AFOSR-TR- 8 35

Edward L. Ginzton Laboratory
W. W. Hansen Laboratories of Physics
Stanford University
Stanford, California

AD A098804

ACOUSTIC MICROSCOPY FOR NONDESTRUCTIVE EVALUATION

OF MATERIALS

Semiannual Technical Report

for the period

1 August 1980 — 31 January 1981

The views and conclusions contained in this
document are those of the authors and should
not be interpreted as necessarily represent-
ing the official policies, either expressed
or implied, of the Defense Advanced Research
Projects Agency or the U.S. Government.

Principal Investigator: Professor C.F. Quate

G.L. Report No. 3232

March 1981

TABLE OF CONTENTS

I. INTRODUCTION AND SUMMARY

The prime event during this interval was the conference in London as sponsored by the Rank Foundation. As mentioned in the last quarterly, it was devoted entirely to the subject of scanning microscopy. Our work was given a great deal of credit by the various speakers -- all of whom recognize some of the inherent advantages of scanning for the various forms of microscopy -- acoustic, optical, and x-ray. The electron microscope was not included since it hs widespread coverage elsewhere.

The book containing the papers has now appeared.[1] It has two important features: 1) it contains a good deal of valuable reference material on this field, and 2) it was printed within 3 months of the conference. This conference signals the start for a new community of workers with a common interest and this spreading of the work into other laboratories is the first sign of maturity for this new technology. A second sign of maturity is the entrance of commercial instrument manufacturers into this field. We have previously reported that Leitz Co. of Wetzlar, West Germany has undertaken a program to construct a prototype instrument. We can now report that in Japan, Olympus Optical Company has undertaken a strong effort in this field and they too are following the methods developed in our laboratory. We have received copies of the enclosed bulletin[2] as put out by Hitachi, also in Japan -- but we know very little of that effort other than that reported in this publication.

Our own work, as reported below, consists of further improvements in the instrument. We have extended the operation to higher frequencies (3.6 GHz with a wavelength of 0.4 micrometers). We have built new hardware and

Noninvasive Method for Visualization of Interior Region of Sample

Acoustic Microscope

In recent years, ultrasonic technology has been progressing by leaps and bounds. With utilization of 1 GHz (10^9 Hz) waves now a possibility, it has become feasible to develop acoustic microscopes with high resolutions on the sub-micron order. Intensive research is in fact being directed toward the development of such microscopes at Stanford University in the U.S.A. as well as other research facilities throughout the world.

This is an area in which Hitachi has put in a lot of effort, too. In 1978, the company came out with a scanning transmission acoustic microscope with three micron resolution. Then, in the autumn of 1979, this same system was perfected into a reflection acoustic microscope with sub-micron resolution.

Fine Images Obtained Using a Micro Lens with High Numerical Aperture

How the reflection microscope works:

1. A piezoelectric film is excited by pulse with a high frequency carrier wave, causing it to generate an ultrasonic wave.

2. The ultrasonic wave is sharply focused by a spherical lens in the sensor section and directed onto the test sample which is moved two-dimensionally so as to be scanned by the ultrasonic beam.

3. The reflected wave from the sample is picked up by the sensor section and is then converted into electrical signals for visual display on a cathode ray tube.

Main Features

1. Fine images can be readily obta'ned thanks to two new developments, a lens system capable of focusing the ultrasonic sound down to a diameter of less than one micron and a scanning table almost perfectly free of vertical fluctuation.

2. The physical properties of materials with complex structures can be clearly determined since the amplitude mode conventionally used in converting the ultrasonic wave into a visual image has been supplemented by the incorporation of a newly developed interference mode which modulates the wave into an interference image.

Cells Can Be Observed in Their Natural Living State

The resolution of acoustic microscopes has already reached about the same level as that of conventional optical microscopes, thus opening up numerous potential fields of application. Areas where acoustic microscopes are likely to prove immediately useful include medicine and biology, where they can be used to observe cells *in vivo*. They are also useful in physics and engineering, where they offer a means for noninvasively examining minute samples. One particularly important application of this type is in the inspection of the interior condition of semiconductor devices. Although acoustic microscopes are today used almost exclusively for structure observation, it will, with the development of measurement techniques for obtaining quantitative physical parameters, become possible to use them for determining microscopic properties as well. This will open the way for quant.tative analysis of the image characteristics of medical ultrasonic diagnostic equipment and put the acoustic microscope on the road toward development as an analytical instrument.

Hitachi

developed new software to enable us to record the image in digital form on floppy discs. We have devised a system for recording two simultaneous images -- each with a different frequency. The difference frequency can be varied as we wish.

This we believe will lead us into the field of acoustic "spectroscopy", a important concept since the evidence suggest that the objects that we investigate are sensitive to the acoustic frequency.

We have done further work on materials -- both inconel and manganese ferrite.

We have been advised by such people as Marchsesault, Director of Research at Xerox in Toronto, and Sloan at Dupont that our preliminary work on polymers indicates that we are in a position to tackle some of the more important problems encountered with these materials. With this in mind, we have extended the theory for imaging of polymer samples.[*] It turns out that we should be able to measure in a quantitative manner both the material density and the velocity of source point-by-point over the image being imaged. This will provide us with a wealth of information of use to the polymer chemists.

The work on adhesion of chrome on glass as reported in the last semiannual report has now appeared in print. This paper has brought the largest response of any single paper we have published. Thin films and problems of adhesion seem to represent generic problems of great interest to a large number of workers. Adhesion is difficult to measure and our method has great appeal to those working in the field.

A strong effort has been placed on photoacoustics during the interval covered by this report. We now have an argon laser properly modulated at microwave frequencies and images are beginning to appear. The work that we

[*]See Figs. 3, 4, and 5 of Quarterly Report marked G.L. Report No. 3173.

have done, as reported here, concerns the theoretical effort which culminates in curves which show the photoacoustics response for various combinations of materials. The photoacoustic response relates the mgnitude of the acoustic power generated per unit of absorbed optical power.

All in all, this has been a rather productive period which has given us new inspiration to continue the momentum of our present program of research.

II. NEW INSTRUMENTAL ADVANCES

A significant amount of effort was spent on the design and construction of a new system that allows digital control and digital storage of the images. The system is "stand alone" so that it can be transported to different microscopes. It incorporates two Z-80 microprocessors -- one to control the information fed to the disc, and the second to act as buffer. This second feature will permit us to record the images at a much faster rate than has been possible with previous systems. Our ability to deal with digital signals lets us work in the realm that has been called "digital image processing". We can now record a histogram and reprocess the signal by adjusting the histogram so that it is more or less evenly distributed over the area of the image. It is known that processing of this sort can improve the image detail in significant ways. The other system which is now easy to implement is the straightforward technique of differentiating the signal to reduce the image contrast and bring out the features such as edges. A striking example has been published by Hollis of IBM (see book[1] edited by Ash).

We now have in place a new system that permits us to record two simultaneous images of the same area. The two images can differ in frequency

by a fixed amount. With this technique we make use of two parallel channels each with a train of acoustic pulses differing from each other by the specified interval. The pulse trains are interlaced in time and this permits us to separate them at the output with proper gating techniques. We are now in the process of extending the technique so that we can vary the frequncy differnce in a continous fashion and display this in the image. It will permit us to monitor and display those features of the object that are sensitive to frequency. This flexibility will enhance our ability to extract more and more information from the objects under observation.

III. ADVANCES WITH ACOUSTIC LENS

Our work has continued on the theory, design, and fabrication of acoustic lenses. This has permitted us to build lens with a smaller diameter (now with a radius of 16 μm). This is culminated in a high instrument operating with a wavelength of 0.4 micrometers in water.

In Fig. 1 we see an aluminum line 1μ thick on a silicon substrate with a 2μ sputtered glass overlay. The acoustic images were taken with lens of radius equal to 44 microns and operating at 2.6 GHz. The line is 15 μ wide. It has been intentionally damaged with a diamond indenter as part of an electromigration study. The optical micrograph in Fig. 1(b) is an oil immersion interference contrast picture. Of special interest in the acoustic image in Fig. 1(a) is the network of cracks in the aluminum line which are not evident in the optical image of Fig. 1(b). The dark area of the indentation in Fig. 1(a) is seen to be different in its acoustic response from the other indented areas and from the rest of the aluminum line. A possible explanation is that the indenter has broken loose the bond between the aluminum and the

(a) ACOUSTIC 1st FOCUS
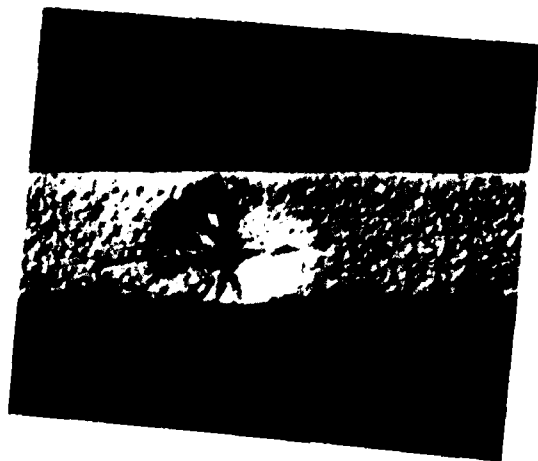
(b) OPTICAL
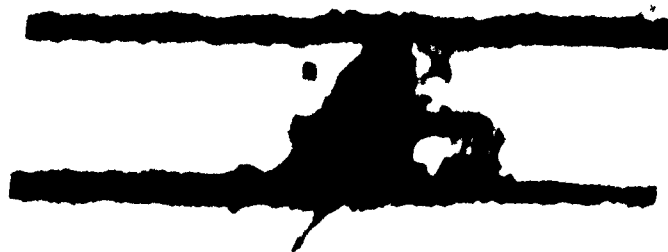
(c) ACOUSTIC 2nd FOCUS

ALUMINUM LINE ON SILICON WITH QUARTZ OVERLAY

FIGURE 1

silicon below or between the aluminum and the quartz above. We know from our previous studies that adhesion failure gives rise to strong contrast in acoustic micrographs. An alternative possibility is that the indenter has removed the glass layer from this area.

IV. MATERIAL STUDIES

We have continued to study the nickel alloy, Inconel. The image of Fig. 2 with its striking contrast is one of the best that we have recorded to date. We see there both the grain boundaries and the curved lines and the slip planes as the straight lines. The slip planes are more difficult to delineate with chemical etching procedures, yet in the acoustic micrographs they show up with a contrast equal to that of the grain boundaries. The important feature in these images is the strength of the acoustic reflection at the grain boundaries. The acoustic response in this form tells us something of the elastic properties of the boundaries. As yet we have not unraveled this source of contrast but it continues to interest us.

A second material that we have studied during this interval is a sample of manganese ferrite. It is a material commonly used for magnetic recording heads -- a material of some technical importance. Our comparison between the optical and acoustic micrographs shows that the surface features appear in both, but the grain boundaries appear only in the acoustic micrographs. The relative orientation of the grains can be deduced from the change in contrast between adjacent grains. The one defect is seen as a chip at the narrow junction between three of the grains. As a result of this study, our friends at Honeywell Laboratory in Denver have provided us with samples of actual recording heads. We hope to be able to present the results of that study in

INCONEL ALLOY
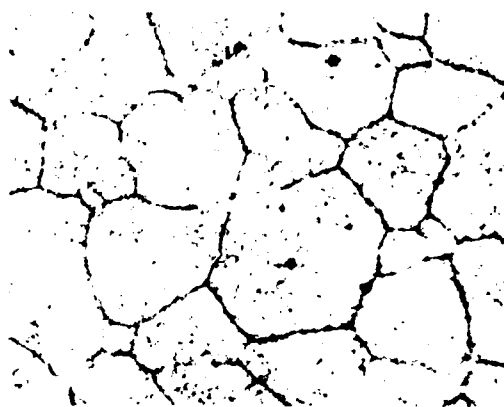
(a) OPTICAL, POLISHED

(b) OPTICAL, ETCHED

(c) ACOUSTIC $Z = -0.5\mu$
    2.7 GHz

(d) ACOUSTIC $Z = -1.0\mu$
    2.7 GHz

FIGURE 2

our next report.

We mentioned in our introduction that the publication of a paper on film adhesion has attracted attention. One instance of this which is of direct interest to the Air Force is the call we received from the Hughes Laboratory at Santa Barbara. They are experiencing problems with the adhesion of Lead Sulphide films to the sapphire substrate. These devices are used as infrared detectors. The project is being done for the Space Missle Division in Los Angeles. Dr. Jim Knight at Santa Barbara has provided us with defective detectors and we are currently in the process of characterizing these devices with acoustic microscopy.

V. PHOTOACOUSTIC MICROSCOPY

From our previous reports the reader will be aware of our strong interest in photoacoustics as a new method for imaging. In essence, it will allow us to monitor and image the optical energy absorbed by the object that is under scrutiny. The modulated optical beam periodically heats the sample and generates an acoustic wave in the liquid surrounding the sample. This wave is picked up in the acoustic lens and the image is formed with mechanical scanning as in the conventional acoustic microscope. The new system is operating with acoustic waves near 900 MHz. We are now recording our first traces with a good signal-to-noise ratio.

Our plan is to present, in this section, the results of the theoretical calculations that we have been performing in order to predict that magnitude of the acoustic wave that can be expected for a given amount of absorbed optical power.

1. Scanning Photoacoustic Microscopy

In the photoacoustic effect absorbed light is converted into sound by the thermal expansion of the absorber and its surroundings. It is the basis of photoacoustic spectroscopy, where the received acoustic signal detected by a microphone is measured as a function of the optical wavelength of light absorbed by a solid, liquid, or gas.[3,4] It can be used to measure very small concentrations of materials, or very small absorption coefficients.[5,6] Early flaw detection results by von Gutfeld[24] pointed to the possibility of microscopy based on photoacoustics.

In the work to be described here we will first review the work that was done prior to this reporting interval in order to remind the reader what was done and to prepare for the next report where we expect images of superior quality as recorded on the new machine. In the later section on theory we report the work that was done during this interval. We see there that the results are presented in forms of curves. These are most useful in predicting the acoustic output. Figure 3 shows the experimental setup that was used initially. It has now been replaced with an argon laser that is modulated with an acousto-optic modulator at a single frequency. An acoustic lens of radius of 200 μm was used as the receiver.

- 9 -

The confocal arrangement means that we collect a substantial fraction of the generated acoustic energy. This is essential to overcome acoustic losses in the water used as coupling fluid from sample to lens. The use of the acoustic lens ensures that our output acoustic signal is collected only from the heated spot on the sample. A potential advantage of the high acoustic frequency is the ability to generate acoustic efficiently with short modulated optical pulses. We shall see later that the strength of the photoacoustic signal is a strongly increasing function of the optical modulation frequency for some materials.

The sample was scanned with a scanner from a conventional acoustic microscope, modified to scan at 1 Hz fast scan rate. Position was detected in both x and y directions perpendicular to the acoustic lens axis. These signals controlled the position of the CRT spot. The intensity of the cathode ray display was proportional to the amplified and detected acoustic power in a pulse.

The photoacoustic signal is generated by the intensity modulation of the absorbed laser light. Later we will discuss the theory of photoacoustic generation and develop a detailed model predicting photoacoustic output for given laser input for different geometries. For now we note that the acoustic wave equation in the presence of thermal expansion for a semi-infinite isotropic solid is:[7]

$$\frac{\partial^2 T}{\partial z^2} - \frac{1}{v_s^2} \frac{\partial^2 T}{\partial t^2} = \frac{B\beta}{c_{11}} \frac{\partial^2 \theta}{\partial t^2}$$
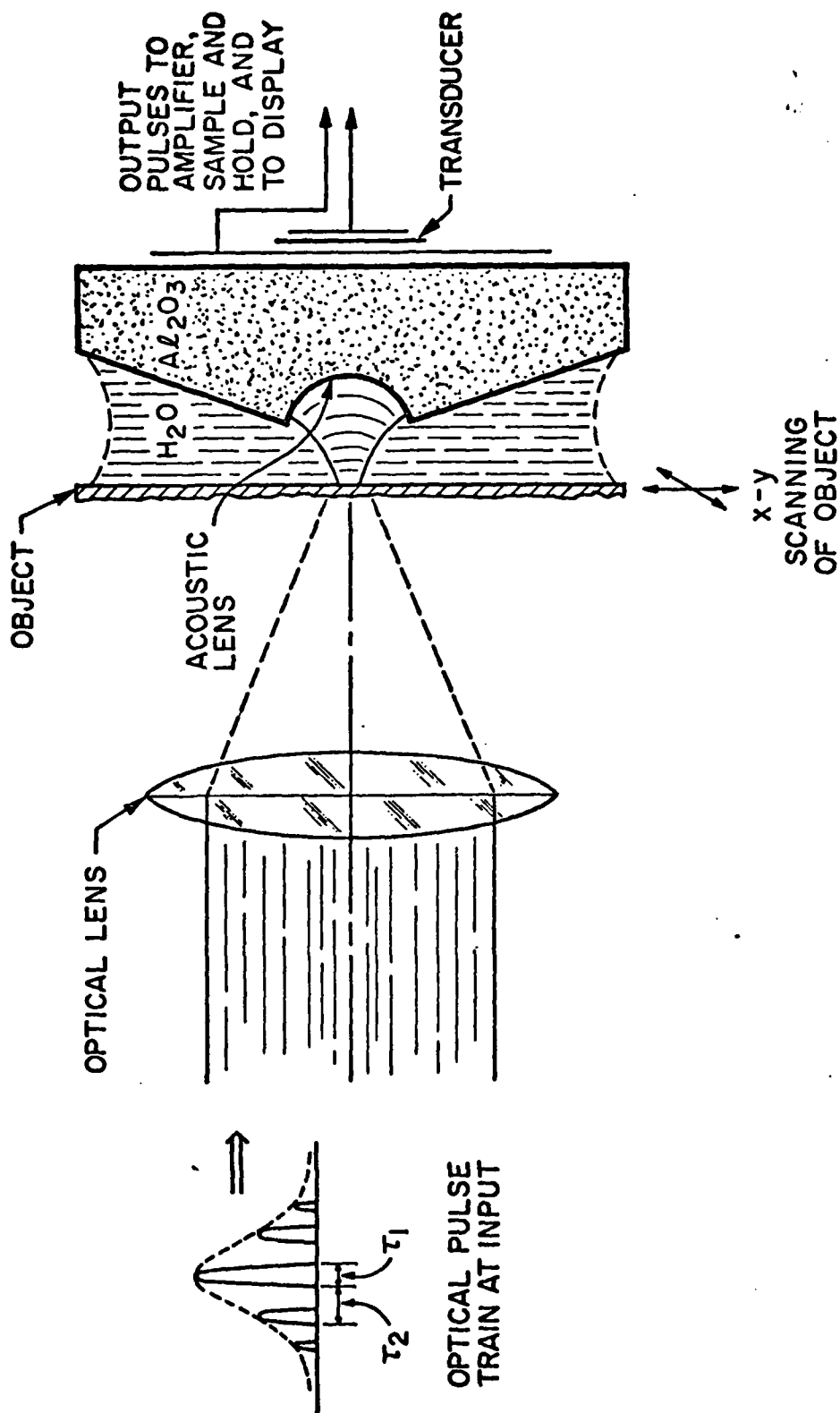
FIG. 3--The photoacoustic setup.

where

T = stress

V_s = sound velocity

B = bulk modulus

β = linear coefficient of thermal expansion

c_{11} = stiffness

θ = temperature rise.

By inspection of this equation we can see the right hand side is the driving or source term for the stress wave $T(z,t)$. One can also see that the frequency spectrum of the temperature variation $\theta(z,t)$ will determine the spectrum of the generated acoustic waves.

Now the temperature rise θ is proportional to optical power absorbed, providing the absorption coefficient α is not a function of temperature. Thus the acoustic spectrum is determined by the spectrum of the modulation of optical power absorbed by the sample.

We also notice that in terms of power, with $\theta \propto P_{optical}$ and $P_{acoustic} \propto T^2$ then we have $P_{acoustic} \propto (P_{optical})^2$.

In order to produce acoustic images with this system the system was confocally aligned, so that the optical lens and the acoustic lens are focused on overlapping spots. This is a disadvantage of the present system as compared to other systems, which typically use a microphone or hydrophone in a gas or liquid cell as the acoustic receiver. There the difficult and precise alignment of the system is not required.

The resolution we expect in this confocal imaging system is better than we get from one lens alone. Basically, we expect the overall imaging system transfer function to be the convolution of the transfer functions of each

lens.[23] This means that higher spatial frequencies in the object are passed by the imaging system and by the criteria discussed elsewhere. This means greater resolution. A complicating factor here is that acoustic waves will be produced from a source larger than the optical spot size due to thermal diffusion. Thus at 840 MHz the thermal diffusion length in gold is 0.23 μ. If we have an optical spot size of 2.0 μ we will have a thermal spot size (where the temperature is modulated at 840 MHz) of ~ 2.5 μ. The square-law nature of the photoacoustic generation process acts to offset this by shrinking the effective spot size.

To produce confocal alignment of optical and acoustic lenses, the acoustic lens acted as the lens of a reflection acoustic microscope to image a scanned finder grid. A scanning optical reflection micro- scope was constructed by picking off with a beam splitter a portion of the light returning through the optical lens from the other side of the same finder grid. The optical reflection microscope image was formed by focussing this returning light onto a photodiode whose output con- trolled the intensity of the display. The same X and Y position signals from the scanner were used to position the spot on the face of the display. By adjusting the positions of the optical and acoustic lenses with micrometers on their respective stages, one could bring the two reflection images — optical and acoustic — into approximate coincidence. One could improve alignment by forming a difference image by subtracting acoustic and optical signals in a differential amplifier. Finally input laser power was increased, the acoustic system was converted to receive-only mode, and one looked for photoacoustic pulses on an oscilloscope triggered by the laser shot. The signals were typically not visible without further search by systematically 'walking'

- 13 -

one set of stage micrometers around the position of rough coincidence already arrived at. Once located, a photoacoustic signal could be kept in sight for several hours. The images could be made over various areas of the sample.

To produce the image, the detected, sampled and held photoacoustic pulse supplied the intensity control for the display, while sample position sensors X and Y controlled CRT spot position.

The earliest images produced with this technique were anything but nondestructive. In particular, images of a 1 mil (25 μ) thick Al foil and a Cr/Al finder grid pattern were imaged with this technique and these images have been published elsewhere.[8] Damage to the samples due to the high temperatures reached during imaging was severe. Holes were burned through the 1 mil Al foil, and both Al and Cr in the grid pattern were severely damaged. The melting temperature of Aluminum is 660 C; that of Chromium is 1857 C. We conclude that local temperature changes of 2000 C or more were produced in this first imaging effort.

In a second round of imaging with this photoacoustic system the scanning and positioning system was improved. In Fig. 4 we show optical and photoacoustic images of a gold finder grid 1500 A thick evaporated on a microscope cover slip. 1.8 μ of sputtered glass (λ/4 at 840 MHz) was deposited on top of the gold, on half of the finder grid pattern, including the letter 'V' as shown. The sputtered glass layer was intended to serve as a quarterwave acoustic transformer from gold into water. It was observed to function as such, since the portion of the finder grid covered with the sputtered glass was observed to have ~6 dB higher photoacoustic signal than the portion of the grid not

GLASS/Au/GLASS
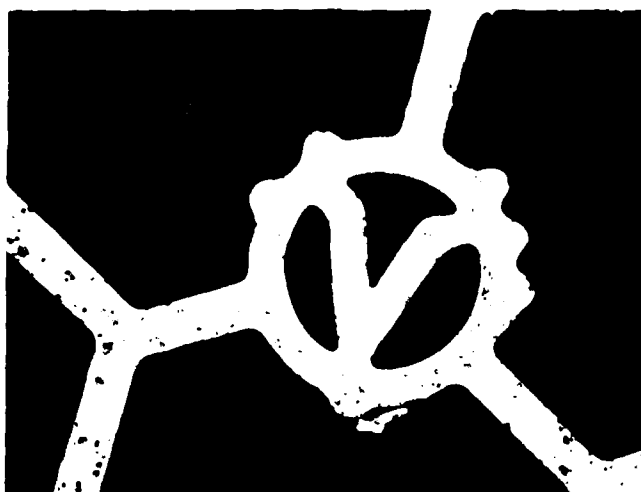
OPTICAL REFLECTION
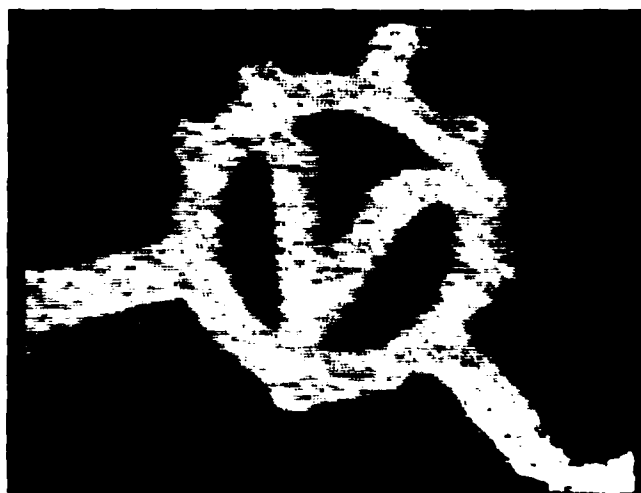
PHOTOACOUSTIC

OPTICAL $\lambda = 1.06\mu$
ACOUSTIC $f = 840$ MHz
$\lambda = 1.83\mu$

FIG. 4 --Photoacoustic image of chrome on glass.

- 15 -

covered with this glass.

In the optical reflection microscope picture of the letter 'V', individual glass particles from the sputtering process are visible on the gold pattern. Many of these are recognizable as dark areas in the photoacoustic image as well. Presumably they act as scattering centers for the photoacoustic pulses.

At the bottom of the circular band surrounding the letter 'V' is an imperfection in the pattern visible in the optical micrograph which is not visible in the photoacoustic image. It is a small area of metal which was evaporated onto photoresist in the process of laying down the grid pattern. It did not break away cleanly in the liftoff procedure. This area of metal is still attached to the well adhered grid pattern, but is not itself well adhered to the glass substrate. The area in question was evaporated onto photoresist, which was dissolved away during liftoff. It is laying on the glass substrate and is covered with the sputtered glass.

The lack of adhesion is shown by the photoacoustic picture, which simply does not show this area at all. The photoacoustic picture was taken before the optical picture. If we assume this piece of metal was left on at liftoff, it must have been physically present in the sample when the photoacoustic image was made. It must have been the different boundary conditions at the gold-glass interface which resulted in no photoacoustic signal. As we shall see, the theory of photoacoustic generation predicts that light absorbed at a free surface is much less efficient in generating a photoacoustic signal than a constrained surface. The non-adhering metal area we have been discussing is seen to act as a free surface.

- 16 -

The optical micrograph in Fig. 4 was taken after the photoacoustic imaging. There is no visible damage in the optical picture. In other pictures taken of other areas of the same glass/gold/glass grid it was found that with optical power approximately twice that in Fig. 4, the gold started to melt. The melting point of gold is 1064 C. We conclude that temperature changes of several hundred degrees C were encountered in the photoacoustic imaging of Fig. 4.

In Figs. 5 and 6 we see photoacoustic images of an integrated circuit. This circuit, a test silicon on sapphire device manufactured by RCA, was illuminated by the laser pulses through the sapphire substrate. The laser light was absorbed at the bottom of the layers making up the integrated circuit structure. Sound propagated from the front (top) side of the devices to the acoustic lens. The photoacoustic signal is absent where there are no optical absorbers present. Different image intensity is seen for different types of device layers. A feature worthy of note is that areas of uncovered silicon (visible as lightly covered areas in the optical pictures) give much weaker photoacoustic response than areas of a aluminum or aluminum-covered silicon (black in the optical pictures).

2. Theory of Photoacoustic Generation

To predict the photoacoustic response we will adopt a plane-wave model. The incoming intensity-modulated light will be absorbed and raise the temperature of the absorbing region. The heat diffusion process will determine temperature rise as a function of position. This temperature function is used as the driving term in the acoustic

SILICON ON SAPPHIRE IC

(a) OPTICAL TRANSMISSION

|← 100 μ →|
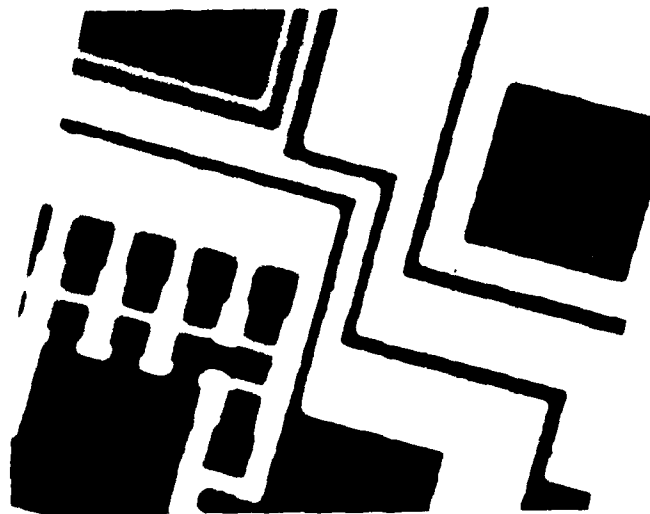
(b) PHOTOACOUSTIC

FIGURE 5

SILICON ON SAPPHIRE IC

(a) OPTICAL TRANSMISSION

100μ
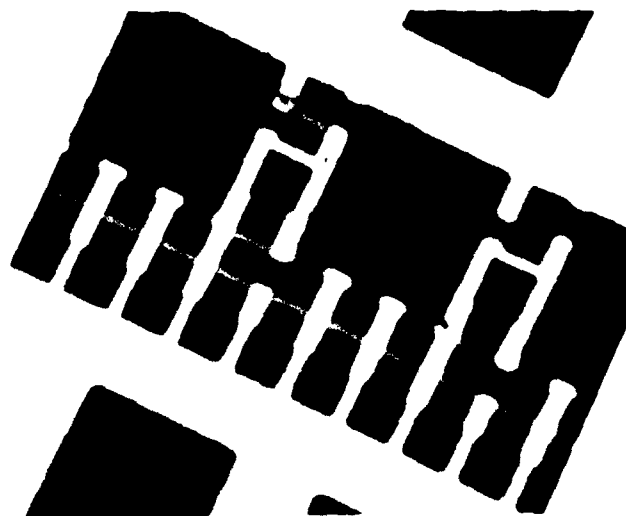
(b) PHOTOACOUSTIC

FIGURE 6

field equations, which are solved to find the acoustic power in the far field. The method of coupled modes[9] is used to solve for the generation from the distributed source region.

Figures 7 and 8 show the specific models we are postulating. In Fig. 7 light enters as a plane wave of intensity I_0 through transparent medium I . It is absorbed in medium II, the light intensity varying as $I_0 e^{-\alpha z}$. Heating and resultant thermal expansion of the heated boundary region generates acoustic waves that we detect in the far field of region I or region II. We eventually assume the incoming light is intensity modulated with angular frequency ω , and the resultant acoustics are at the same frequency. In Fig. 8 we make region II a layer of thickness L and there the light is attenuated as $I_0 e^{-\alpha z}$. Region III is transparent. We will solve for the temperature distribution as a function of position, and use this as the driving term in the acoustic field equations. We will solve these with coupled mode variables for the far-field acoustic strain and power.

3. Two-Layer Model: Heat Flow

The theory of heat conduction[10] tells us that heat will flow whenever we have a temperature gradient in space. For the case of one-dimensional heat flow, we will have:

$$f = -k \frac{\partial \theta}{\partial z} \tag{5.1}$$

where f is the heat flux in watt/m^2, θ is the temperature, and K

- 20 -

REGION I | REGION II

$$I = I_0 e^{-\alpha z}$$

$a'_{-1}(z)$

$a'_{+2}(z)$

$a'_{-2}(z)$

$z = 0$

(a)

I | II

$$\theta_1 = \theta_{11} e^{\tau_1 z} \qquad \theta_2 = \theta_{20} e^{-\tau_2 z} + \theta_{22} e^{-\alpha z}$$

$z = 0$
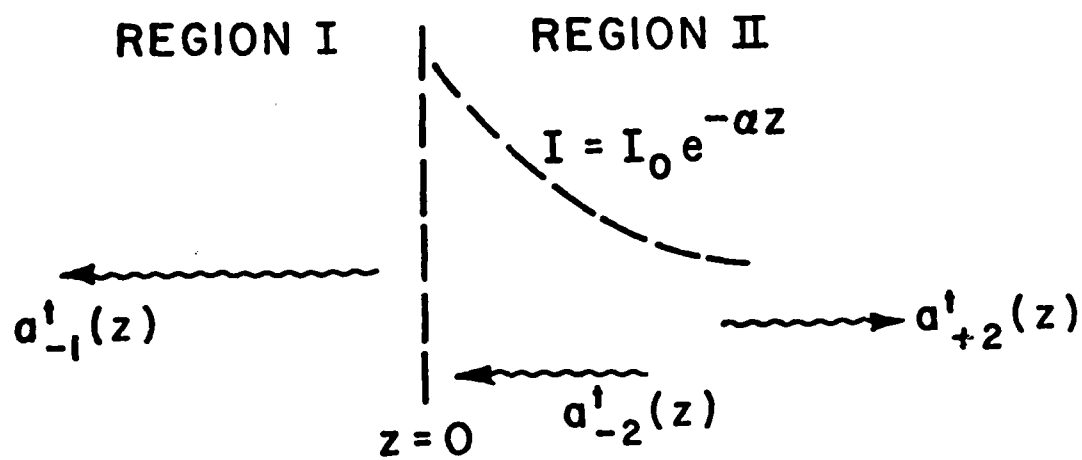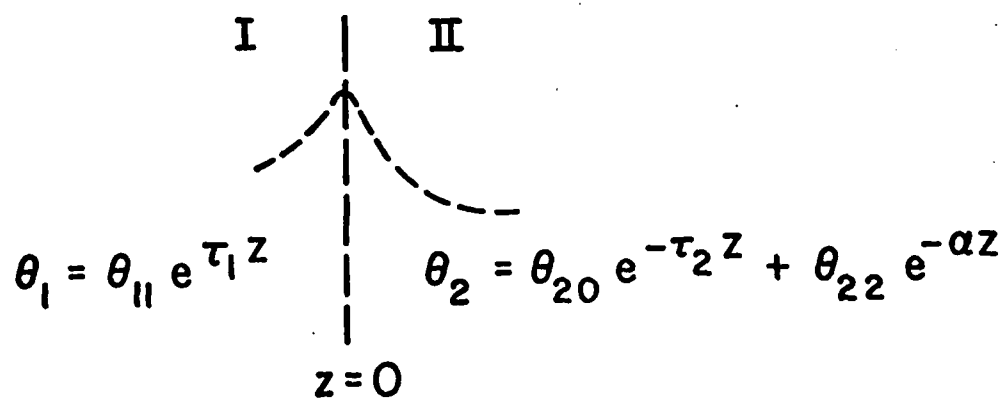
(b)

FIG. 7. (a) Production of the thermal wave, two-region case.
(b) Temperature profile for the two-region case.

REGION I   II   III

(a)

(b)
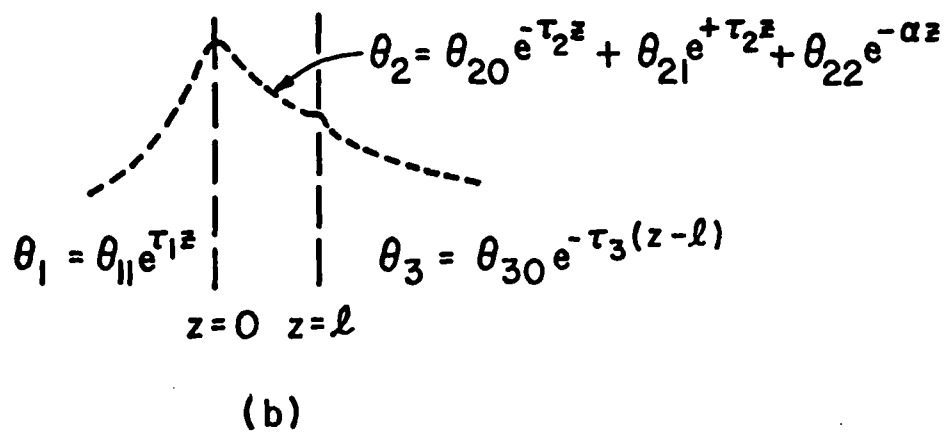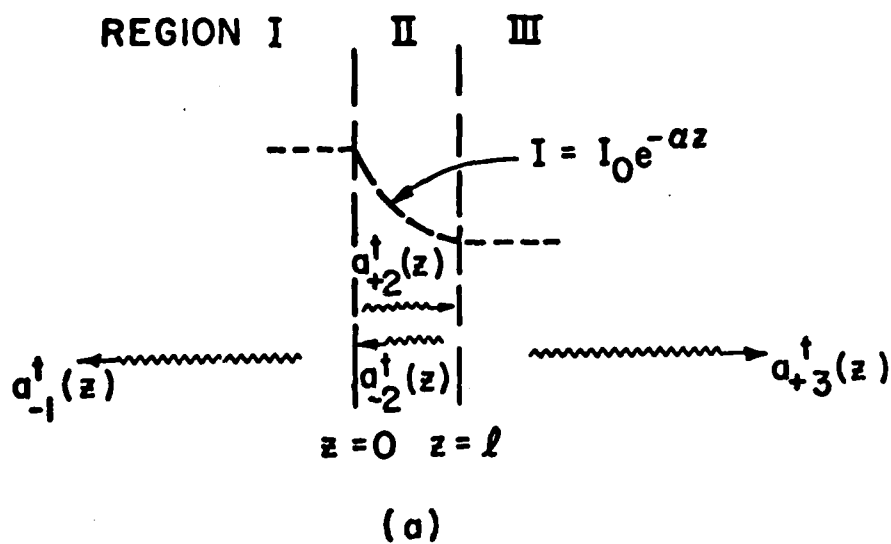
FIG. 8. (a) Thermal waves in the three-region case.
(b) Temperature profile three regions.

is the thermal conductivity in (watt/km). If the heat flux changes with position z, there is heat being deposited or generated in the medium. The rate of heat absorption in a volume element $\Delta z \Delta A$ is:

$$-\left(\frac{\partial f}{\partial z}\, \Delta z\right) \Delta A$$

where the negative sign accounts for the fact that if $\partial f/\partial z$ is a negative number, net energy is being absorbed in the medium, if we assume a flow of heat toward positive values of z.

The medium may also be heated by absorption of optical energy. For light traveling towards $+z$ where the intensity varies as

$$I = I_o e^{-\alpha z}$$

we will have energy absorbed by the medium equal to:

$$-\left(\frac{\partial I}{\partial z}\, \Delta z\right) \Delta A$$

for a volume element $\Delta z \Delta A$. Both the change in heat flux and the absoprtion of optical energy will cause a change in the temperature. For a volume $\Delta z \Delta A$ this will correspond to rate of energy absorption

$$\rho C \frac{\partial \theta}{\partial t}\, \Delta z \Delta A$$

where ρ = density; C = specific heat . Equating heat absorbed to heat required for temperature change θ, we find that:

$$\rho C \frac{\partial \theta}{\partial t} = -\left(\frac{\partial f}{\partial z} + \frac{\partial I}{\partial z}\right) \tag{5.2}$$

We now assume sinusoidal excitation, and this gives:

$$\frac{\partial f}{\partial z} = -j\omega\rho C\theta + \alpha I_0 e^{-\alpha z} \tag{5.3}$$

$$\frac{\partial \theta}{\partial z} = -\frac{1}{K} f \tag{5.4}$$

where (5.4) simply restates the definition of heat flux f .

The standard method of solving these equations for the temperature $\theta(z)$ is to eliminate the variable f . One is left with the diffusion equation, and there is a large literature devoted to solving this equation under a variety of boundary conditions.[10,21] However, to point out the advantages of coupled modes,[9] we will use this method to solve for the temperature distribution.

We multiply Eqs. (5.4) by Z_t and add it to Eq. (5.3):

$$\frac{\partial}{\partial z}(f + Z_t \theta) = -\frac{Z_t}{K}\left(f + \frac{j\omega\rho CK}{Z_t}\theta\right) + \alpha I_0 e^{-\alpha z} \tag{5.5}$$

Now let:

$$Z_t^2 = j\omega\rho CK$$

or

$$Z_t = (1 + j)\sqrt{\frac{\omega\rho CK}{2}} \tag{5.6}$$

and we have:

$$\frac{\partial}{\partial z}(f + Z_t \theta) = -\frac{Z_t}{K}(f + Z_t \theta) + \alpha I_0 e^{-\alpha z} \tag{5.7}$$

- 24 -

or, letting

$$a_+^t = f + Z_t \theta \qquad (5.8)$$

we have

$$\frac{\partial a_+^t}{\partial z} = -\frac{Z_t}{K} a_+^t + \alpha I_0 e^{-\alpha z} \qquad (5.9)$$

Similarly, if we multiply Eq. (5.4) by Z_t and subtract from Eq. (5.3), we get

$$\frac{\partial a_-^t}{\partial z} = \frac{Z_t}{K} a_-^t + \alpha I_0 e^{-\alpha z} \qquad (5.10)$$

where

$$a_-^t = f - Z_t \theta \quad . \qquad (5.11)$$

The advantage of transforming to normal mode variables is that we have uncoupled the equations without having to go to a second order equation. Equations (5.9) and (5.10) can now be manipulated to a form that is directly integrable. We let:

$$a_+^t = d_+^t e^{-\tau z}$$

$$a_-^t = d_-^t e^{+\tau z} \qquad (5.12)$$

where

$$\tau = \frac{Z_t}{K} = (1 + j) \sqrt{\frac{\omega \rho C}{2K}} \qquad (5.13)$$

Then Eqs. (5.9), (5.10) become:

$$\frac{\partial d_+^t}{\partial z} = \alpha I_0 \, e^{-(\alpha - \tau)z} \tag{5.14}$$

$$\frac{\partial d_-^t}{\partial z} = \alpha I_0 \, e^{-(\alpha + \tau)z} \tag{5.15}$$

We now apply these equations to the two regions I and II. In region II we will have, by simple integration of (5.14):

$$d_{+2}^t(z) - d_{+2}^t(0) = \alpha I_0 \int_0^z e^{-(\alpha - \tau_2)\zeta} \, d\zeta$$

where ζ is the dummy position variable of integration. Integration gives:

$$d_{+2}^t(z) = -\frac{\alpha I_0}{\alpha - \tau_2} \left(e^{-(\alpha - \tau_2)} - 1 \right) + d_{+2}^t(0) \tag{5.16}$$

Similarly, for the negative-traveling mode in region II,

$$d_{-2}^t(\infty) - d_{-2}^t(z) = \alpha I_0 \int_z^\infty e^{-(\alpha + \tau_2)\zeta} \, d\zeta \tag{5.17}$$

Since we have no heat flow from $+\infty$, $d_{-2}^t(\infty) = 0$, and

$$d_{-2}^t(z) = -\frac{\alpha I_0}{\alpha + \tau_2} e^{-(\alpha + \tau_2)z} \tag{5.18}$$

We can now put these back in terms of a_+^t and a_-^t to get:

$$a_{+2}^t(z) = +\frac{\alpha I_0}{\alpha - \tau_2} \left(e^{-\tau_2 z} - e^{-\alpha z} \right) + a_{+2}(0) \, e^{-\tau_2 z} \tag{5.19}$$

- 26 -

$$a_{-2}^{t}(z) = -\frac{\alpha I_0}{\alpha + \tau_2} e^{-\alpha z} \qquad (5.20)$$

In region I we have no sources of heat, and hence Eqs. (5.10) and (5.11) simplify to:

$$\frac{\partial a_{+1}^{t}}{\partial z} = -\frac{Z_{t1}}{K_1} a_{+1}^{t} = -\tau_1 a_{+1}^{t}$$

and

$$\frac{\partial a_{-1}^{t}}{\partial z} = \frac{Z_{t1}}{K_1} a_{-1}^{t} = \tau_1 a_{-1}^{t} \ .$$

Since $a_{+1}(-\infty) = 0$, we will have

$$a_{+1}^{t}(z) = 0$$

and

$$a_{-1}^{t}(z) = a_{-1}^{t}(0) e^{\tau_1 z} \qquad (5.21)$$

What remains is to match boundary conditions at the interface $Z = 0$. There we must have continuity of the temperature θ and the heat flux f . For the latter (f) we must have:

$$a_{+1}^{t}(0) + a_{-1}^{t}(0) = a_{+2}^{t}(0) + a_{-2}^{t}(0) \qquad (5.22)$$

For the former (θ) we will have:

$$\delta_{21}\left(a_{+1}^{t}(0) - a_{-1}^{t}(0)\right) = a_{+2}^{t}(0) - a_{-2}^{t}(0) \qquad (5.23)$$

Substitution of our results for $a_{+1}^{t}(z)$, $a_{-1}^{t}(z)$, $a_{+2}^{t}(z)$ and $a_{-2}^{t}(z)$ into these gives:

- 27 -

$$a^t_{-1}(0) = -\frac{2\alpha I_0}{(\delta_{21} + 1)(\alpha + \tau_2)} \tag{5.24}$$

$$a^t_{+2}(0) = -\frac{(1 - \delta_{21})\alpha I_0}{(1 + \delta_{21})(\alpha + \tau_2)} \tag{5.25}$$

where we have let $\delta_{21} = Z^t_2/Z^t_1$.

Using Eqs. (5.19), (5.20), and (5.21) we can write for the temperature distributions:

$$\theta_1(z) = \theta_{11}e^{\tau_1 z} \tag{5.26}$$

$$\theta_2(z) = \theta_{20}e^{-\tau_2 z} + \theta_{22}e^{-\alpha z} \tag{5.27}$$

where:

$$\theta_{11} = \frac{\alpha I_0}{Z^t_1(1 + \delta_{21})(\alpha + \tau_2)} \tag{5.28}$$

$$\theta_{20} = \frac{\alpha I_0 \left(1 + \delta_{21}(\alpha/\tau_2)\right)}{\tau_2 Z^t_2 \left(\frac{\alpha^2}{\tau_2^2} - 1\right)(1 + \delta_{21})} \tag{5.29}$$

$$\theta_{22} = \frac{-\alpha I_0}{\tau_2 Z^t_2 \left(\frac{\alpha^2}{\tau^2} - 1\right)} \tag{5.30}$$

If we let

$$\theta_{02} = \frac{\alpha I_0}{\tau_2 Z^t_2 \left(\frac{\alpha^2}{\tau_2^2} - 1\right)} \tag{5.31}$$

It may be shown that:

$$\theta_{20} = \theta_{02} \frac{\left(1 + \delta_{21} \frac{\alpha}{\tau_2}\right)}{\left(1 + \delta_{21}\right)} \qquad (5.32)$$

$$\theta_{22} = - \theta_{02} \qquad (5.33)$$

Again we have defined:

$$z_{1,2}^t = (1 + j) \sqrt{\frac{\omega}{2} \rho_{1,2} C_{1,2} K_{1,2}} \qquad (5.34)$$

$$\tau_{1,2} = \frac{z_{1,2}^t}{K_{1,2}} \qquad (5.35)$$

$$\delta_{21} = \frac{z_2^t}{z_1^t} = \sqrt{\frac{\rho_2 C_2 K_2}{\rho_1 C_1 K_1}} \qquad (5.36)$$

To calculate the maximum temperature excursion of the sample, we note that the peak temperature will be at $z = 0$, where

$$\theta_1(0) = \theta_{11} = \theta_2(0) = \theta_{20} + \theta_{22} \ .$$

In Table 5.1 are listed some calculated peak ac temperature excursions at the interface $z = 0$ for a variety of combinations of materials for a 100 MHz modulation frequency, with 10^{10} W/m^2 = 10 mW/μ^2 absorbed. We note the remarkable similarity in results for various types of medium 1 used with the metals and silicon. This is because the metals are better heat conductors than the first media (pyrex, sapphire, water), so the first medium is of minor consequence.

- 29 -

TABLE 5.1.   Maximum Temperature Excursion at 100 MHz for Optical
Intensity Absorbed $I_o = 10^{10} W/m^2 = 10 \ mW/\mu^2$.

Medium 1	Medium 2	$\alpha, \ m^{-1}$ [9]	Temperature θ_{11}
Pyrex	Aℓ	1.12 E8	19 C
Sapphire	Aℓ	1.12 E8	16 C
Water	Aℓ	1.12 E8	19 C
Pyrex	Au	7.60 E7	18 C
Sapphire	Si	3.29 E6	16 C
Pyrex	Water	1.00 E5	0.37 C
Pyrex	Water	1.00 E6	3.7 C

4.   Two-Layer Model: Acoustic Generation

Having solved for the temperature profile excited by light inten-
sity modulated at radian frequency ω , we can proceed to calculate the
generation of acoustic waves. The coupling from a fluctuating tempera-
ture distribution to propagating sound wave is via the coefficient of
thermal expansion.

For a one-dimensional isotropic model, Hooke's law takes the
form:

$$T = c_{11}S - B\beta'\theta \qquad (5.37)$$

where T = stress , S = strain , c_{11} = stiffness , B = bulk modulus ,
β' = linear thermal expansion coefficient , θ = temperature change.
Bulk modulus B rather than c_{11} is used in the second term because
by the nature of thermal expansion the stress it causes is a hydro-
static pressure increase rather than a directed traction force.

For sound propagation in one dimension (z) in an isotropic medium we have:

$$\frac{\partial u}{\partial z} = -\frac{\partial S}{\partial t} \qquad (5.38)$$

where u = particle velocity. This is just the time derivative of the definition of strain. Substituting in (5.37) we have:

$$\frac{\partial u}{\partial z} = -\frac{1}{c_{11}}\frac{\partial T}{\partial t} - \beta\frac{\partial \theta}{\partial t} \qquad (5.39)$$

where $\beta = B\beta'/c_{11}$. Newton's second law for this case is:

$$\frac{\partial T}{\partial z} = -\rho\frac{\partial u}{\partial t} \qquad (5.40)$$

Equations (5.39) and (5.40) are two coupled equations in the variables T (stress) and u (particle velocity) . Letting $Z_0 = \rho V_s$, where Z_0 = acoustic impedance, V_s = sound velocity, we define

$$a_+ = T + Z_0 u \qquad (5.41)$$

$$a_- = T - Z_0 u \qquad (5.42)$$

where a_+ and a_- (with no superscript as in a_+^t, a_-^t) are positive and negative traveling acoustic normal modes.

We assume that temperature waves and sound waves are time harmonic and hence $\partial/\partial t \rightarrow j\omega$. Then

$$\frac{\partial T}{\partial z} = -j\omega\rho u \qquad (5.43)$$

and

$$\frac{\partial u}{\partial z} = -\frac{j\omega}{c_{11}} T - j\omega\beta\theta \qquad (5.44)$$

To transform to normal modes we multiply Eq. (5.44) by Z_0 and add to Eq. (5.43):

$$\frac{\partial}{\partial z}(T + Z_0 u) = -j\frac{\omega Z_0}{c_{11}}T - j\omega\rho U - j\omega\beta Z_0\theta \qquad (5.45)$$

With $c_{11} = \rho V_s^2$ and $k = \omega/V_s$:

$$\frac{\partial}{\partial z}(T + Z_0 u) = -jk(T + Z_0 u) - jkc_{11}\beta\theta \qquad (5.46)$$

or:

$$\left(\frac{\partial}{\partial z} + jk\right)a_+ = -jkc_{11}\beta\theta \qquad (5.47)$$

Similarly, if we multiply Eq. (5.44) by Z_0 and subtract it from Eq. (5.43) we get:

$$\frac{\partial}{\partial z}(T - Z_0 u) = \frac{j\omega}{V_s}(T - Z_0 u) + j(\omega/V_s)c_{11}\beta\theta \qquad (5.48)$$

or

$$\left(\frac{\partial}{\partial z} - jk\right)a_- = +jkc_{11}\beta\theta \qquad (5.49)$$

We make a change of variables to carry out integration:

$$a_+ = d_+ e^{-jkz} \quad \text{and} \quad a_- = d_- e^{+jkz}$$

This changes Eqs. (5.47) and (5.49) to:

$$\frac{\partial d_+}{\partial z} = -jkc_{11}\beta\theta e^{jkz} \qquad (5.50)$$

and

$$\frac{\partial d_-}{\partial z} = +jkc_{11}\beta\theta e^{-jkz} \qquad (5.51)$$

If we now assume θ is different from 0 over a region extending from z_1 to z_2 we can integrate these equations:

$$d_+(z) - d_+(z_1) = -jkc_{11}\beta \int_{z_1}^{z} \theta e^{+jk\zeta} \, d\zeta \qquad (5.52)$$

and

$$d_-(z_2) - d_-(z) = +jkc_{11}\beta \int_{z}^{z_2} \theta e^{-jk\zeta} \, d\zeta \qquad (5.53)$$

which yield:

$$a_+(z) = -jkc_{11}\beta e^{-jkz} \int_{z_1}^{z} \theta e^{+jk\zeta} \, d\zeta + a_+(z_1)e^{-jk(z-z_1)} \qquad (5.54)$$

and

$$a_-(z) = -jkc_{11}\beta e^{+jkz} \int_{z}^{z_2} \theta e^{-jk\zeta} \, d\zeta + a_-(z_2)e^{+jk(z-z_2)} \qquad (5.55)$$

Let us now return to the specific case of the two semi-infinite media meeting in the plane $z = 0$, with optical energy incident from the left in transparent medium I and absorbed in medium II. In medium II we have previously found the temperature in Eq. (5.27) to be:

$$\theta_2(z) = \theta_{20}e^{-\tau_2 z} + \theta_{22}e^{-\alpha z}$$

- 33 -

Putting this in Eqs. (5.54) and (5.55) with $z_1 = 0$, $z_2 = \infty$, we find:

$$a_{+2}(z) = -\frac{jk_2\beta_2 c_{112}\theta_{20}}{(jk_2 - \tau_2)}\left(e^{-\tau_2 z} - e^{-jk_2 z}\right)$$

$$- \frac{jk_2 c_{112}\beta_2\theta_{22}}{(jk_2 - \alpha)}\left(e^{-\alpha z} - e^{-jk_2 z}\right)$$

$$+ a_{+2}(0)\, e^{-jk_2 z} \qquad (5.56)$$

$$a_{-2}(z) = -jk_2 c_{112}\beta_2\left[\frac{\theta_{20}}{\tau_2 + jk_2}e^{-\tau_2 z} + \frac{\theta_{22}}{\alpha + jk_2}e^{-\alpha z}\right] \qquad (5.57)$$

We have set $a_{-2}(\infty) = 0$, since there are no sources of sound in the far field, either on the right or the left. For region I, using $\theta_1(z) = \theta_{11}e^{\tau_1 z}$ (Eq. (5.26)), with $z_1 = -\infty$, $z_2 = 0$, we substitute in Eqs. (5.54) and (5.55) to find:

$$a_{+1}(z) = -\frac{jk_1\beta_1 c_{111}\theta_{11}}{\tau_1 + jk_1}e^{\tau_1 z} \qquad (5.58)$$

and

$$a_{-1}(z) = \frac{jk_1\beta_1 c_{111}\theta_{11}}{jk_1 - \tau_1}\left[e^{jk_1 z} - e^{\tau_1 z}\right] + a_{-1}(0)\, e^{jk_1 z} \qquad (5.59)$$

At the interface at $z = 0$ we require continuity of stress T and particle velocity u. Since $2T = a_+ + a_-$ and $2Z_0 u = a_+ - a_-$,

- 34 -

the boundary conditions can be written as:

$$a_{+1}(0) + a_{-1}(0) = a_{+2}(0) + a_{-2}(0) \tag{5.60}$$

$$\Delta_{21}\left(a_{+1}(0) - a_{-1}(0)\right) = a_{+2}(0) - a_{-1}(0) \tag{5.61}$$

where we have defined $\Delta_{21} = Z_{02}/Z_{01}$. Substituting the values for the various a's from Eqs. (5.56), (5.57), (5.58), and (5.59), into Eqs. (5.60) and (5.61), we can solve these equations for the remaining previous unknowns, $a_{+2}(0)$ and $a_{-1}(0)$. The results are:

$$
\begin{aligned}
a_{+2}(0) = {} & \frac{2Z_{02}}{Z_{01}+Z_{02}} \left[\frac{-jk_1\beta_1 c_{111}\theta_{11}}{\tau_1 + jk_1} \right] \\
& - \left(\frac{Z_{01}-Z_{02}}{Z_{01}+Z_{02}}\right) jk_2 c_{112}\beta_2 \left[\frac{\theta_{22}}{\alpha + jk_2} + \frac{\theta_{20}}{\tau_2 + jk_2} \right]
\end{aligned}
\tag{5.62}
$$

$$
\begin{aligned}
a_{-1}(0) = {} & -\frac{2Z_{01}}{Z_{01}+Z_{02}} \left[jk_2 c_{112}\beta_2 \left(\frac{\theta_{22}}{\alpha + jk_2} + \frac{\theta_{20}}{\tau_2 + jk_2} \right) \right] \\
& + \left(\frac{Z_{01}-Z_{02}}{Z_{01}+Z_{02}}\right) \left[\frac{jk_1\beta_1 c_{111}\theta_{11}}{\tau_1 + jk_1} \right]
\end{aligned}
\tag{5.63}
$$

Finally, in the far-field region where the sound will be observed, Eqs. (5.56) and (5.57) simplify somewhat because in the far field all terms containing exponentials with real parts go to 0, leaving only terms containing $e^{\pm jkz}$. Then in this limit we will have:

$$a_{+2}(z) \cong \left\{ jk_2 c_{112}\beta_2 \left[\frac{\theta_{22}}{jk_2 - \alpha} + \frac{\theta_{20}}{jk_2 - \tau_2} \right] + a_{+2}(0) \right\} e^{-jk_2 z} \quad (5.64)$$

$$a_{-1}(z) \cong \left\{ \frac{jk_1 c_{111}\beta_1 \theta_{11}}{jk_1 - \tau_1} + a_{-1}(0) \right\} e^{jk_1 z} \quad (5.65)$$

If we substitute in for $a_{+1}(0)$, $a_{-1}(0)$, and get θ_{ij}, we get, after some rearrangement,

$$a_{+2}(z) = \left\{ - \frac{2jk_1\beta_1 c_{111}\Delta_{21}\left(\frac{\alpha}{\tau_2} - 1\right)\delta_{21}}{\tau_1(1+\Delta_{21})(1+\delta_{21})\left(1 + j\frac{k_1}{\tau_1}\right)} - \frac{jk_2 c_{112}\beta_2}{\tau_2} \right.$$

$$\times \left\{ \left[\frac{1}{1 - j\frac{k_2}{\tau_2}} + \left(\frac{1 - \Delta_{21}}{1 + \Delta_{21}}\right)\left(\frac{1}{1 + j\frac{k_2}{\tau_2}}\right) \right] \left(\frac{1 + \delta_{21}\frac{\alpha}{\tau_2}}{1 + \delta_{21}} \right) \right.$$

$$\left. \left. - \left(\frac{\tau_2}{\alpha}\right)\left[\frac{1}{1 - j\frac{k_2}{\alpha}} + \left(\frac{1 - \Delta_{21}}{1 + \Delta_{21}}\right)\left(\frac{1}{1 + j\frac{k_2}{\alpha}}\right) \right] \right\} \right\} \theta_{02} e^{-jk_2 z}$$

$$(5.66)$$

$$a_{-1}(z) = \left\{ \frac{jk_1 c_{111}\beta_1 \delta_{21}\left(\frac{\alpha}{\tau_2} - 1\right)}{\tau_1(1 + \delta_{21})} \left[\left(\frac{1 - \Delta_{21}}{1 + \Delta_{21}}\right)\left(\frac{1}{1 + j\frac{k_1}{\tau_1}}\right) - \frac{1}{1 - j\frac{k_1}{\tau_1}} \right] \right.$$

$$\left. - \frac{2jk_2 c_{112}\beta_2}{\tau_2(1 + \Delta_{21})} \left[\frac{\left(1 + \delta_{21}\frac{\alpha}{\tau_2}\right)}{(1 + \delta_{21})\left(1 + j\frac{k_2}{\tau_2}\right)} - \frac{\tau_2/\alpha}{1 + j\frac{k_2}{\alpha}} \right] \right\} \theta_{02} e^{jk_1 z}$$

$$(5.67)$$

- 36 -

These expressions are the complete solutions for the far-field acoustic modes, and are rather complicated as they stand. We would like to consider them in limiting cases of interest. First, suppose we have strong optical absorbtion ($\alpha \gg \tau_2$; $\alpha \gg k_2$) and moderate diffusion ($\tau_i \gg k_i$; $i=1,2$). We will keep terms of the form $\Delta_{21}(k_2/\tau_2)$, because Δ_{21} may be large. Then substitution of these limits and substantial rearrangement gives:

$$a_{-1}(z)e^{-jk_1 z} = -\frac{2I_0\delta_{21}}{(1+\Delta_{21})(1+\delta_{21})}\left[\frac{V_{s2}\beta_2}{C_2}\right]$$

$$\times \left[1 + \left(1 + j\frac{k_1}{\tau_1\Delta_{21}}\right)\left(\frac{\beta_1}{\beta_2}\right)\left(\frac{\kappa_1}{\kappa_2}\right)^{1/2}\right] \qquad (5.68)$$

$$a_{+2}(z)e^{jk_2 z} = -\frac{2I_0\delta_{21}}{(1+\Delta_{21})(1+\delta_{21})}\left[\frac{V_{s2}\beta_2}{C_2}\right]$$

$$\times \left[1 + j\Delta_{21}\frac{k_2}{\tau_2} + \left(\frac{\beta_1}{\beta_2}\right)\left(\frac{\kappa_1}{\kappa_2}\right)^{1/2}\right] \qquad (5.69)$$

where κ_i = thermal diffusivity = $(K_i/\rho_i c_i)$.

We can simplify even further by assuming that medium 1 has properties identical to medium 2 (except that 1 is transparent while 2 absorbs light). Then we find that:

$$a_{+2}(z)e^{jk_2 z} = a_{-1}(z)e^{-jk_1 z} = -\frac{I_0}{2}\left[\frac{V_s\beta}{C}\right]\left[2 + j(k/\tau)\right] . \qquad (5.70)$$

In the low-frequency limit as $k/\tau \to 0$,

$$a_{+2}(z)e^{jk_2 z} = a_{-1}(z)e^{-jk_1 z} = -\left[\frac{V_s \beta}{C}\right] I_0 \qquad (5.71)$$

This reduces the photoacoustic conversion problem to its simplest form. There are no reflections of acoustic or thermal waves.

We see that the simple expression $[V_s \beta/C]$ gives the conversion of light intensity to acoustic stress wave amplitude directly. In terms of acoustic intensity, we have in this limiting ideal case:

$$I_{ac} = \frac{1}{8}\left[\frac{V_s}{\rho}\right]\left[\frac{\beta}{C}\right]^2 I_0^2 = \eta I_0^2 \qquad (5.72)$$

The proportionality constant η between I_{ac} and I_0^2 is seen as an intrinsic conversion factor characterizing a material. It is the efficiency of conversion of light to sound in the absence of effects due to mismatch in the properties of materials.

In Table 5.2 we list the thermal and acoustic properties of selected materials. The intrinsic conversion factor η for these materials is listed in the table. We note that the only gas in the table, STP air, is by far the most efficient converter, owing to its high expansion coefficient and low density. The liquids in the table are more efficient than the solids, again owing to larger expansion coefficients. The conducting solids listed are more efficient than the semiconductors and insulators, although one could find metallic substances such as Invar, which would have conversion efficiency zero owing to a vanishing expansion coefficient.

- 38 -

TABLE 5.2. Thermal and Acoustic Properties of Selected Materials (20 C unless noted)

Material	Thermal Conductivity K (W/m/K)	Density ρ (kg/m³)	Heat Capacity C (J/kgK)	Stiffness $c_{11} = \rho v_s^2$ (N/m²)	Adjusted Linear Coefficient of Thermal Expansion $\beta = \frac{B\beta'}{c_{11}}$ (K⁻¹)	Diffusivity $\kappa = K/\rho C$ (m²/sec)	Longitudinal Sound Velocity v_s (m/sec)	Intrinsic Conversion Factor $\eta = \frac{1}{8}\left[\frac{v_s}{\rho}\right]\left[\frac{\beta}{c}\right]^2$ (m²/W)
STP air	.241	1.225	741	.142 E6	.34 E-2	.265 E-3	340	.550 E-8
Acetone	.198	790	2176	.106 E10	.50 E-3	.115 E-6	1158	.967 E-14
Methanol	.155	791	2547	.936 E9	.40 E-3	.769 E-7	1088	.424 E-15
Water	.650	1000	4185	.237 E10	.69 E-4	.155 E-6	1540	.522 E-16
Nitrogen (75 K)	.138	824	1948	.638 E9	.17 E-3	.859 E-7	880	.102 E-14
Pyrex	1.26	2290	975	.730 E11	.27 E-6	.564 E-6	5646	.236 E-19
Sapphire	33	3986	433	.494 E12	.30 E-5	.191 E-4	11130	.168 E-16
Carbon (average)	80	2000	711	.320 E11	.52 E-5	.562 E-4	4000	.133 E-16
Silicon	84	2340	728	.166 E12	.45 E-5	.490 E-4	8415	.171 E-16
Aluminum	300	2699	917	.109 E12	.18 E-4	.121 E-3	6356	.113 E-15
Molybdenum	179	10220	138	.470 E12	.29 E-5	.127 E-3	6780	.170 E-16
Gold	345	19200	130	.189 E12	.13 E-4	.138 E-3	3140	.210 E-15

Refs. for Table 5.2: 12, 23, 24, 25, 16, 17, 18, 19

Returning now to the case of two different media in the limiting case of $k_1 \ll \tau_1$, $k_2 \ll \alpha$, $\tau_2 \ll \alpha$, as expressed in Eqs. (5.68), (5.69) we note that the positive and negative traveling modes a_{-1} and a_{+2} are equal and independent of frequency (provided the frequency is sufficiently small enough that $(k_1/\tau_1\Delta_{21}) \ll 1$ and $\Delta_{21}(k_2/\tau_2) \ll 1$). The acoustic intensities carried away to the far fields by these modes are unequal, however, since

$$I_{ac} = \frac{|a_\pm|^2}{8Z_0} \; .$$

The acoustic intensity will be inversely proportional to the acoustic impedance. We are postulating conditions here corresponding to a thin plane transducer at the boundary between two half-spaces. The ratio of the acoustic intensities radiated into the two regions in this case is just what we have found.

At frequencies where $\Delta_{21}(k_2/\tau_2)$ or $(k_1/\Delta_{21}\tau_1)$ cannot be neglected compared to 1, the acoustic mode amplitudes in Eqs. (5.68) and (5.69) become frequency-dependent. Assume for example, that $\Delta_{21}(k_2/\tau_2) \sim 1$, but $(k_1/\Delta_{21}\tau_1) \ll 1$. This obviously may happen if $\Delta_{21} \gg 1$. As an example, if medium 2 = gold, medium 1 = water, and $\Delta_{21} = 39.1$, then Eqs. (5.68) and (5.69) become:

$$a_{-1}(z)e^{-jk_1 z} = -\frac{2I_0\delta_{21}}{(1+\Delta_{21})(1+\delta_{21})}\left[\frac{V_{s2}\beta_2}{C_2}\right]\left[1 + \left(\frac{\beta_1}{\beta_2}\right)\left(\frac{\kappa_1}{\kappa_2}\right)^{1/2}\right] \quad (5.73)$$

$$a_{+2}(z)e^{jk_2 z} = -\frac{2I_0 \delta_{21}}{(1+\Delta_{21})(1+\delta_{21})} \left[\frac{V_{s2}\beta_2}{C_2}\right]$$

$$\times \left[1 + \left(\frac{\beta_1}{\beta_2}\right)\left(\frac{\kappa_1}{\kappa_2}\right)^{1/2} + \left(\frac{1+j}{\sqrt{2}}\right)\left(\Delta_{21}\frac{\kappa_2^{1/2}}{V_{s2}}\right)\omega^{1/2}\right] \quad (5.74)$$

In this case the negative-traveling mode is seen to remain flat as a function of frequency, whereas the positive-traveling mode has the form $A + (1+j)B\omega^{1/2}$ where A and B are real expressions. The acoustic intensity then has the form $I_{ac} \propto A^2 + 2AB\omega^{1/2} + 2B^2\omega$.

In Fig. 9 are plotted the intensities, I_1 , and I_2 of acoustics generated in media 1 and 2 for the combinations methanol-aluminum $(\Delta_{21} = 21)$; water-aluminum $(\Delta_{21} = 11)$; pyrex-aluminum $(\Delta_{21} = 1.33)$; sapphire-aluminum $(\Delta_{21} = .39)$. Aluminum is medium 2 in each case. The full expressions [Eqs. (5.66) and (5.67)] with no approximation are used. A listing of the program used is given in Appendix C. The ordinates are acoustic far-field intensity in watt/m^2 for optical absorption of 1 watt/m^2. The main features of these graphs are in accord with our previous discussion. I_1 is, in each case, nearly frequency-independent as we expect. I_2 is flat at low frequencies, and is approaching a value of:

$$I_{20} = \left\{\left[\frac{2\delta_{21}}{(1+\Delta_{21})(1+\delta_{21})}\right]\left[1 + \left(\frac{\beta_1}{\beta_2}\right)\left(\frac{\kappa_1}{\kappa_2}\right)^{1/2}\right]\right\}^2 \cdot \frac{1}{8}\left[\frac{V_{s2}}{\rho_2}\right]\left[\frac{\beta_2}{C_2}\right]^2 \quad (5.75)$$

at the left edge of the graph in Fig. 9. The limiting value of I_1 at the lower frequencies, I_{10} , is related by the ratio of acoustic
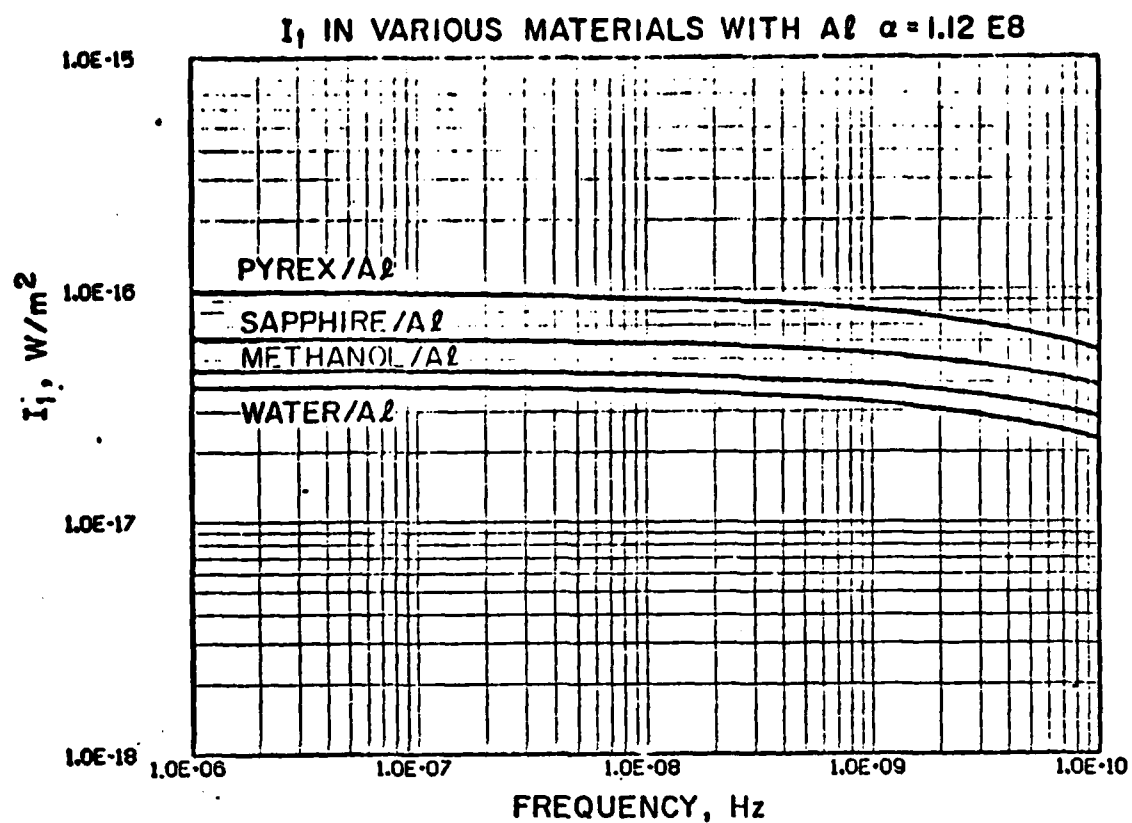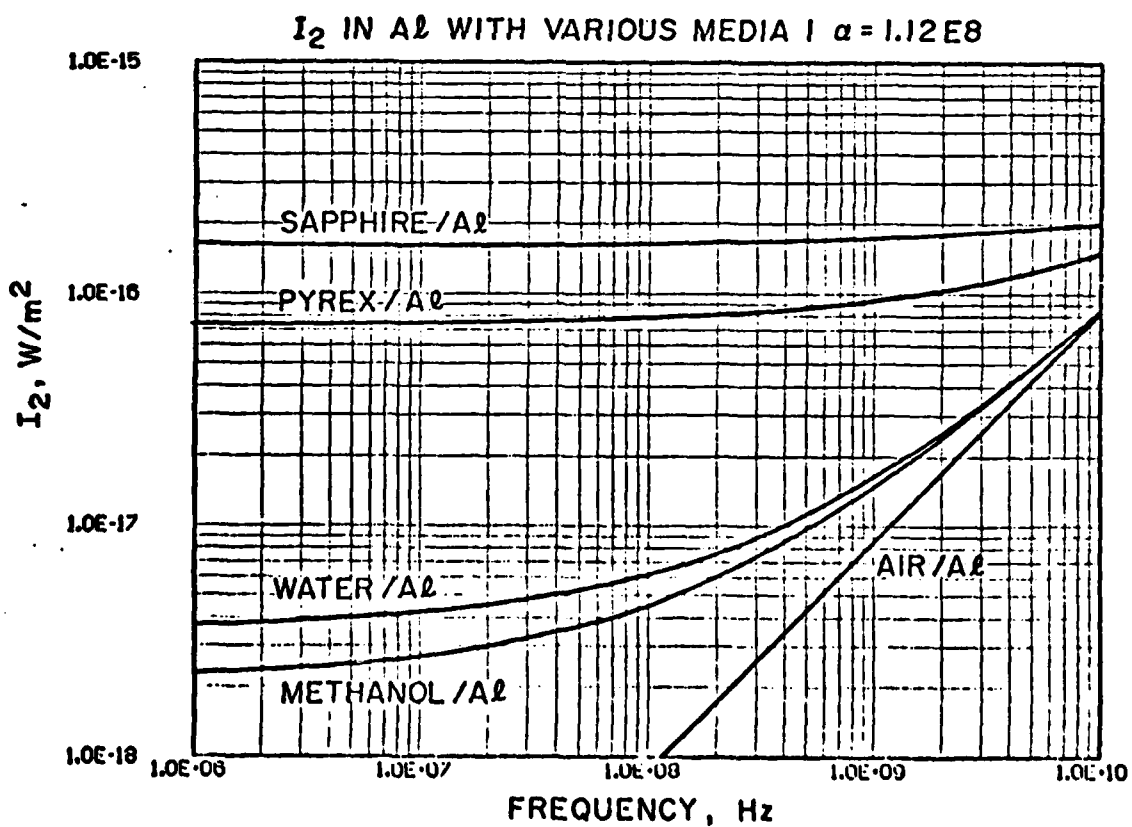
FIGURE 9

impedances:

$$I_{10} = I_{20}\left(\frac{Z_{02}}{Z_{01}}\right) \tag{5.76}$$

At higher frequencies I_2 becomes an increasing function of frequency as $\Delta_{21}(k_2/\tau_2)$ is no longer negligible. For example, at 100 MHz, $|\Delta_{21}(k_2/\tau_2)| = 0.91$ for the combination (1 = methanol, 2 = aluminum). In the range 100 MHz − 1 GHz the average increase of I_1 with ω is $\propto \omega^{.55}$, in line with an initial dependence as $\omega^{1/2}$, approaching proportionality to ω at higher frequencies.

Thus far we have assumed $\alpha \gg \tau_2$, and thus have been dealing with strong optical absorptions. Since α is independent of modulation frequency and $\tau \propto \omega^{1/2}$, at some frequency this assumption fails to be valid and we have rather different behavior than we have seen thus far.

If we still assume $k_1 \ll \tau_1$, $k_2 \ll \tau_2$, and $k_2 \ll \alpha$, but we now assume $\tau_2 \gg \alpha$, and keep terms involving $\Delta_{21}(k_2/\alpha)$, then we find Eq. (5.66) and (5.67) become:

$$a_{+2}(z)e^{jk_2 z} \cong -\left(\frac{2}{1 + \Delta_{21}}\right)\left[\frac{V_{s2}\beta_2}{c_2}\right]I_0\left(1 + j\Delta_{21}\frac{k_2}{\alpha}\right) \tag{5.77}$$

$$a_{-1}(z)e^{-jk_1 z} \cong -\frac{2\alpha I_0}{(1 + \Delta_{21})}\left[\frac{V_{s2}\beta_2}{c_2}\right]$$

$$\times \left[\frac{1}{\tau_2}\left(\frac{\beta_1}{\beta_2}\right)\left(\frac{\kappa_1}{\kappa_2}\right)^{1/2}\left(\frac{\delta_{21}}{1 + \delta_{21}}\right) + \frac{1}{\alpha}\right] \tag{5.78}$$

Let us dispose of Eq. (5.78) for a_{-1} by noting that since $\tau_2 \propto (1+j)\omega^{1/2}$, a_{-1} has the form: $a_{-1}(z)e^{-jk_1z} \cong A(1+j)\omega^{-1/2} + B$ where A and B are real constants. Thus in this limit

$$I_1 \propto 2A^2\omega^{-1} + 2AB\omega^{-1/2} + B^2 \ .$$

The equation (5.77) for a_{+2} in this limit is quite interesting in that it gives an acoustic intensity proportional to ω^2 for $\Delta_{21} \gg 1$. Cases in point are the combinations (medium 1 = 10^{-5} atm air; medium 2 = silicon; $\Delta_{21} = 6 \times 10^9$) and (medium 1 = water; medium 2 = silicon; $\Delta_{21} = 13$). The high values for Δ_{21} mean that both first media look more or less like free surfaces to higher-impedance silicon. For silicon with incident optical radiation of wavelength 8000 Å, $\alpha = 3.29 \times 10^6 m^{-1}$. In this case $|\tau_2/\sqrt{2}/\alpha| = 1$ at frequency 169 MHz. For comparison, this value of α is a factor of 34 smaller than that for Al used in Fig. 9. For Al, $|\tau_2/\sqrt{2}/\alpha| = 1$ at 483 GHz! Hence no trace of this effect will be found in Fig. 9. Equation (5.66) is plotted as a function of frequency for several first media with silicon as medium 2 in Fig. 10.

In Fig. 10 we see that for a range of frequencies for the combination water/silicon from about 200 MHz to about 2 GHz, I_2 in silicon is a rapidly increasing function of frequency, the variation approaching $I_2 \propto \omega^2$. In this range of frequencies the relation (5.77) is a good approximation to the exact equation (5.66), which is plotted. For example, for water/silicon at 1 GHz, Eq. (5.77) predicts $I_2 = 8.7 \times 10^{-18}$ W/m^2; the exact value from the graph is 9.1×10^{-18} W/m^2.

The approximation in Eq. (5.77) breaks down at the highest frequencies in Fig. 10 because k_2/α is no longer small and the curves reach a maximum at ~ 4 GHz.

We see that for the approximately free-surface case, in cases where $|\tau_2| > \alpha$, there is strong reason to prefer high-frequency modulation. An immediate case in point is electron-beam/acoustic microscopy, where medium 1 would be vacuum, medium 2 a solid, and α would now correspond to the electron-beam attenuation coefficient. The acoustic signal is detected with a piezoelectric transducer in contact with medium 2. A graph for vacuum/Si I_2 would have the same $I_2 \propto \omega^2$ characteristic for values of α such that $|\tau_2/\sqrt{2}\alpha| > 1$. The graph shown for air/silicon shows a signal increasing by two orders of magnitude between 100 MHz and 1 GHz for $\alpha = 3.29 \times 10^6 m^{-1}$. A corresponding increase will be observed at lower frequencies for smaller α .

To exhibit the dependence of acoustic intensity on absorption coefficient, Fig. 11 plots Eq. (5.66) for I_2 in silicon for the combinations 10^{-5} atm air/Si, water/si, pyrex/Si, and sapphire/Si, as a function of absorption coefficient α . A modulation frequency of 100 MHz is assumed. For high values of α at the right side of the graph, we find I_2 is independent of α , as is predicted by Eq. (5.69). In this regime we get a huge variation in generated acoustic intensity depending on the acoustic impedance mismatch (and thermal mismatch) across the boundary. Thus the I_2 signal level in silicon is 30 dB higher with sapphire as medium 1 than with 10^{-5} atm air (approximating vacuum) as medium 1. This large dependence of acoustic signal on loading conditions of the surface has earlier been noted by White and von Gutfeld.

Physically we may understand this in terms of the reflection of waves at the boundary between medium 1 and medium 2. If the boundary

- 45 -

I$_2$ IN Si WITH VARIOUS MEDIA $\alpha = 3.29\ E6$

SAPPHIRE/Si

PYREX/Si

WATER/Si

IE-5 ATM AIR/Si

FREQUENCY, Hz

FIGURE 10

I$_2$ IN Si WITH VARIOUS FIRST MEDIA 100 MHz

SAPPHIRE/Si

PYREX/Si

WATER/Si

IE-5 ATM AIR/Si

ALPHA, m^{-1}
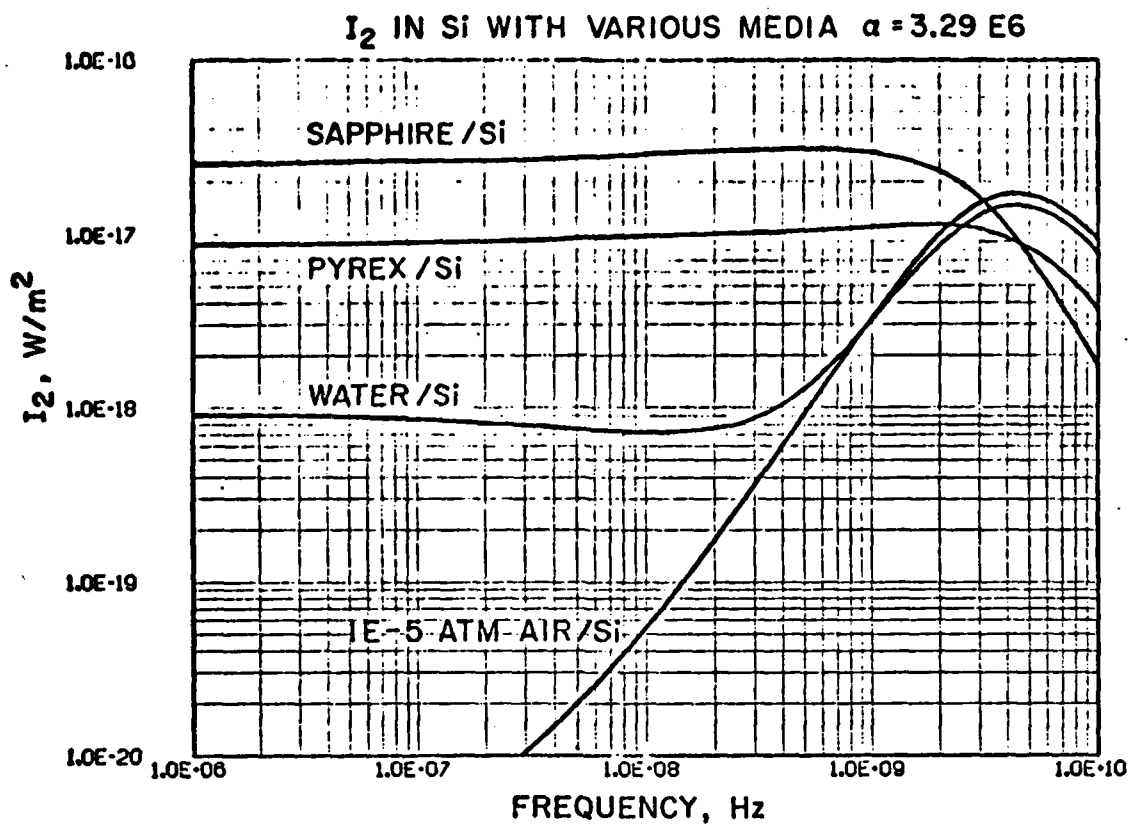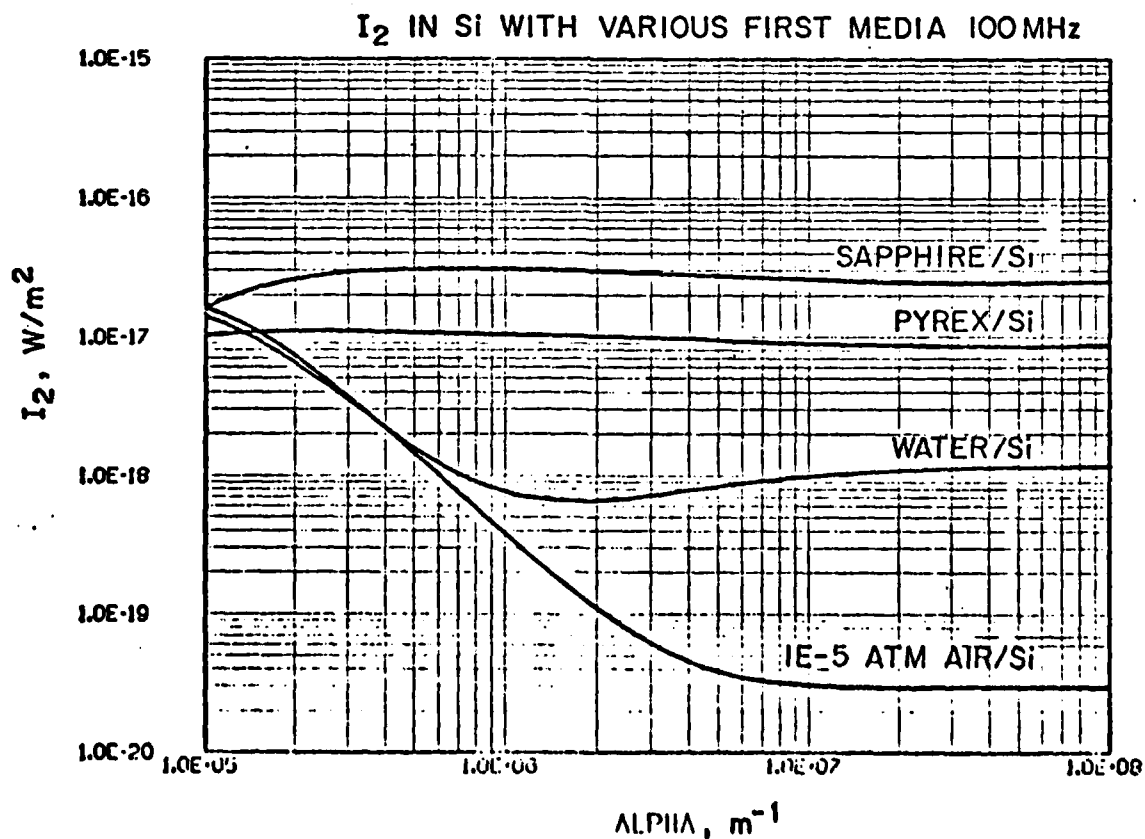
FIGURE 11

is a free surface, the negative traveling acoustic wave is completely reflected at the free surface boundary with a 180° phase change. When $\alpha \gg k_2$ and $|\tau_2| \gg k_2$, the positive traveling acoustic wave and reflected negative traveling wave are out of phase and cancel, leading to small acoustic intensity in the far field. If medium 1 and medium 2 have equal acoustic impedances, there is no reflection at the boundary, and far-field acoustic intensity comes only from the positive-traveling wave. If medium 1 has infinite acoustic impedance the negative traveling acoustic wave in medium 2 is reflected at the boundary with no phase change. If again $\alpha \gg k_2$ and $|\tau_2| \gg k_2$, the positive traveling acoustic wave and reflected wave are in phase, leading to a large far-field acoustic intensity in medium 2.

As we move toward smaller values of α in the left side of Fig. 11, the graphs converge to near equality, as is predicted by Eq. (5.77). The water/Si and 10^{-5} atm air/Si curves in particular are falling off as α^{-2} in the range of α between $10^5 m^{-1}$ and $10^6 m^{-1}$. For these materials, in the regime where $\Delta_{21}(k_2/\alpha) \gg 1$, Eq. (5.77) simplifies to

$$a_{+2}(z)e^{jk_2 z} \cong -2j \left[\frac{\beta}{\alpha c_2}\right] \omega I_o \qquad (5.79)$$

or

$$I_2 \cong \frac{1}{2\rho_2 V_{s2}} \left[\frac{\beta}{\alpha c_2}\right]^2 \omega^2 I_o^2 \qquad (5.80)$$

which corresponds to the $1/\alpha^2$ dependence seen in Fig. 10 for water/Si and 10^{-5} atm air/Si.

The two-medium case may be compared with White, whose classic paper[7] considers absorbtion in an infinitely thin boundary layer of a semi-infinite medium, and their diffusion and expansion due to heating. He considers two cases relevant to our results: a perfectly constrained surface, and a free surface. For the free surface, White predicts, in the limit $|\tau_2| \gg k_2$, in our notation, that far-field stress

$$|T_2| = \frac{\beta_2 \kappa_2^{1/2} \omega^{1/2}}{c_2} \qquad (5.81)$$

where this is a rearrangement of White's Eq. (5.10). For the case vacuum/gold, Eq. (5.81) predicts, for $f = 100$ MHz , the far-field stress in Gold $T_2 = [3.2 \times 10^{-5} \ (N/m^2)]$. Using Eq. (5.66) for the case STP air/gold one obtains $T_2 = 2.6 \times 10^{-5} \ (N/m^2)$, a discrepancy of 20% in stress, 44% in power.

White's other relevant case, the perfectly constrained surface, predicts the stress in medium 2 for the case $|\tau_2| \gg k_2$

$$|T_2| = \frac{\beta_2 V_{s2}}{c_2} I_0 \qquad (5.82)$$

where we have rearranged White's Eq. (5.10) to fit our notation. Recall that Eq. (5.71) for far-field stress in the matched boundary case becomes

$$|T_2| = \frac{1}{2} \frac{\beta_2 V_{s2}}{c_2} I_0 \qquad (5.83)$$

- 48 -

when we convert mode amplitude a_{+2} to stress. The doubling as we go from the matched case (5.83) to the perfectly constrained case (5.82) ·may be attributed to the reflection of the negative-propagating acoustics generated in medium 2 at the $Z_{01} = \infty$ boundary.

For example, in the case sapphire/aluminum at 100 MHz, Eq. (5.66) leads to stress $T_2 = 1.24 \times 10^{-4}$ N/m^2 whereas Eq. (5.82) gives $T_2 = 1.73 \times 10^{-4}$ N/m^2 . There is about 3 dB difference between the two values, somewhat more than in the free-surface predictions just considered. Considering the range of acoustic and thermal properties available in real materials, Eq. (5.82) seems somewhat less useful for the case of solid-solid interfaces than Eq. (5.81) is for gas-solid or liquid-solid interfaces.

5. Three-Layer Model: Heat Flow

We now consider the 3-layer geometry of Fig. 8 in which light enters through transparent semi-infinite medium 1 on the left and is absorbed in medium 2, with optical intensity $I(z) = I_o e^{-\alpha z}$ in medium 2. Medium 2 is an infinite slab of thickness ℓ which contacts medium 1 at $z = 0$ and semi-infinite medium 3 at $z = \ell$. Medium 3 is assumed to be transparent. Our procedure is to first solve for the temperature ⌣ .bution in space, and then use this as the distributed source for positive and negative traveling acoustic modes. We shall be concerned finally with the far-field modes in media 1 and 3, and their associated acoustic power. Parker[20] studied the case where medium 1 was glass, medium 2 a negligible-thickness absorbing layer, and 3 the gas in a photoacoustic cell. Rosencwaig and Gersho[21] solved for the pressure in a

- 49 -

gaseous medium 1 when medium 2 was an absorbing solid and medium 3, a backing material. von Gutfeld and Budd[22] considered a 3-layer case where medium 2 absorbed all optical power in an infinitesimally thin surface layer. They found the acoustic signal in liquid medium 3 to be strongly dependent on layer thickness and choice of liquid.

Our analysis to follow is applicable to any choice of media 1, 2, 3 and we arrive at exact analytic expressions for far-field acoustic amplitudes with no initial assumptions on the relative sizes of optical and thermal skin depths or acoustic k-vector.

We proceed as in the single-interface case. In medium 2, proceeding as in Eqs. (5.16) and (5.17), but noting that integration in the latter is now from z to ℓ , we arrive at the 3-layer analogs of Eqs. (5.19) and (5.20):

$$a_{+2}^t(z) = \frac{\alpha I_0}{(\alpha - \tau_2)} \left[e^{-\tau_2 z} - e^{-\alpha z} \right] + a_{+2}^t(0) e^{-\tau_2 z} \tag{5.84}$$

$$a_{-2}^t(z) = \frac{\alpha I_0 e^{\tau_2 z}}{(\alpha + \tau_2)} \left[e^{-(\alpha+\tau_2)\ell} - e^{-(\alpha+\tau_2)z} \right] + a_{-2}^t(\ell) e^{-\tau_2(\ell-z)} \tag{5.85}$$

Since the heat source exists only in medium 2, in media 1 and 3 we will have:

$$a_{-1}^t(z) = a_{-1}^t(0) e^{\tau_1 z} \tag{5.86}$$

$$a_{+3}^t(z) = a_{+3}^t(\ell) e^{-\tau_3(z-\ell)} \tag{5.87}$$

and $a_{+1}^t(z) = a_{-3}^t(z) = 0$. The boundary conditions are that heat flux f and temperature θ are continuous at $z = 0$ and at $z = \ell$. Application of these permits us to evaluate the unknowns $a_{-1}^t(0)$, $a_{+2}^t(0)$, $a_{-2}^t(\ell)$ and $a_{+3}^t(\ell)$. Then in region i we recall that temperature $\theta_i(z) = (a_{+i}^t(z) - a_{-i}^t(z))/2Z_i^t$. Solving for $\theta_i(z)$ in region 1, we have:

$$\theta_1(z) = \theta_{11} e^{\tau_1 z} \tag{5.88}$$

In region 3:

$$\theta_3(z) = \theta_{30} e^{-\tau_3(z-\ell)} \tag{5.89}$$

In region 2:

$$\theta_2(z) = \theta_{20} e^{-\tau_2 z} + \theta_{21} e^{+\tau_2 z} + \theta_{22} e^{-\alpha z} \tag{5.90}$$

where solution of the boundary condition equations yields:

$$\theta_{11} = -\frac{\delta_{21}\theta_{02}}{D_t} \left[-(1-\delta_{23})\left(\frac{\alpha}{\tau_2} + 1\right)e^{-\tau_2\ell} + (1+\delta_{23})\left(\frac{\alpha}{\tau_2} - 1\right)e^{\tau_2\ell} \right.$$
$$\left. + 2\left(1 - \delta_{23}\frac{\alpha}{\tau_2}\right)e^{-\alpha\ell} \right] \tag{5.91}$$

$$\theta_{30} = \frac{\delta_{23}\theta_{02}}{D_t} \left[(1-\delta_{21})\left(1 - \frac{\alpha}{\tau_2}\right)e^{-(\alpha+\tau_2)\ell} + (1+\delta_{21})\left(1 + \frac{\alpha}{\tau_2}\right)e^{-(\alpha-\tau_2)\ell} \right.$$
$$\left. - 2\left(1 + \delta_{21}\frac{\alpha}{\tau_2}\right) \right] \tag{5.92}$$

$$\theta_{20} = -\frac{\theta_{02}}{D_t}\left[(1 + \delta_{23})\left(1 + \delta_{21}\frac{\alpha}{\tau_2}\right)e^{\tau_2\ell} - (1 - \delta_{23})\left(1 - \delta_{23}\frac{\alpha}{\tau_2}\right)e^{-\alpha\ell}\right]$$

$$(5.93)$$

$$\theta_{21} = \frac{\theta_{02}}{D_t}\left[(1 - \delta_{23})\left(1 + \delta_{21}\frac{\alpha}{\tau_2}\right)e^{-\tau_2\ell} - (1 + \delta_{21})\left(1 - \delta_{23}\frac{\alpha}{\tau_2}\right)e^{-\alpha\ell}\right]$$

$$(5.94)$$

$$\theta_{22} = -\theta_{02} \qquad (5.95)$$

where

$$\delta_{ij} = z_i^t/z_j^t = \sqrt{\frac{\rho_i C_i K_i}{\rho_j C_j K_j}} \quad ; \qquad (5.96)$$

θ_{02} is given by Eq. (5.31), and

$$D_t = (1 - \delta_{21})(1 - \delta_{23})e^{-\tau_2\ell} - (1 + \delta_{21})(1 + \delta_{23})e^{\tau_2\ell} \qquad (5.97)$$

These solutions for the temperature distribution in the 3-medium geometry agree with the harmonic part of the solution given by Rosencwaig and Gersho[21] for a similar 3-medium geometry.

6. Three-Layer Model: Acoustic Generation

With the temperature distribution in the 3 regions known, we can solve for the acoustic modes. Since there are sources [non-vanishing $\theta_i(z)$] in all 3 regions, we will have positive and negative traveling

modes in each region. For region 1,

$$a_{+1}(z) = -jk_1c_{111}\beta_1 e^{-jk_1z} \int_{-\infty}^{z} \theta_1(\zeta)e^{jk_3\zeta} \, d\zeta + a_{+1}(-\infty)e^{jk_1z} \qquad (5.98)$$

where the third subscript on c_{111} designates the region. Since $a_{+1}(-\infty) = 0$ (no acoustic sources at $-\infty$) with Eq. (5.88) we are led to:

$$a_{+1}(z) = -\frac{jk_1c_{111}\beta_1\theta_{11}}{\tau_1 + jk_1} e^{\tau_1z} = E_1 e^{\tau_1z} \qquad (5.99)$$

Similarly, for the negative traveling mode

$$a_{-1}(z) = -jk_1c_{111}\beta_1 e^{jk_1z} \int_{z}^{0} \theta_1(\zeta)e^{-jk_1\zeta} \, d\zeta + a_{-1}(0)e^{jk_1z} \qquad (5.100)$$

which yields

$$a_{-1}(z) = \frac{jk_1c_{111}\beta_1\theta_{11}}{(jk_1 - \tau_1)} e^{jk_1z} \left[1 - e^{-(jk_1-\tau_1)z}\right] + a_{-1}(0)e^{jk_1z} \qquad (5.101)$$

In region 3 we have:

$$a_{-3}(z) = -jk_3c_{113}\beta_3 e^{jk_3z} \int_{z}^{\infty} \theta_3(\zeta)e^{-jk\zeta} \, d\zeta + a_{-3}(+\infty)e^{jk_3z} \qquad (5.102)$$

No acoustic sources at $z = +\infty$ means $a_{-3}(+\infty) = 0$, and then substitution of Eq. (5.89) results in:

$$a_{-3}(z) = \frac{-jk_3c_{113}\beta_3\theta_{30}}{(jk_3 + \tau_3)} e^{-\tau_3(z-\ell)} = E_3 e^{-\tau_3(z-\ell)} \qquad (5.103)$$

- 53 -

For the positive-traveling mode in region 3 we will have:

$$a_{+3}(z) = -jk_3 c_{113} \beta_3 \, e^{-jk_3 z} \int_{\ell}^{z} \theta_3(\zeta) e^{jk_3 \zeta} \, d\zeta + a_{+3}(\ell) e^{-jk_3(z-\ell)}$$

(5.104)

We substitute Eq. (5.89) for θ_3 and get:

$$a_{+3}(z) = \frac{-jk_3 c_{113} \beta_3 \theta_{30}}{(jk_3 - \tau_3)} \left[e^{-\tau_3(z-\ell)} - e^{-jk_3(z-\ell)} \right] + a_{+3}(\ell) e^{-jk_3(z-\ell)}$$

(5.105)

In region 2 we will have:

$$a_{+2}(z) = -jk_2 c_{112} \beta_2 e^{-jk_2 z} \int_{0}^{z} \theta_2(\zeta) e^{jk_2 \zeta} \, d\zeta + a_{+2}(0) e^{-jk_2 z}$$

(5.106)

Substitution of Eq. (5.90) in this expression yields:

$$a_{+2}(z) = -jk_2 c_{112} \beta_2 e^{-jk_2 z} \left[\frac{\theta_{20}}{jk_2 - \tau_2} \left(e^{(jk_2 - \tau_2)z} - 1 \right) + \frac{\theta_{21}}{jk_2 + \tau_2} \right.$$

$$\left. \times \left(e^{(jk_2 + \tau_2)z} - 1 \right) + \frac{\theta_{22}}{jk_2 - \alpha} \left(e^{(jk_2 - \alpha)z} - 1 \right) \right] + a_{+2}(0) e^{-jk_2 z}$$

(5.107)

Let us define E_{22} as the entire first term on the right evaluated at $z = \ell$, that is:

$$a_{+2}(\ell) = E_{22} + a_{+2}(0) \, e^{-jk_2 \ell}$$

(5.108)

Likewise, the negative mode will be:

$$a_{-2}(z) = -jk_2 c_{112} \beta_2 e^{jk_2 z} \int_z^{\ell} \theta_2(\zeta) e^{-jk_2 \zeta} d\zeta + a_{-2}(\ell) e^{jk_2(z-\ell)} \tag{5.109}$$

Substitution of Eq. (5.90) and integration gives us:

$$a_{-2}(z) = +jk_2 c_{112} \beta_2 e^{jk_2 z} \left[\frac{\theta_{20}}{(jk_2 + \tau_2)} \left(e^{-(jk_2 + \tau_2)\ell} - e^{-(jk_2 + \tau_2)z} \right) \right.$$

$$+ \frac{\theta_{21}}{(jk_2 - \tau_2)} \left(e^{-(jk_2 - \tau_2)\ell} - e^{-(jk_2 - \tau_2)z} \right)$$

$$\left. + \frac{\theta_{22}}{(jk_2 + \alpha)} \left(e^{-(jk_2 + \alpha)\ell} - e^{-(jk_2 + \alpha)z} \right) \right]$$

$$+ a_{-2}(\ell) e^{jk_2(z-\ell)} \tag{5.110}$$

We define E_{20} as the entire first term on the right side of this equation at $z = 0$; that is:

$$a_{-2}(0) = E_{20} + a_{-2}(\ell) e^{-jk_2 \ell} \tag{5.111}$$

The remaining 4 boundary conditions (the first 2 were vanishing $a_{+1}(-\infty)$ and vanishing $a_{-3}(+\infty)$) are equality of stress $T = (a_+ + a_-)/2$ and particle velocity $u = (a_+ - a_-)/2Z_0$ on both sides of the boundaries at $z = 0$ and $z = \ell$.

T at z = 0 :

$$a_{+1}(0) + a_{-1}(0) = a_{+2}(0) + a_{-2}(0)$$

or $$E_1 + a_{-1}(0) = a_{+2}(0) + E_{20} + a_{-2}e^{-jk_2\ell} \qquad (5.112)$$

u at z = 0 :

$$\frac{Z_{02}}{Z_{01}}\left[a_{+1}(0) - a_{-1}(0)\right] = a_{+2}(0) - a_{-2}(0)$$

or: $$\Delta_{21}\left[-a_{-1}(0) + E_1\right] = a_{+2}(0) - a_{-2}(\ell)e^{-jk_2\ell} - E_{20}$$

$$(5.113)$$

T at z = ℓ :

$$a_{+3}(\ell) + a_{-3}(\ell) = a_{+2}(\ell) + a_{-2}(\ell)$$

or: $$a_{+3}(\ell) + E_3 = a_{+2}(0)e^{-jk_2\ell} + E_{22} + a_{-2}(\ell) \qquad (5.114)$$

V at z = ℓ :

$$\Delta_{23}\left[a_{+3}(\ell) - E_3\right] = a_{+2}(0)e^{-jk_2\ell} + E_{22} - a_{-2}(\ell) \qquad (5.115)$$

Equations (5.112), (5.113), (5.114), and (5.115) are a set of 4 equations in the remaining 4 unknowns: $a_{-1}(0)$, $a_{+2}(0)$, $a_{-2}(\ell)$, and $a_{+3}(\ell)$. We need find only $a_{-1}(0)$ and $a_{+3}(\ell)$ to write down

the far field behavior. Solution yields:

$$a_{-1}(0) = \frac{1}{D}\left[\left(-(1-\Delta_{23})(1+\Delta_{21})e^{-jk_2\ell} + (1+\Delta_{23})(1-\Delta_{21})e^{jk_2\ell}\right)E_1\right.$$

$$\left. - 2(1+\Delta_{23})e^{jk_2\ell}E_{20} - 2(1-\Delta_{23})E_{22} - 4\Delta_{23}E_3\right] \qquad (5.116)$$

$$a_{+3}(\ell) = -\frac{1}{D}\left[4\Delta_{21}E_1 + 2(1-\Delta_{21})E_{20} + 2(1+\Delta_{21})e^{jk_2\ell}E_{22}\right.$$

$$\left. + \left((1-\Delta_{21})(1+\Delta_{23})e^{-jk_2\ell} - (1+\Delta_{21})(1-\Delta_{23})e^{jk_2\ell}\right)E_3\right]$$

$$(5.117)$$

where

$$D = (1-\Delta_{21})(1-\Delta_{23})e^{-jk_2\ell} - (1+\Delta_{21})(1+\Delta_{23})e^{jk_2\ell} \qquad (5.118)$$

Letting z approach $-\infty$ in Eq. (5.101) and letting z approach $+\infty$ in Eq. (5.105) results in the far field modes:

$$a_{-1}(z) = \frac{jk_1 c_{111}\beta_1\theta_{11}}{(jk_1 - \tau_1)}e^{jk_1 z} + a_{-1}(0)e^{jk_1 z} \qquad (5.119)$$

$$a_{+3}(z) = \frac{jk_3 c_{113}\beta_3\theta_{30}}{(jk_3 - \tau_3)}e^{-jk_3(z-\ell)}$$

$$+ a_{+3}(\ell)e^{-jk_3(z-\ell)} \qquad (5.120)$$

If we now substitute (5.116) and (5.117) in these equations, making

use of (5.103) and (5.99), we obtain:

$$a_{-1}(z) = -\frac{2}{D}\left\{\frac{E_1}{(jk_1 - \tau_1)}\left[(1 - \Delta_{23})(jk_1 - \Delta_{21}\tau_1)e^{-jk_2\ell}\right.\right.$$

$$\left.- (1 + \Delta_{23})(jk_1 + \Delta_{21}\tau_1)e^{jk_2\ell}\right]$$

$$\left. + (1 + \Delta_{23})e^{jk_2}E_{20} + (1 - \Delta_{23})E_{22} + 2\Delta_{23}E_3\right\}e^{jk_1 z}$$

$$(5.121)$$

$$a_{+3}(z) = -\frac{2}{D}\left\{\frac{E_3}{(jk_3 - \tau_3)}\left[(1 - \Delta_{21})(jk_3 - \Delta_{23}\tau_3)e^{-jk_2\ell} - (1 + \Delta_{21})\right.\right.$$

$$\left.\times (jk_3 + \Delta_{23}\tau_3)e^{jk_2\ell}\right]$$

$$\left. + (1 - \Delta_{21})E_{20} + (1 + \Delta_{21})e^{jk_2\ell}E_{22} + 2\Delta_{21}E_1\right\}e^{-jk_3(z-\ell)}$$

$$(5.122)$$

These expressions are our final equations for the far-field acoustic modes in regions 1 and 3. Since $a_{+1}(z) = 0$ in the far field of region 1, and $a_{-3}(z) = 0$ in the far field of region 3, these expressions give the far-field stress and particle velocity, and acoustic power:

(far-field stress) $T_1(z) = \dfrac{a_{-1}(z)}{2}$ (5.123)

(far-field particle velocity) $u_1(z) = -\dfrac{a_{-1}(z)}{2Z_{01}}$ (5.124)

- 58 -

(far-field acoustic intensity) $\qquad I_1(z) = -\dfrac{1}{8}\dfrac{a_{-1}(z)a_{-1}^{*}(z)}{Z_{01}}$ $\qquad$ (5.125)

(far-field stress) $\qquad T_3(z) = \dfrac{a_{+3}(z)}{2}$ $\qquad$ (5.126)

(far-field particle velocity) $\qquad u_3(z) = \dfrac{a_{+3}(z)}{2Z_{03}}$ $\qquad$ (5.127)

(far-field acoustic intensity) $\qquad I_3(z) = \dfrac{1}{8}\dfrac{a_{+3}(z)a_{+3}^{*}(z)}{Z_{03}}$ $\qquad$ (5.128)

We now consider the examples listed in Table 5.3. A Fortran program to calculate far-field acoustic intensities I_1 and I_3 from Eqs. (5.125) and (5.128), using Eqs. (5.121) and (5.122) was implemented. This program's listing is included as Appendix D.

First we consider the effects of the third medium, which is the new element. The effects of adding the third medium on both I_1 and I_3 can be profound. If medium 3 is an efficient thermal-acoustic generator, such as acetone, large signal enhancements are possible, for very thin films, as von Gutfeld and Budd have observed. Also, the 2-3 boundary means we can get both a reflected wave in medium 2, and thickness resonance effects.

In Fig. 12 and Fig. 13 we see intensity I_1 and I_3 in the far field of medium 3 for pyrex as medium 1, aluminum as medium 2, and 4 different third media: acetone, water, methanol, and aluminum. Aluminum as the third medium reduces the 3-layer problem to the 2-layer case already studied and is included for comparison.

TABLE 5.3. Photoacoustic Generation in 3-region Systems

Discussed in Section 5.7

Graphs	Figure	Points Illustrated
Pyrex/Al/Acetone Pyrex/Al/Al Pyrex/Al/Methanol Pyrex/Al/Water	5-12	Effect on I_1 and I_3 of changing medium 3 for different layer thickness.
Pyrex/Mo/Acetone Sapphire/Mo/Acetone	5-14	Effect on I_3 of changing medium 1 for different layer thickness.
Pyrex/Al/Water Pyrex/Au/Water Pyrex/Si/Water Pyrex/Mo/Water	5-15	Effect on I_3 of changing medium 2 for different layer thickness.
Pyrex/Mo/Water	5-16	Effect on I_3 of changing modulation frequency for different layer thickness.
Sapphire/Carbon/Acetone Sapphire/Carbon/Water	5-17 5-18	Effect on I_1 and I_3 of changing layer thickness. $\lambda/4$ thickness resonance.
Sapphire/Al/Water Sapphire/Si/Water	5-19	Contrast in a photoacoustic image.

PYREX/Aℓ WITH VARIOUS MEDIA 3
I_1 IN PYREX   100 MHz

NORMALIZED LAYER THICKNESS $A_2 L$
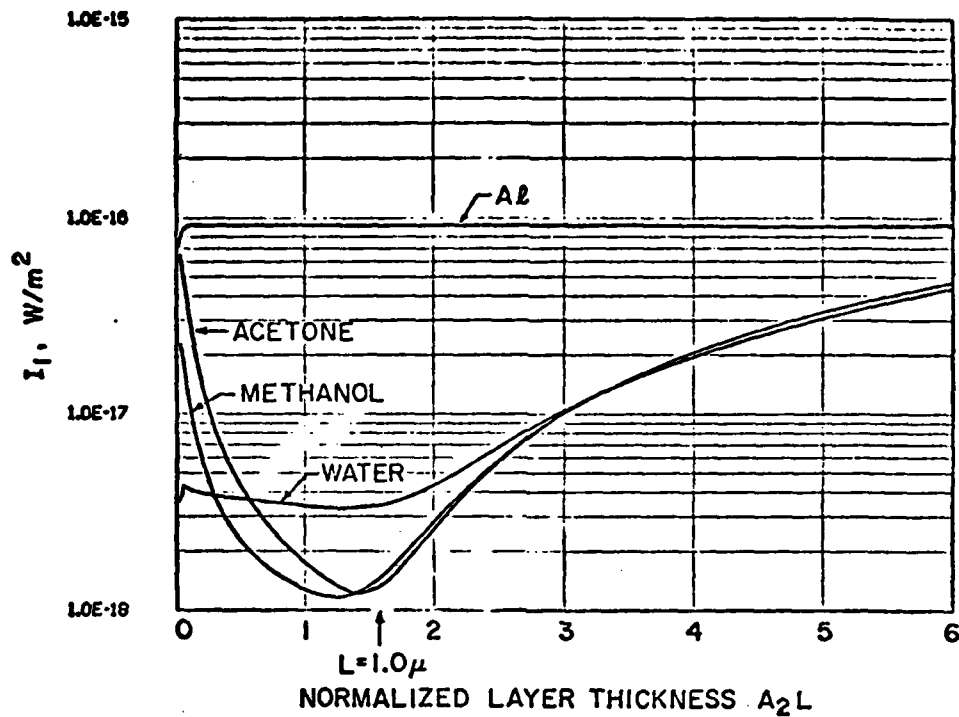
FIGURE 12

PYREX/Aℓ WITH VARIOUS MEDIA 3
I_3 100 MHz

NORMALIZED LAYER THICKNESS $A_2 L$

FIGURE 13

- 61 -
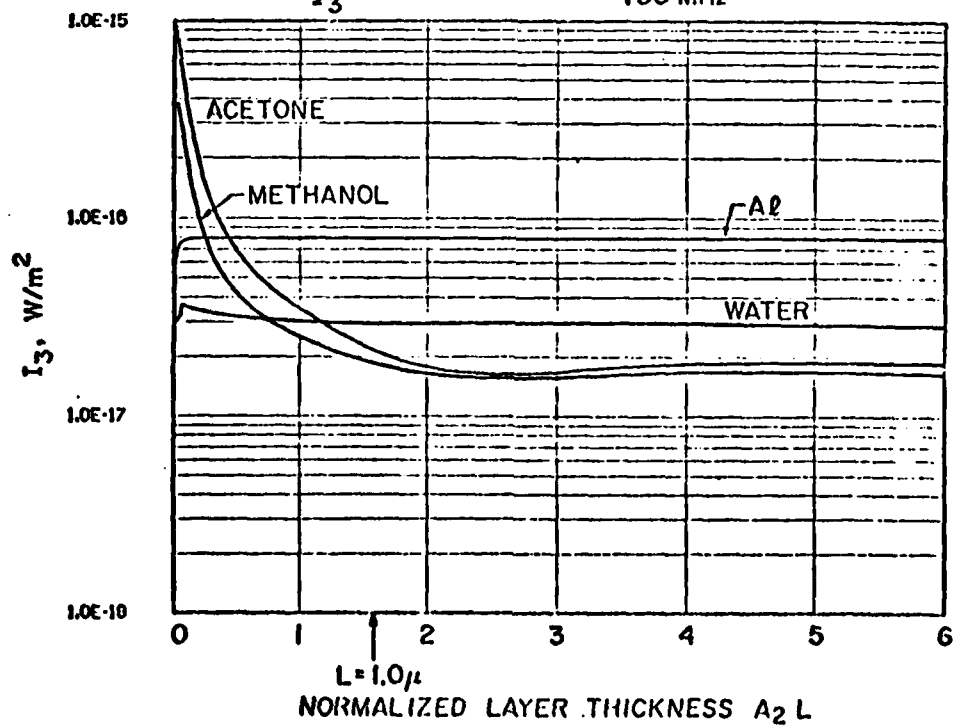
For the case of aluminum at an optical wavelength 0.95μ, optical absorption constant is $\alpha = 1.12 \times 10^8 \text{ m}^{-1}$. For 100 MHz modulation, thermal attenuation constant $a_2 = |\tau_2/\sqrt{2}| = 1.61 \times 10^6 \text{ m}^{-1}$. The two graphs are plotted as a function of normalized layer thickness a_2L. The effects of finite (rather than infinite) α are seen only at the extreme left, where $\alpha L \cong 1$ or less, and thus $a_2L \ll 1$. In this region all the curves approach zero as $a_2L \to 0$, since not all the light is being absorbed.

For the case of I_3 in the region from roughly $a_2L = 0.03$ to $a_2L = 0.3$ (200 Å to 2000 Å thickness) in Fig. 13, both methanol and acetone give a large signal enhancement over the 2-region case where the Al extends to $+\infty$. The intrinsic conversion factors η from Table 5.2 are in the ratio

$$\text{Acetone:Methanol:Al:Water:: } 185:81:2:1$$

The intensities I_3 in Fig. 13. are in the same order for thin Al films. Physically, since $a_2L \ll 1$, most of the heat generated at the pyrex/aluminum interface reaches the aluminum/medium 3 interface, where the transmitted heat wave in the third medium generates acoustics in medium 3 by the expansion of medium 3. When medium 3 has a large intrinsic conversion factor η, large signal enhancement is possible.

For thicker layers we have a diminishing amplitude thermal wave reaching medium 3, and the acoustic wave intensity decreases as the square of the thermal wave amplitude. For $a_2L \gtrsim 2$ in the present case, essentially all the sound reaching the far field of region 3 is created in region 2 (Al) and transmitted across the boundary from 2 to 3.

- 62 -

When medium 3 is one of the liquids the impedance mismatch at this boundary with Al is large. For example, $\Delta_{23} = Z_{02}/Z_{03} = 18.7$ for medium 2 = Al, medium 3 = acetone.

For this reason, the signals I_3 in the liquids are considerably smaller for thermally thick films than for the matched case when medium 3 is Al. We note that if one were to insert a fourth medium with $Z_{04} = \sqrt{Z_{02}Z_{03}}$ of $\lambda/4$ thickness between medium 2 and 3, the signals in the liquids would rise to the same value as the 2-medium pyrex/Al case, as shown in Fig. 12.

Resonance behavior is not much in evidence for the I_3 graphs only because medium 1, in this case pyrex, is a rather good acoustic match to Aluminum ($Z_{02}/Z_{01} = \Delta_{21} = 1.33$) and thus the power reflection coefficient of a wave traveling toward medium 1 in medium 2 is only 0.061. We will see examples later where I_3 exhibits strong resonance effects with substantial mismatch in impedance between media 1 and 2.

Looking at the far-field acoustic intensity I_1 in pyrex for the same four combinations, Fig. 12, we find that in every case the addition of a third medium decreases the signal for the range of thickness shown. The sharp increase in I_1 as $aL \to 0$ for the methanol and acetone graphs is to be understood as sound produced in region 3. The liquids with high conversion factors η receive a heat wave produced in medium 2 (Al) near the 1-2 boundary which has not been completely damped by the time it reaches the 2-3 boundary, for $a_2L \lesssim 2$. Sound produced in medium 3 propagates in the negative z direction as well as the positive z direction. A percentage (19% in the case of medium 2 = aluminum, medium 3 = acetone) of the negative-traveling sound power in medium 3 crosses the 2-3 boundary into

- 63 -

medium 2, where, because of the good impedance match between medium 1 (pyrex) and medium 2 (aluminum), there is negligible reflection at the 1-2 boundary, and the sound travels to the far field of medium 1. This accounts for the sharp rise in I_1 for a very thin region 2.

The I_1 graphs in Fig. 12 show a drop of almost 20 dB from the 2-medium case of pyrex/Al for thermally thick (but still acoustically thin) layers near $aL \sim 1.5$. To explain this, we should note that in no case is much sound produced in pyrex itself. From Table 5.2, $n_2/n_1 = 4800$ for 1 = pyrex, 2 = aluminum. The substantial I_1 signal in the 2-layer pyrex/Al case is sound generated by thermal expansion of Al which crosses the 1-2 boundary. When we have a third low-impedance medium terminating region 2 for $L \ll \lambda$, the wave traveling toward $+z$ in medium 2 is reflected at nearly full amplitude but at opposite phase. This wave interferes with the wave traveling towards $-z$ originally, resulting in drastically reduced I_1. As the layer becomes thicker, I_1 increases as the two waves get back in phase with each other, which happens at the $\lambda/4$ thickness, $a_2 L \cong 25$ for 100 MHz, not shown in Fig. 12. This would be a 16 μ thick Al region.

To see the effect of the first medium on the sound transmitted to the far field of medium 3, we compare the cases Sapphire/Mo/Acetone with Pyrex/Mo/Acetone in Fig. 14. The I_3 for Sapphire is lower for thin film thickness because Sapphire is a better heat conductor than pyrex ($K_{sapphire}/K_{pyrex} = 26$) and thus less heat will reach acetone, whose very efficient expansion is responsible for the far-field sound in the case of a thin Mo film. In the thick-film case, the

- 64 -

SAPPHIRE/MO//ACETONE I_3 100 MHz

PYREX/MO//ACETONE I_3 100 MHz

PYREX/MO/ACETONE

SAPPHIRE/MO/ACETONE

NORMALIZED THICKNESS $A_2 L$.

I_3 W/m^2

FIGURE 14

- 65 -
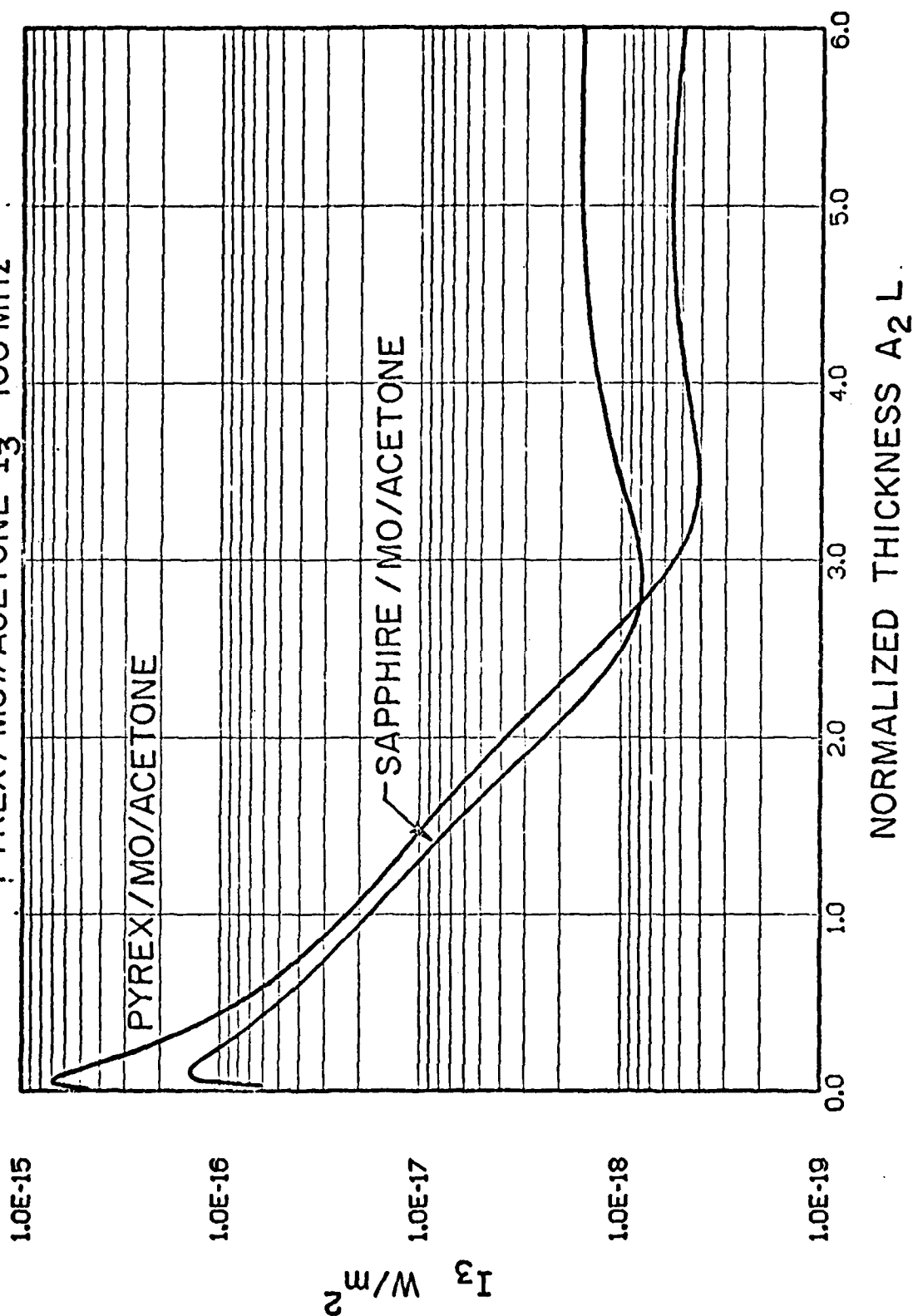
sound reaching the far field of medium 3 is actually produced in media 1 and 2. Sapphire has a much higher intrinsic conversion factor η in Table 5.2: $\eta_{sapphire}/\eta_{pyrex} = 710$. It is therefore more efficient as a photoacoustic generator than pyrex, and is in fact more efficient than molybdenum. It is also a more efficient constraint on molybdenum $(z_{o,sapphire} \cong 3.4 \, z_{o,pyrex})$. Both these effects lead to higher far-field acoustic power in acetone in the thick film case.

We next consider the effects of a change in the second medium when the first and third media are kept fixed. In Fig. 15 we have again plotted Eqs. (5.128), using Eq. (5.122) for four different second media: gold, molybdenum, aluminum, and silicon. Medium 1 is pyrex in all cases and medium 3 is water. There are several factors to consider to account for the differences we observe.

Firstly, the silicon curve has a more gradual rise at small film thickness. This is because the optical absorbtion constant α for silicon $(3.29 \times 10^6 \, m^{-1}$, optical $\lambda = 8000$ A) is a factor of at least 13 smaller than the α values for the other materials. A thicker Si layer is required to absorb all the light.

The curves for Al and Si in Fig. 15 are flat as a function of layer thickness, whereas the Mo and Au graphs are decreasing functions. The difference is the acoustic impedance match with medium 1, pyrex. Aluminum $(\Delta_{21} = Z_{02}/Z_{01} = 1.33)$ and Si $(\Delta_{21} = 1.52)$ are fairly well matched to pyrex. For a wave in medium 2 striking the 1-2 boundary, the power reflection coefficients are 0.02 and 0.04, respectively, versus 0.47 and 0.42 for Mo and Au. This means that acoustic thickness resonance effects will not be much in evidence in the far-field in medium 3,

- 66 -

I_3 IN WATER FOR VARIOUS MEDIA #2

MEDIUM I = PYREX   100 MHz

FIGURE 15

LAYER THICKNESS IN μ

I_3, W/m^2
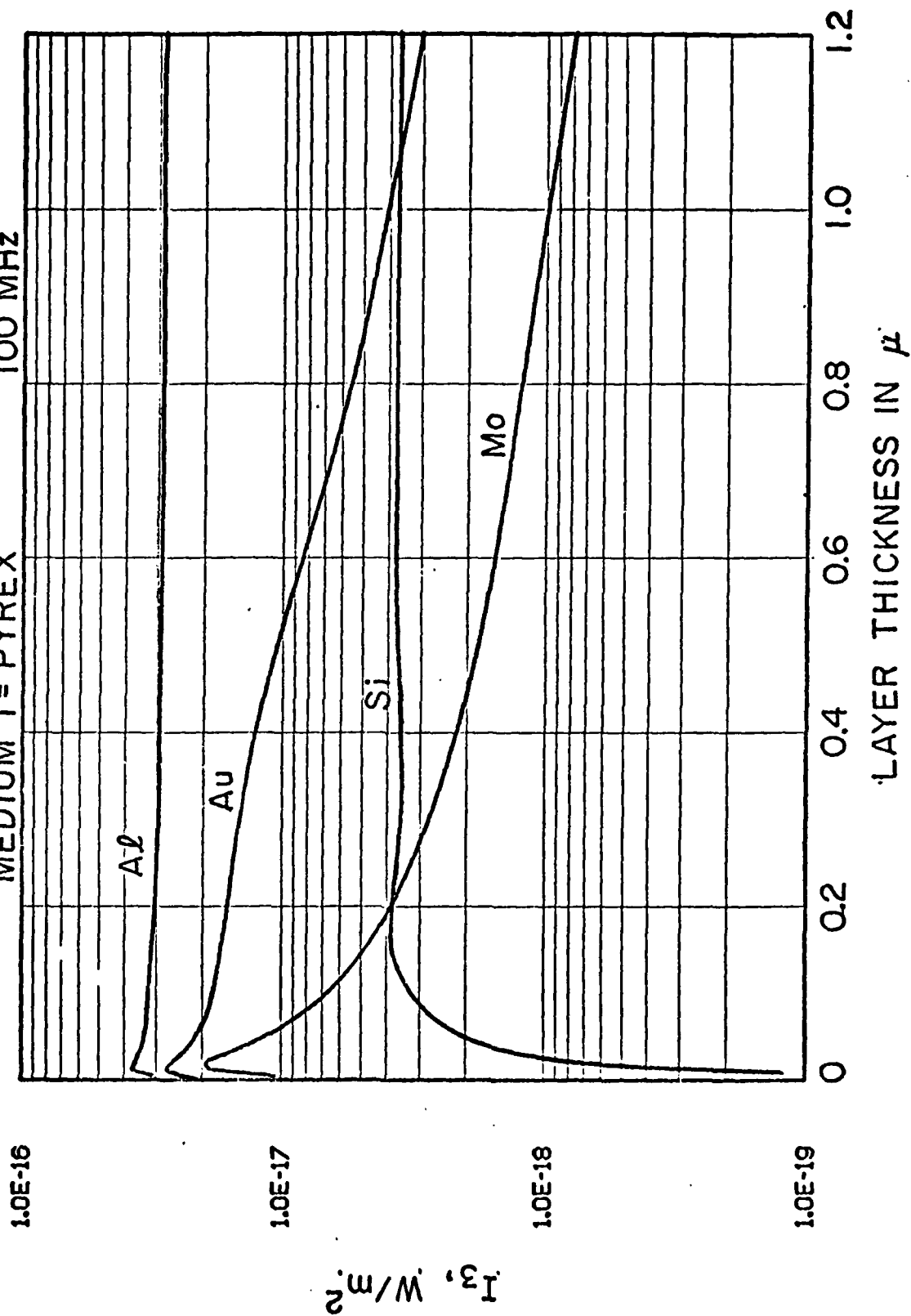
there being only the portion of the positive traveling wave in medium 2 that is transmitted across the 2 - 3 boundary to consider. Gold and Mo, being poor acoustic matches to pyrex, exhibit thickness resonance effects due to multiple reflections within the layer. Both exhibit a half-wave resonance maximum (at thickness 34 μ for Mo, 16 μ for Au) and a quarter-wave minimum. In the thin layer region shown, the Mo and Au curves are decreasing towards their quarter-wave minimum off the right side of the graph. The details of the Mo layer thickness resonance will be considered shortly. We emphasize that because of the large acoustic impedance mismatch between all four solids and water, the sound intensity in water is very low compared to the sound intensity we would have if medium 2 had extended to ∞ .

In Fig. 16 we have plotted intensity in the far field in water for the combination pyrex/molybdenum/water, also studied by von Gutfeld and Budd. We see here the effect of changing modulation frequency of the incoming light. In the region at the extreme left, for film thickness approaching zero, the far-field acoustic intensity goes to zero because the film thickness is less than the optical penetration depth and the light is not all absorbed. For optical $\lambda = 1.0$ μ , in molybdenum $1/\alpha = 224$ Å , in accord with the turning point at the extreme left of each graph in Fig. 16.

In the region of film thickness from roughtly 0.04 μ to 1μ , the far-field intensity I_3 in water decreases with increasing film thickness at each frequency. This is because the thermal wave in the molybdenum film is attenuated with attenuation constant

$$a_2 = \frac{\omega}{2\kappa_2} = |\tau_2|/\sqrt{2} .$$

- 68 -

PYREX MO//WATER I₃ AT THREE FREQUENCIES

FIGURE 16

- 69 -
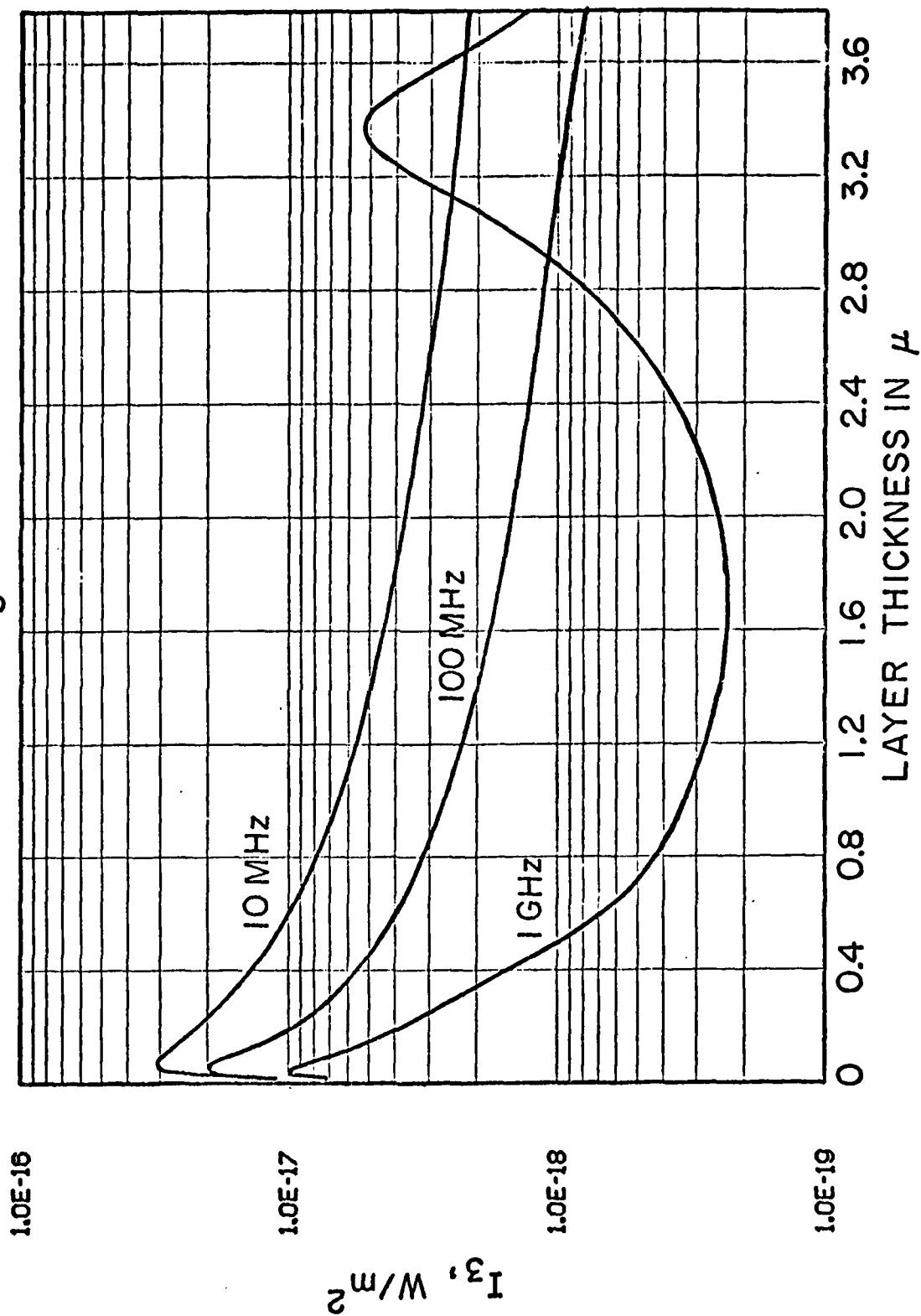
Thus $a \propto \sqrt{\omega}$ means a smaller amplitude thermal wave reaches the water. Water has approximately the same intrinsic conversion factor η as molybdenum, as we see in Table 5.2. Water is a better thermal match to molybdenum $(Z_{Mo}^{t}/Z_{H_2O}^{t} = 9.6)$ than an acoustic match $(Z_{o,Mo}/Z_{o,H_2O} = 45)$. Thus sound in the far field of water is most efficiently generated by the thermal wave heating the water directly, since sound generated inside the Mo film doesn't get out efficiently.

This analysis breaks down in the right hand region of the 1 GHz graph in Fig. 16. At film thickness 3.4 μ the 1 GHz graph reaches a peak about 3 dB below the very thin film peak at about 0.04 μ thickness. At 3.4 μ thickness the film acts as a half-wave acoustic resonator, since the acoustic wavelength in Mo at 1 GHz is 6.8 μ. Due to the large reflection coefficients at each boundary, acoustic waves in the Mo film are reflected many times back and forth within the layer, some energy being transmitted into water on each pass. The transmitted waves in water are all in phase when $L = \lambda/2$, and hence we get maximum intensity with this condition, as Fig. 16 shows. The $\lambda/2$ thickness resonance condition is appropriate when both boundaries are low impedance boundaries as in this case.

Cases exhibiting a quarter-wave resonance thickness for the central layer are sapphire/carbon/acetone and sapphire/carbon/water, for which I_3 and I_1 are graphed as a function of film thickness in Figs. 17 and 18. The carbon data are an average of thin-film carbon specimens. The thermal diffusion constant a for carbon at 1 GHz is such that $aL = 7.5$ corresponds to film thickness $L = 1.0\mu$. The sound wavelength in carbon at 1 GHz is 4μ , giving us the quarter-wave resonator we see.

SAPPHIRE/CARBON//ACETONE, WATER I_3 I GHz

SAPPHIRE/CARBON/ACETONE

SAPPHIRE/CARBON/WATER

NORMALIZED LAYER THICKNESS A_2L

FIGURE 17

SAPPHIRE/CARBON //ACETONE, WATER I_1 I GHz

SAPPHIRE/CARBON/ACETONE

SAPPHIRE/CARBON/WATER

NORMALIZED LAYER THICKNESS A_2L
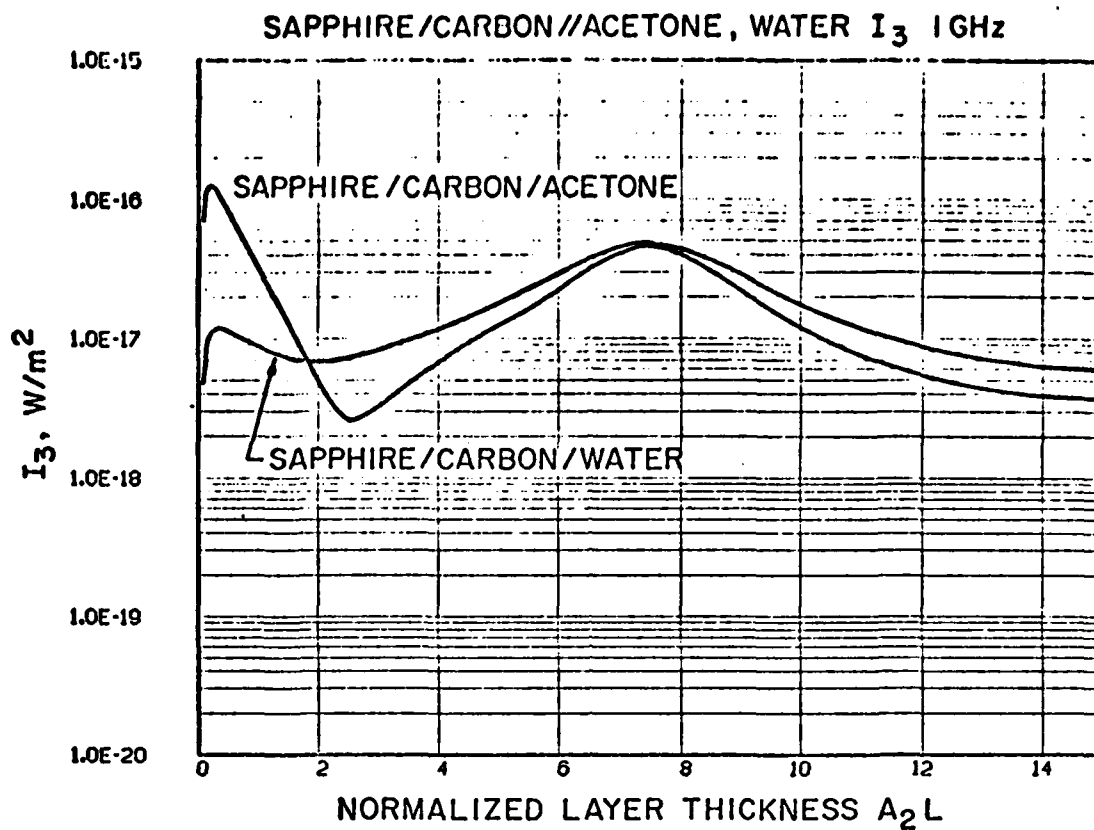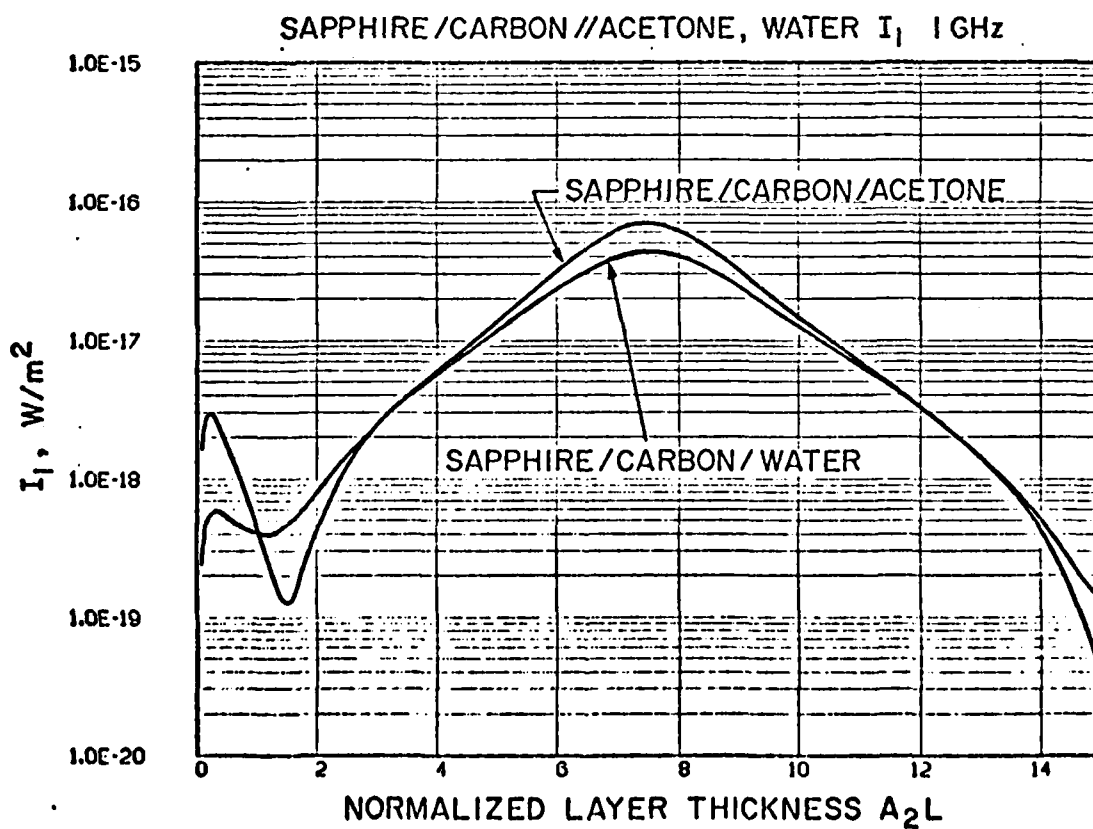
FIGURE 18

We expect quarter-wave resonance in this case because carbon $z_0 = 8 \times 10^6$) is intermediate in acoustic impedance between sapphire $(z_0 = 44 \times 10^6)$ and water $(z_0 = 1.5 \times 6)$. In general, $L = \mathscr{N} \lambda/4$, where $\mathscr{N}$ is an odd integer, satisfies this resonance condition. In fact, carbon is very close to the geometric mean $(z = 8.2 \times 10^6)$ between the impedances of sapphire and water and thus acts as an ideal quarter-wave transformer between sapphire. Thus the acoustic mode traveling to the right in sapphire (medium 1) in Fig. 8 is not reflected at the sapphire/Mo boundary. Similarly the acoustic mode traveling toward medium 2 in medium 3 is not reflected. In this matching-layer-resonator case we expect I_1 and I_3 to be equal. We see from Figs. 17 and 18 that I_1 and I_2 are very nearly equal for $L = \lambda/4 \cong 7.5/a_2$ for Sapphire/Carbon/Water. This is somewhat less true for Sapphire/Carbon/Acetone, where the ideal matching layer would have $z_0 = 6.4 \times 10^6$ mks rayl, 20% less than the carbon value.

The resonance behavior of photoacoustic generation in layers is important in that layer thickness is then an important source of contrast in photoacoustic images. One can imaging extracting layer thickness information from photoacoustic images if one can tune modulation frequency over a substantial range.

Finally, to illustrate the application of these results to a real photoacoustic image, we have plotted the response I_3 in water for the cases Sapphire/Aluminum/Water and Sapphire/Silicon/Water in Fig. 19. In Figs. 5 and 6 we saw areas of this nature and noted the silicon on sapphire areas gave much weaker response than the aluminum on sapphire areas. The aluminum areas are 1.0 µ thick while the polycrystalline silicon regions are 0.5 µ thick. Figure 19 predicts a difference in response in the far field of ~ 11 dB, consistent with what we saw in Figs. 5 and 6.

SAPPHIRE/Aℓ/WATER I_3 840 MHz
SAPPHIRE/Si/WATER I_3 840 MHz

LAYER THICKNESS IN μ

I_3, W/m^2

FIGURE 19

- 73 -
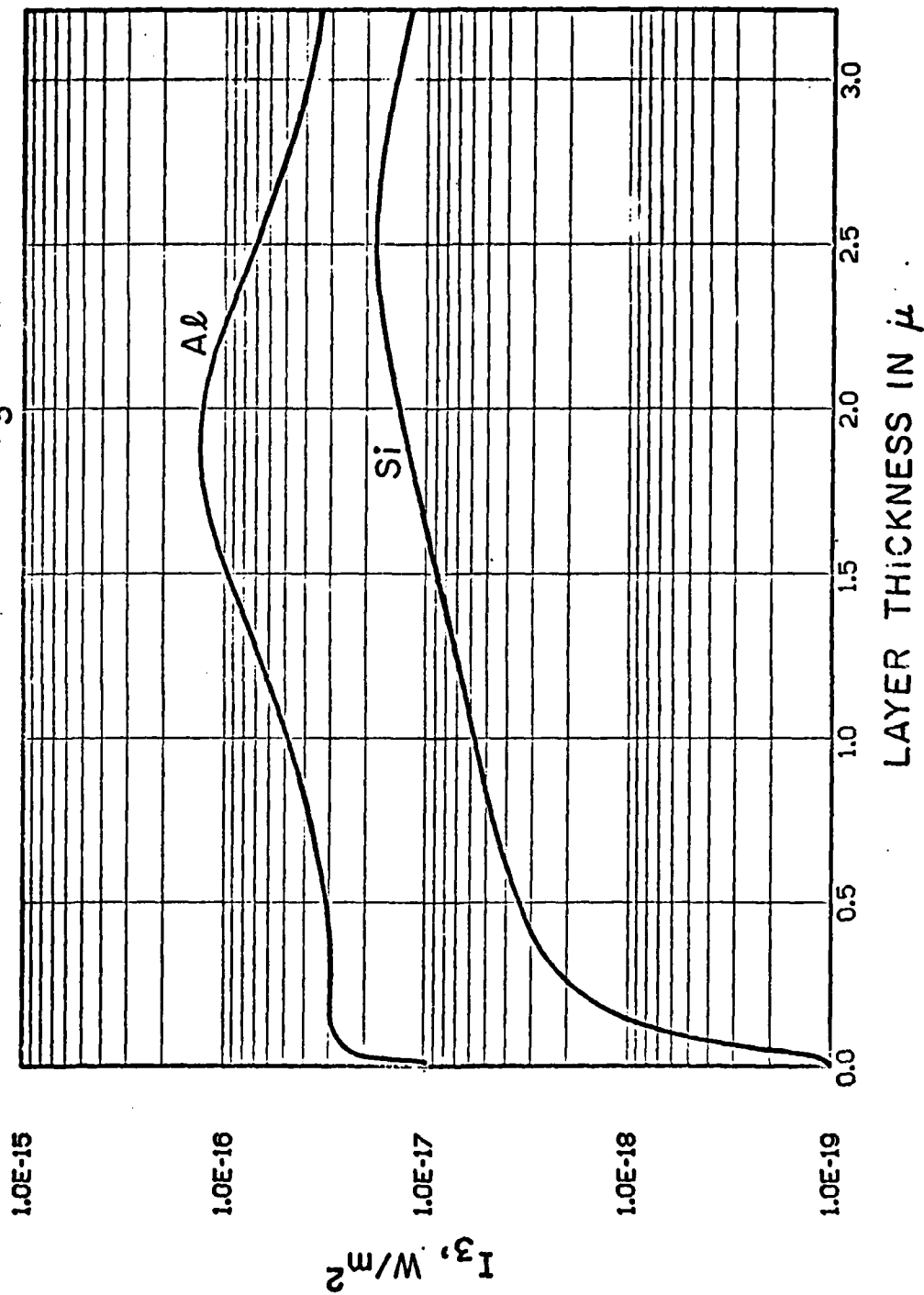
VI. OTHER EVENTS

As mentioned earlier we have had visits from Dr. Milton Ritchie and Dr. Jim Knight from the Hughes Santa Barbara Research Center. They are asking us to study the adhesion of lead sulphide films in the infrared detectors — a device that is being built under contract with the Air Force (Space Division).

Dr. J. Reffner of American Cyanamide Company has supplied us with a number of samples of polymers for study with acoustic microscopy.

A group from Xerox Research Laboratory in Toronto has visited us and they left with a strong interest in our work.

Jack Baring of Honeywell has supplied us with samples of magnetic recording heads that are defective in the sense that they generate excessive second harmonic.

List of Publications

"Scanned Acoustic Microscopy," E. A. Ash, ed., Chapter II, Academic Press, 1980.

"Film Adhesion Studies with the Acoustic Microscope," by R. C. Bray, C. F. Quate, J. Calhoun, and R. Koch; published in Thin Solid Films, 74, 295-302 (1980).

Seminars

"Microwaves and Acoustic Imaging," Physics Department Colloquim, Princeton University, Princeton, PA

"Acoustic Imaging," Electrical Engineering Department, Stanford University.

Some of our Visitors

T. Destephano and V. Jipson of IBM at Yorktown Heights, New York

Dr. Akiyama of Hitachi in Japan

Dr. J. Zelich of Hughes Aircraft Company.

Dr. P. Liao of Bell Labs

Dr. H. Fritsche of Leitz in West Germany

Dr. K. Wishnuff of National Semiconductor

Dr. D. Jonney of Los Alamos, New Mexico

Dr. J. McGroddy of IBM at Yorktown Heights, New York

Dr. C. Tracy of GM Research Labs.

Dr. F. Jamerson of GM Research Labs.

Dr. K. McKay of Avantek.

REFERENCES

1. Scanned Acoustic Microscopy, E.A. Ash, ed. (Academic Press, 1980).

2. "Noninvasive Method for Visualization of Interior Region of Sample; Acoustic Microscope," by Hitachi, published in New Technology.

3. Y.-H Pao, Optoacoustic Spectroscopy and Detection, New York: Academic Press, 1977.

4. A. Rosencwaig, Photoacoustics and Photoacoustic Spectroscopy, New York: Wiley, 1980.

5. L. B. Kreuzer, et al., Science $\underline{177}$, 347 (1972).

6. C.K.N. Patel, et al., Science $\underline{184}$, 1173 (1974).

7. R. M. White, J. Appl. Phys. $\underline{34}$, 3559 (1963).

8. H. K. Wickramasinghe, R. C. Bray, V. Jipson, C. F. Quate, and J. R. Salcedo, Appl. Phys. Lett. $\underline{33}$, 912 (1978).

9. B. A. Auld, Acoustic Fields and Waves in Solids, New York: Wiley, 1973, Chapter 6.

10. H. S. Carslaw and J. C. Jaeger, Conduction of Heat in Solids, Oxford: Clarendon Press, 1959.

11. G. Hass and L. Hadley, "Optical Properties of Metals," in D. E. Gray, ed., AIP Handbook, 3rd. Edition, New York: McGraw-Hill, 1972.

12. Reference 9, V.I., Appendix 2A.

13. D. E. Gray, ed., AIP Handbook, New York: McGraw-Hill, 1972.

14. Landölt-Börnstein, Numerical Data and Functional Relationships in Science and Technology, K.-H. Hellwege and A.M. Hellwege, eds., Group III, Vol. 1. Berlin: Springer, 1966.

15. N. B. Vargaftik, Tables on the Thermophysical Properties of Liquids and Gases, New York: Wiley, 1975.

16. Landölt-Börnstein, Group II, V. 5, W. Schaafs, ed., Berlin: Springer, 1967.

17. V. J. Johnson, ed., Properties of Materials at Low Temperatures (Phase 1): A Compendium, New York: Pergamon, 1961.

18. I. A. Blech, "Properties of Materials," in D. G. Fink, ed., Electronics Engineers' Handbook, New York: McGraw-Hill, 1975.

19. R. C. Weast, ed., Handbook of Physics and Chemistry, 56th edition, Cleveland: CRC Press, 1975.

20. J. G. Parker, Appl. Opt. 12, 2974 (1973).

21. A. Rosencwaig and A. Gersho, J. Appl. Phys. 47, 64 (1976).

22. R. J. von Gutfeld and H. F. Budd, Appl. Phys. Lett. 34, 617 (1979).

23. R. A. Lemons, Acoustic Microscopy by Mechanical Scanning, Ph.D. Thesis, Stanford University, 1975, p. 71.

24. R. J. von Gutfeld, "Thermoelastically Generated MHz Elastic Waves from Constrained Surfaces," in Proc. 1977 Ultrasonics Symposium, pp. 397-402.

0.1
0.2
0.3
0.4
0.5
0.6
0.7
0.8
0.9
1.
2.
3.
4.
5.
6.
7.
8.
9.
10.
11.
12.
13.
14.
15.
16.
17.
18.
19.
20.
21.
22.
23.
24.
25.
26.
27.
28.
29.
30.
31.
32.
33.
34.
35.
36.
37.
38.
39.
40.
41.
42.
43.
44.
45.
46.
47.
48.
49.
50.
51.

APPENDIX A

PROGRAM TO CALCULATE THE REFLECTANCE FUNCTION
OF N LAYEFS ON A SUESTRATE AS A FUNCTION OF
SINE OF ANGLE OF INCIDENCE.

```
//REFLEC JOB 'F17SE7,181','B BBAY',CLASS=E
/*JOBPARM DEST=SELF
// EXEC WATFIV
//GO.SYSIN DD *
$WATFIV
C
C    THIS PROGRAM CALCULATES THE REFLECTANCE FUNCTION (MAGNITUDE
C AND PHASE) FOR A PLANE ACOUSTIC WAVE INCIDENT ON A MULTI-
C LAYER TARGET, AS A FUNTION OF ANGLE OF INCIDENCE. IT ALSO CALCULATES.
C TRANSMISSION FROM THE LIQUID THROUGH MANY LAYERS INTO A SOLID .
C THE MATHEMATICS FOLLOWS RA LEMCES' THESIS, "ACOUSTIC MICROSCOPY
C BY MECHANICAL SCANNING", STANFORD UNIVERSITY, 1975, BUT DIFFEBS
C IN THAT THE INCIDENT WAVE IS IN THE LIQUID. ISOTROPIC SOLIDS
C ARE ASSUMED. .
C
      COMMON/CCALC/ALPHA(8),BETA(8),P(8),FP(8),Q(8),QP(8),
     1C11(8),C12(8),C44(8),K(8),KAPPA(8),SIGMA,NP2
      REAL*8 THICK(9),RHO(9),C11,C12,C44,SIGMA,K,KAPPA,
     2MAGAOP(46,2),MAGBCP(46,2),MAGA3(46,2),THETA,SIGSQ,TH,PI,X1,X2,X3,
     3X4,X5,X6,PHIACF(46,2),PHIBCF(46,2),PHIA3(46,2),COSTH,
     4XXR,XXI,XXP,XXF,TLM(100),TLF(100),TSM(100),TSP(100),
     5RLM(100),RLP(100)
      COMPLEX*16 Z(3,3),V(3),T(3,3),DFT,DET1,DET2,DET3,AOP,BOP,A3,DCMPLX
     1,ANP1,BNP1,AOER,JAY,PRCD(4,4),ALPHA,BETA
     2,MAT1(4,4),MAT2(4,4),TOTMAT(4,4),P,PP,Q,QP
      PI=3.141592653589793
      JAY=(0.0D0,1.0D0)
C
$SPACE 3
      READ,N
      NP1=N+1
      NP2=N+2
      NM1=N-1
      DO 701 I=1,N
      C11(I)=1.0
      C44(I)=1.C
701   RHO(I)=1.0
      DO 100 I=1,NP2
  100 READ,C11(I),C44(I),RHO(I),THICK(I)
      DO 110 I=1,NP2
      C12(I)=C11(I)-2.*C44(I)
  110 K(I)=DSQRT(RHO(I)/C11(I))
      DO 115 I=2,NP2
  115 KAPPA(I)=DSQRT(RHO(I)/C44(I))
      WRITE (6,50)
50    FORMAT(1H1, 12X,'SOLID C',5X,'SOLID 1',5X,'SOLID 2',5X,'SOLID 3',
     15X,'SOLID 4',5X,'LIQUID',/)
      WRITE (6,51) (C11(I),I=1,6),(C12(I),I=1,6),(C44(I),I=1,6),
     1(RHO(I),I=1,6),  (THICK(I),I=1,6)
51    FORMAT(///,5X,'C11= ',6E12.3//,5X,'C12= ',6E12.3//
     1,5X,'C44= ',6E12.3//,5X,'RHC= ',6E12.3//, 5X,'THICK=',6E12.3///)
```

```
52.      C
53.      $EJECT
54.      $SPACE 3
55.      C    CALCULATE A PRODUCT CF LAYER TRANSFER MATRICES,
56.      C IN PROD. IN WHAT FOLLOWS, SIGMA IS TANGENTIAL COMP OF INCIDENT
57.      C SLOWNESS; ALPHA IS PERPENDICULAR COMPONENT CF TRANSMITTED
58.      C LONGITUDINAL SLOWNESS, AND EETA IS PERPENDICULAR COMPONENT
59.      C CF TRANSMITTED SHEAR SLOWNESS; P,PP,Q,QP ARE LAYER THICKNESS
60.      C IN RADIANS OF ANGLE - SIN AND CCS.
61.      C
62.              DO 999 NNN = 1,100
63.              THETA = DARSIN((.1D-1)*FLOAT(NNN-1))
64.              SIGMA=K(1)*DSIN(THETA)
65.              SIGSQ=SIGMA**2
66.              DO 120 I=1,NP2
67.       120 ALPHA(I)=CDSQRT((K(I)**2-SIGSQ)*(1.0D0,0.0D0))
68.              DO 125 I=2,NP2
69.       125 BETA(I)=CDSQRT((KAPPA(I)**2-SIGSQ)*(1.0D0,0.0D0))
70.              DO 150 I=2,NP1
71.              TH=2.*PI/K(I)*THICK(I)
72.              P(I)=CDCOS(ALPHA(I)*TH)
73.              PP(I)=CDCOS(EETA(I)*TH)
74.              Q(I)=CDSIN(ALPHA(I)*TH)
75.       150 QP(I)=CDSIN(BETA(I)*TH)
76.              CALL CALCCF(2,MAT1)
77.              DO 151 I=1,NM1
78.              CALL CALCCF(I+2,MAT2)
79.              CALL MATMUL(MAT2,MAT1,PROD)
80.              DO 152 II=1,4
81.              DO 152 JK=1,4
82.       152 MAT1(II,JK)=PRCD(II,JK)
83.       151 CONTINUE
84.              DO 195 I=1,2
85.              DO 195 J=3,4
86.              PROD(I,J) = PRCD(I,J)*JAY
87.       195 CONTINUE
88.              DO 196 I=3,4
89.              DO 196 J=1,2
90.              PROD(I,J) = PRCD(I,J)*JAY
91.       196 CONTINUE
92.      C
93.      $EJECT
94.      $SPACE 3
95.              CALL SIMEC(PRCD,ANP1,BNP1,AOPR)
96.              XXR=ANP1
97.              XXI=ANP1*(-JAY)
98.              TLM(NNN)=CDABS(ANP1)
99.              TLP(NNN)=DATAN2(XXI,XXR)
100.     C
101.             XXR=BNP1
102.             XXI=BNP1*(-JAY)
103.             TSM(NNN)=CDABS(BNP1)
104.             IF(TSM(NNN) .LT. .1E-6) GO TO 331
105.             TSP(NNN)=DATAN2(XXI,XXR)
106.     C
107.      331 XXR=AOPR
108.             XXI=AOPR*(-JAY)
109.             RLM(NNN)=CDABS(AOPR)
110.             RLP(NNN)=DATAN2(XXI,XXR)
111.      999 CONTINUE
```

- 79 -

```fortran
112.    C
113.          WRITE(6,950)
114.     950  FORMAT('1  TRANSMITTED LONGITUDINAL AMPLITUDE AND PHASE'/)
115.          DO 951 I=1,100
116.          WRITE(6,952) TLM(I), TLE(I)
117.     952  FORMAT(' ',3X,E12.5,3X,E12.5)
118.     951  CONTINUE
119.    C
120.          WRITE(6,953)
121.     953  FORMAT('1  TRANSMITTED SHEAR AMPLITUDE AND PHASE'/)
122.          DO 955 I=1,100
123.          WRITE(6,954) TSM(I), TSE(I)
124.     954  FORMAT(' ',3X,E12.5,3X,E12.5)
125.     955  CONTINUE
126.    C
127.          WRITE(6,956)
128.     956  FORMAT('1  REFLECTED LONGITUDINAL AMPLITUDE AND PHASE'/)
129.          DO 958 I=1,100
130.          WRITE(6,957) RLM(I), RLE(I)
131.     957  FORMAT(' ',3X,E12.5,3X,E12.5)
132.     958  CONTINUE
133.    C
134.          STOP
135.          END
136.    C
137.    $EJECT
138.    C
139.    C    SIMEQ SETS UP A SYSTEM OF 4 EQUATIONS IN 4 UNKNOWNS
140.    C AND USES CRAMER'S RULE TO SOLVE FOR 3 OF THEM: REFLECTED
141.    C AMPLITUDE, TRANSMITTED LONGITUDINAL AMPLITUDE, AND
142.    C TRANSMITTED SHEAR AMPLITUDE. PHASE IS PRESENT IN THE
143.    C COMPLEX AMPLITUDES. THE FOURTH UNKNOWN, THE X COMPONENT
144.    C OF PARTICLE VELOCITY IN THE SOLID JUST PAST THE LIQUID/
145.    C SOLID INTERFACE, IS NOT OF INTEREST.
146.    C
147.          SUBROUTINE SIMEQ(MATR,ANP,BNP,AOP)
148.          COMMON/CCALC/ALPHA(8),EETA(8),P(8),PP(8),Q(8),QP(8),
149.         1C11(8),C12(8),C44(8),K(8),KAPPA(8),SIGMA,NP2
150.          COMPLEX*16 MATT(4,4),MATF(4,4),CONST(4),TEMP(4),
151.         1DET11,DET12,DET13,DET14,ANP,BNP,AOP,ALPHA,BETA,
152.         2P,PP,Q,QP,E
153.          REAL*8 C11,C12,C44,K,KAPPA,SIGMA,BSIM
154.    C
155.          BSIM = 2.*C44(NP2)*SIGMA
156.          MATT(1,1) = SIGMA/K(NP2)
157.          MATT(2,1) = - (C11(NP2)*K(NP2) - 2.*C44(NP2)*
158.         1 SIGMA*SIGMA/K(NP2))
159.          MATT(1,2) = - EETA(NP2)/KAPPA(NP2)
160.          MATT(2,2) = BSIM*MATT(1,2)
161.          MATT(3,1) = ALPHA(NP2)/K(NP2)
162.          MATT(3,2) = SIGMA/KAPPA(NP2)
163.          MATT(4,1) = - BSIM*ALPHA(NP2)/K(NP2)
164.          MATT(4,2) = -C44(NP2)*(SIGMA*SIGMA-EETA(NP2)*BETA(NP2))/
165.         1KAPPA(NP2)
166.          MATT(1,3) = -MATR(1,1)
167.          MATT(2,3) = -MATR(2,1)
168.          MATT(3,3) = -MATR(3,1)
169.          MATT(4,3) = -MATR(4,1)
170.    C
171.    C    E IS THE IMPEDANCE OF THE LIQUID;
```

- 80 -

```
172.      C    P IS TANGENT OF INCIDENCE ANGLE.
173.      C
174.             E = C11(1)*K(1)
175.             P = ALPHA(1)/K(1)
176.             MATT(1,4) = MATR(1,2)*E + MATR(1,3)*P
177.             MATT(2,4) = MATR(2,2)*E + MATR(2,3)*P
178.             MATT(3,4) = MATR(3,2)*E + MATR(3,3)*P
179.             MATT(4,4) = MATR(4,2)*E + MATR(4,3)*P
180.      C
181.      C    THE MATRIX OF COEFFICIENTS OF THE SET OF 4
182.      C EQUATIONS IN THE 4 UNKNOWNS ANE, ENE, AOP IS
183.      C NOW READY. NEXT PUT THE CONSTANTS IN THESE
184.      C EQUATIONS IN 4-VECTOR CONST(I).
185.      C
186.             CONST(1) = -MATR(1,2)*E+MATR(1,3)*P
187.             CONST(2) = -MATR(2,2)*E+MATR(2,3)*P
188.             CONST(3) = -MATR(3,2)*E+MATR(3,3)*P
189.             CONST(4) = -MATR(4,2)*E+MATR(4,3)*P
190.      C
191.      C    NOW USE CRAMER'S RULE TO SOLVE.
192.      C
193.             CALL CDET4(MATT,DET11)
194.             DO 731 I = 1,4
195.             TEMP(I) = MATT(I,1)
196.             MATT(I,1) = CONST(I)
197.       731   CONTINUE
198.             CALL CDET4(MATT,DET12)
199.             ANP = DET12/DET11
200.             DO 732 I = 1,4
201.             MATT(I,1) = TEMP(I)
202.             TEMP(I) = MATT(I,2)
203.             MATT(I,2) = CONST(I)
204.       732   CONTINUE
205.             CALL CDET4(MATT,DET13)
206.             BNP = DET13/DET11
207.             DO 733 I = 1,4
208.             MATT(I,2) = TEMP(I)
209.             TEMP(I) = MATT(I,4)
210.             MATT(I,4) = CONST(I)
211.       733   CONTINUE
212.             CALL CDET4(MATT,DET14)
213.             AOP = DET14/DET11
214.             RETURN
215.             END
216.      C
217.      C
218.      $EJECT
219.      C    CALCOF CALCULATES THE TRANSFER MATRIX OF THE ITH LAYER
220.      C AND PUTS THE RESULT IN A. SEE IPHCNS' EC. 5.10
221.      C
222.             SUBROUTINE CALCOF (I,A)
223.             COMMON/CCALC/ALPHA(8),EETA(8),P(8),PP(8),Q(8),QP(8),
224.            1C11(8),C12(8),C44(8),K(8),KAPPA(8),SIGMA,NP2
225.             REAL*8 C11,C12,C44,SIGMA,K,KAEEA,CA,CB,CC,SIGSQ,KA,KSQ,
226.            1KAP,KAPSQ,DIFFC,CKSQ,CKAESQ
227.             COMPLEX*16 ALPHA,BETA,E,EE,C,CE,A(4,4),ALPH,ALPHSQ,BET,
228.            1BETSQ,PA,PPA,CA,CPA,DIFFSC,CSCASQ
229.             CA=C11(I)
230.             CB=C12(I)
231.             CC=C44(I)
```

- 81 -

```
232.            SIGSQ=SIGMA**2
233.            ALPH=ALPHA(I)
234.            ALPHSQ=ALPH**2
235.            BET=BETA(I)
236.            BETSQ=BET**2
237.            KA=K(I)
238.            KSQ=KA**2
239.            KAP=KAPPA(I)
240.            KAPSQ=KAP**2
241.            DIFFC=CA-CB
242.            DIFFSQ=SIGSQ-BETSQ
243.            PA=P(I)
244.            PPA=PP(I)
245.            QA=Q(I)
246.            QPA=QP(I)
247.            CKSQ=CA*KSQ
248.            CKAPSQ=CC*KAPSQ
249.            CSCASQ=CB*SIGSQ+CA*ALPHSQ
250.            A(1,1)=(DIFFC*SIGSQ*PA+CSCASQ*PPA)/CKSQ
251.            A(1,2)=SIGMA/CKSQ*(PPA-PA)
252.            A(1,3)=-SIGMA*DIFFSQ/(ALPH*KAPSQ)*QA-2.*BET*SIGMA/KAPSQ*QPA
253.            A (1,4)=-SIGSQ/(ALPH*CKAPSQ)*QA-BET/CKAPSQ*QPA
254.            A(2,1)=CSCASQ*DIFFC*SIGMA/CKSQ*(PPA-PA)
255.            A(2,2)=(CSCASQ*PA+DIFFC*SIGSQ*PPA)/CKSQ
256.            A(2,3)=CSCASQ*DIFFSQ/(ALPH*KAPSQ)*QA-2*DIFFC*SIGSQ*BET/KAPSQ*QPA
257.            A(2,4)=CSCASQ*SIGMA/(ALPH*CKAPSQ)*QA-DIFFC*SIGMA*BET/CKAPSQ*QPA
258.            A(3,1)=DIFFC*ALPH*SIGMA/CKSQ*QA-SIGSQ/(BET*CKSQ)*QPA
259.            A(3,2)=-ALPH/CKSQ*QA-SIGSQ/(BET*CKSQ)*QPA
260.            A(3,3)=(-DIFFSQ*PA+2.*SIGSQ*PPA)/KAPSQ
261.            A(3,4)=SIGMA/CKAPSQ*(PPA-PA)
262.            A(4,1)=-2.*CC*DIFFC*ALPH*SIGSQ/CKSQ*QA+CC*CSCASQ*DIFFSQ/(BET*CKSQ)
263.           1*QPA
264.            A(4,2)=2.*CC*ALPH*SIGMA/CKSQ*QA+CC*DIFFSQ*SIGMA/(BET*CKSQ)*QPA
265.            A(4,3)=2.*CC*DIFFSQ*SIGMA/KAPSQ*(PA-PPA)
266.            A(4,4)=(2.*SIGSQ*PA-DIFFSQ*PPA)/KAPSQ
267.            RETURN
268.            END
269.     C
270.     $EJECT
271.     C   MATMUL MULTIPLES MATRICES A AND B, PUTTING THE
272.     C RESULT IN C.
273.     C
274.            SUBROUTINE MATMUL (A,B,C)
275.            COMPLEX*16 C(4,4),A(4,4),B(4,4)
276.            DO 100 I=3,4
277.            DO 100 J=1,2
278.            A(I,J)=-A(I,J)
279.        100 B(I,J)=-B(I,J)
280.            DO 150 I=1,4
281.            DO 150 J=1,4
282.            C(I,J)=(0.0,0.0)
283.            DO 150 K=1,4
284.        150 C(I,J)=C(I,J)+A(I,K)*B(K,J)
285.            DO 200 I=3,4
286.            DO 200 J=1,2
287.            A(I,J)=-A(I,J)
288.            B(I,J)=-B(I,J)
289.        200 C(I,J)=-C(I,J)
290.            RETURN
291.            END
```

```
292.    C CALDET CALCULATES THE DETERMINANT ON A 3X3 MATRIX D,
293.    C PUTTING THE RESULT IN DET.
294.    C
295.          SUBROUTINE CALDET (D,DET)
296.          COMPLEX*16 D(3,3),DET
297.          DET=D(1,1)*D(2,2)*D(3,3)+D(1,2)*D(2,3)*D(3,1)+D(2,1)*D(3,2)*D(1,3)
298.         1-D(3,1)*D(2,2)*D(1,3)-D(2,1)*D(1,2)*D(3,3)-D(3,2)*D(2,3)*D(1,1)
299.          RETURN
300.          END
301.    C
302.    $SPACE 3
303.    C
304.    C   CDET4 CALCULATES A 4X4 DETERMINANT BY EXPANSION BY
305.    C MINORS ON THE FIRST COLUMN.
306.    C
307.          SUBROUTINE CDET4(D4,DET)
308.          COMPLEX*16 D4(4,4), DET, D3(3,3), TDET
309.    C
310.          DO 831 I=1,3
311.          DO 831 J=1,3
312.          D3(I,J)=D4(I+1,J+1)
313.     831  CONTINUE
314.          CALL CALDET(D3,TDET)
315.          DET=TDET*D4(1,1)
316.          DO 832 J=1,3
317.          D3(1,J)=D4(1,J+1)
318.     832  CONTINUE
319.          CALL CALDET(D3,TDET)
320.          DET = DET - TDET*D4(2,1)
321.          DO 833 J=1,3
322.          D3(2,J) = D4(2,J+1)
323.     833  CONTINUE
324.          CALL CALDET(D3,TDET)
325.          DET = DET + TDET*D4(3,1)
326.          DO 834 J=1,3
327.          D3(3,J) = D4(3,J+1)
328.     834  CONTINUE
329.          CALL CALDET(D3,TDET)
330.          DET = DET - TDET*D4(4,1)
331.          RETURN
332.    C
333.    C   GLASS DATA:
334.    C   0.57600D12      0.20200D12      0.21600D1      0.25D0
335.    C   PYREX DATA (AULD):
336.    C      7.30E11         2.50E11         .232E1         .1E1
337.    C   HEAVY PYREX DATA
338.    C      7.30E11         2.50E11         .280E1         .1E1
339.    C   HEAVY SILICATE FLINT GLASS DATA (AULD):
340.    C      6.13E11         2.18E11         .3879E1        .1E1
341.    C   T-40 GLASS DATA (AULD):
342.    C      6.30E11         2.26E11         .339E1         .1E1
343.    C   LIGHT BORATE CROWN GLASS DATA (AULD):
344.    C      5.82E11         1.81E11         .2243E1        .1E1
345.    C   WATER DATA:
346.    C      2.25E10         0.00E00         1.00E00        1.00E00
347.    C   ALUMINUM DATA:
348.    C      1.11D12         2.50D11         .2695E1        .25E0
349.    C   SAPPHIRE(ASSUME ISOTROPIC) DATA:
350.    C      4.94E12         1.45E12         3.98E00        1.00E00
351.    C   CHROMIUM DATA:
```

```
352.    C          3.50E12           1.01E12        7.20E00      .37E-1
353.    C       POLY SI DATA:
354.    C          1.66D12           .800D12        .233E1
355.    C       QUARTZ  DATA:
356.    C          .87D12            .58D12         .265D1          .04E00
356.1   C        FUSED SILICA DATA:
356.2   C          7.85D11           3.12D11        .220D1
356.3   C        COPPER DATA:
356.4   C          16.9D11           7.54D11        .89D1
356.5   C        COPPER/9.98 AT% AL
356.6   C          16.0D11           7.66D11        .758D1
356.7   C       ALUMINUM/1C % CU ALLOY 122 DATA:
356.8   C          11.7D11           3.0D11         .295D1          .35E0
357.    C       POLYETHYLENE DATA:
358.    C          3.40E10           .260E10        .900E00         1.0D0
359.    C       'VACUUM' DATA:
360.    C          1.0E2             1.0E0          1.0E-6       .1E-3
361.    C       VITRINITE %C DAF = 83.5 (CALC. BERKOWITZ) DATA:
362.    C.         5.7E10            1.43E10        1.3          1.0E0
363.    C       VITRINITE %C DAF = 88.8 (CALC. BERKOWITZ) DATA:
364.    C          7.73E10           1.93E10        1.3EC0       1.0E0
365.    C       EXINITE %C DAF = 83.5 (CALC. BERKOWITZ) DATA:
366.    C          3.27E10           8.18E9         1.2E0        1.0E0
367.    C       EXINITE %C DAF = 88.8 (CALC. BERKOWITZ) DATA:
368.    C          8.21E10           2.C5E10        1.3E0        1.0E0
369.    C       CARBON V=3 DATA:    (Z=7)
370.    C          2.1E11            5.24E10        .233E1          1.0E0
371.    C       CARBON V=4 DATA: (Z=7)
372.    C          2.8E11            7.CE10         .175E1          1.0E0
373.    C       CARBON V=5 DATA:    (Z=7)
374.    C          3.5E11            8.75E10        .140E1          1.0E0
375.    C       CARBON Z=6 DATA:    (V=4)
376.    C          2.4E11            6.0E10         .15E1           1.0E0
377.    C       CARBON Z=8 DATA:    (V=4)
378.    C          3.2E11            8.0E10         .20E1           1.0E0
379.    C       CARBON Z=10 DATA: (V=4)
380.    C          4.0E11            1.0E11         .25E1           1.0E0
381.    C       PLATINUM DATA:
381.1   C          2.27D12           6.4D11         2.14D1          .8E-1
381.2   C       GOLD DATA:
381.3   C          2.07D12           2.85D11        1.93D1          .159E0
381.4   C       TITANIUM DATA:
381.5   C          1.66D12           4.4D11         4.50D0          .21D-1
382.            END
383.    $DATA
384.       2
386.               2.25E10           0.00E00        1.00E00         1.00E00
388.               5.82E11           1.81E11        .2243E1         .77E0
390.               7.30E11           2.5CE11        .232E1          .0E1
392.               7.30E11           2.50E11        .232E1          .1E1
400.    $STOP
```

- 84 -

0.1
0.2
0.3
0.4
0.5
0.6
0.7
0.8
0.9

APPENDIX B

PROGRAM TO CALCULATE THE V(Z) RESPONSE OF AN ACOUSTIC
LENS FOR A SAMPLE WHOSE REFLECTANCE IS GIVEN AS DATA.

```
1.      //VZ JOB 'F173E7,181','R BRAY',CLASS=P,REGION=512K
2.      /*JOBPARM DEST=SELF
3.      // EXEC WATFIV
4.      //GO.SYSIN DD *
5.      $WATFIV
6.      C THIS PROGRAM CALCULATES THE V(Z) RESPONSE OF AN ACOUSTIC
7.      C LENS TO A TARGET WHOSE REFLECTANCE FUNCTION IS SPECIFIED
8.      C AS DATA. THE PUPIL FUNCTION OF THE LENS AND THE BACK
9.      C FOCAL PLANE DISTRIBUTION MUST ALSO BE GIVEN AS DATA.
10.     C OTHER INPUTS ARE ACOUSTIC FREQUENCY, LENS RADIUS AND
11.     C OPENING ANGLE, Z MINIMUM AND MAXIMUM. WATER IS
12.     C ASSUMED AS COUPLING MEDIUM WITH TEMPERATURE 60C.
13.     C THIS PROGRAM NUMERICALLY EVALUATES THE V(Z) INTEGRAL
14.     C IN A.ATALAR'S THESIS (STANFORD UNIVERSITY,1978) GIVEN
15.     C AS EQ. (4.26).  IN ADDITION, THE VARIATION IN PATH
15.1    C LENGTH WITH ANGLE FROM LENS TO FOCUS IS INCORPORATED.
16.     C
16.1          REAL*4 ZG(101),VZLOG(101)
17.           REAL*8 PI,FREQ,RLENS,OPANG,ZMIN,ZMAX,RLM,RLP,
18.          1U1X,U1Y,U1A,U1F,FA(81),FP(81),GAP,F,ZINC,KO,
19.          2AREA,R,VZA,VZX,VZY,VZP,ANG,FX,FY,PX,PY,Z,ALPHA,
19.1         3Q1,Q2,RR,BETAR,ANG1
21.           COMPLEX*16 JAY,REFL(100),P(81),DVZ,
22.          1XEXP,VZ(101),U1(201),VZMAX
22.1    C
23.           PI=3.1415927
24.           JAY=(0.0D0,1.0D0)
25.     C
26.     C FREQ IS ASSUMED TO BE IN GHZ; RLENS AND ZMIN AND ZMAX
27.     C IN MICRONS; OPANG IN DEGREES; REFLECTANCE IN EQUAL
28.     C INCREMENTS (.01) OF SIN(THETA); U1(100) IS U1 AT
29.     C THE LENS APERTURE RADIUS; F IN 1 DEGREE INCREMENTS.
30.           READ,FREQ
31.           READ, RLENS,OPANG
32.           READ,ZMIN,ZMAX
33.           WRITE(6,222) FREQ
34.     222  FORMAT('1    FREQUENCY = ', E10.4, ' GHZ')
35.           WRITE(6,223) RLENS,OPANG
36.     223  FORMAT('0    LENS RADIUS = ',E10.4,' MICRONS; OPENING ANGLE = '
37.          1, E10.4, ' DEGREES')
38.           WRITE(6,224) ZMIN, ZMAX
39.     224  FORMAT('0   ZMIN = ', E12.4, '     ZMAX = ', E12.4,
40.          1' MICRONS')
41.           DO 10 I=1,100
42.           READ,RLM,RLP
43.           RX=RLM*DCOS(RLP*1.D0)
44.           RY=RLM*DSIN(RLP*1.D0)
45.           REFL(I)=DCMPLX(RX,RY)
45.1    10   CONTINUE
46.           WRITE(6,225) REFL(1), REFL(100)
47.     225  FORMAT('0    REFL(1) = ', E12.5, 1X, E12.5, '    REFL(100) = ',
```

```
48.            1 E12.5, 1X, E12.5)
50.            DO 20 I=1,201
51.            READ,U1A,U1P
52.            U1Y = U1A*DSIN(U1P*1.D0)
53.            U1X = U1A*DCOS(U1P*1.D0)
54.            U1(I) = DCMPLX(U1X,U1Y)
55.      20    CONTINUE
56.            WRITE(6,226) U1(1), U1(201)
57.      226   FORMAT('0   U1(1) = ', E12.5, 1X, E12.5, '    U1(201) = ',
58.            1 E12.5, 1X, E12.5)
59.            READ(5,16) (PA(K),K=1,81)
60.            READ(5,16) (PP(K),K=1,81)
61.       16   FORMAT(1H ,5F12.4)
62.            DO 21 I=1,81
63.            PX=PA(I)*DCOS(PP(I)*1.D0)
64.            PY=PA(I)*DSIN(PP(I)*1.D0)
65.            P(I)=DCMPLX(PX,PY)
66.      21    CONTINUE
67.            WRITE(6,227) P(1), P(81)
68.      227   FORMAT('0   P(1) = ', E12.5, 1X, E12.5, '    P(81) = ',
69.            1 E12.5, 1X, E12.5)
70.      C
71.      C
72.            RAP=RLENS*DSIN(OPANG*PI/180.)
73.            P=1.15*RLENS
74.            ZINC=(ZMAX-ZMIN)/100.
75.            KO=2*PI*FREQ/1.5
76.      C
77.      C 1.5 MICRONS PER NANOSECOND, THAT IS: SPEED IN WATER
78.      C CHANGE SPEED FOR ANOTHER LIQUID. LIKEWISE
79.      C .0102 NSEC*NSEC/MICRON IS ATTENUATION CONSTANT IN WATER
79.1     C AT 60C  TEMPERATURE. CHANGE FOR ANOTHER LIQUID OR
79.2     C ANOTHER TEMPERATURE.
80.      C
80.1           ALPHA=.0102*FREQ*FREQ
80.2     C
81.      $EJECT
82.      C  WHAT FOLLOWS IS A DOUBLE LOOP TO CALCULATE V(Z).
83.      C THE INNER LOOP (DO 100 I=1,101) CALCULATES VZ(J) FOR
84.      C A FIXED VALUE OF Z WHICH IS INCREMENTED IN THE OUTER
85.      C LOOP (DO 120 J=1,101).
86.      C
87.            Z=ZMIN
87.1           VZMAX = (0.D0,0.D0)
88.            DO 120 J=1,101
89.            Z=ZMIN+DFLOAT(J-1)*ZINC
90.            ZG(J) = SNGL(Z)
91.      C
92.      C  ZG(J) IS SIMPLY A TABLE OF Z FOR PLOTTING ROUTINES
93.      C
94.            VZ(J) = (0.D0,0.D0)
95.      C
96.            DO 100 I=1,101
97.            R = DFLOAT(I-1)/100.*RAP
98.            AREA = 2*PI*R*RAP/100.
99.            DVZ=U1(I)*U1(I)*AREA
100.     C
101.     C  P COMES AS A FUNCTION OF ANGLE IN DEGREES. CONVERT TO
102.     C THE APPROPRITE VALUE OF RADIUS.
102.1    C  NOTE THIS VERSION EXPECTS A PUPIL FUNCTION IN
```

```
102.2     C 1 DEGREE INCREMENTS, WHEREAS CTEEP VERSIONS EXPECT
102.3     C 2 DEGREE INCREMENTS. OUTPUT FROM PUPIL.80 IS SUITABLE.
103.      C
104.            ANG1=DARSIN(R/(RLENS))
105.            IANG1=IDINT(ANG1*180./3.14159)+1
106.            DVZ=DVZ*P(IANG1)*P(IANG1)
107.      C
108.      C  REFLECTANCE COMES AS A FUNCTION OF SIN OF INCIDENCE
109.      C  ANGLE. FIND APPROPRIATE VALUE FOR A GIVEN RADIUS.
110.      C
111.            IANG=IDINT((R/(1.15*RLENS))*100.)+1
112.            DVZ=DVZ*REFL(IANG)
113.      C
114.            XEXP=CDEXP(JAY*2.*(KO+JAY*ALPHA)*Z*
114.1          1DSQRT(1.-(R/F)*(R/F)))
115.            DVZ=DVZ*XEXP
115.005   C
115.01    C    THE NEXT LINES ACCOUNT FOR VARIABLE WATER ATTENUATION
115.02    C  ON THE WAY TC THE FOCUS
115.03    C
115.04          RR = RLENS*DCOS(ANG1)
115.05          RSTAR = DSQRT((.15*RLENS+RR)*(.15*RLENS+RR) + R*R)
115.06          ANG = DARSIN(R/RSTAR)
115.1           DVZ=DVZ*DEXP(ALPHA*2.*(1.15*RLENS-RSTAR))
115.11    C
116.            VZ(J) = VZ(J)+DVZ
117.      100  CONTINUE
117.1     C
117.2     C    NOW KEEP TRACK OF LARGEST MAGNITUDE TO NORMALIZE LATER.
117.3     C
117.4           Q1 = CDABS(VZ(J))
117.5           Q2 = CDABS(VZMAX)
117.6           IF(Q1 .GT. Q2)  VZMAX = VZ(J)
118.      120  CONTINUE
119.      C
119.1     C  PRINT OUT NUMERICAL VALUE OF VZMAX
119.2     C
119.3           WRITE(6,269) VZMAX
119.4      269  FORMAT('0    VZMAX = ', E12.5, 1X, E12.5)
119.5           Q2 = CDABS(VZMAX)
119.6           WRITE(6,271) Q2
119.7      271  FORMAT('0    MAGNITUDE OF VZMAX = ', E12.5)
120.      $EJECT
120.1     C
120.2     C    NOW NORMALIZE RELATIVE TC MAXIMUM RETURN.
120.3     C
120.4     C*****************************************************
120.5     C DEFINE VZMAX AS GLASS VZMAX TC COMPARE DIFFERENT
120.6     C VZ CURVES CN SAME SCALE. THIS VZMAX IS FOR A
120.65    C 24 MICRON, 66 DEGREE LENS & 'LAYER' TARGET.
120.7     C*****************************************************
120.9           VZMAX=(0.15880D-01,0.54380D-01)
121.            WRITE(6,190)
122.       190  FORMAT('1  V(Z) AMPLITUDE IN DB AND PHASE')
123.            DO 200 I=1,101
123.1           VZ(I) = VZ(I)/VZMAX
124.            VZA=20.*DLOG10(CDABS(VZ(I)))
125.            VZLOG(I) = SNGL(VZA)
126.            VZX=VZ(I)
127.            VZY=VZ(I)*(-JAY)
```

- 87 -

```
128.          VZP=DATAN2(VZI,VZT)
129.          WRITE(6,201) VZA,VZP
130.   201    FORMAT(' ',2X,E12.5,3X,E12.5)
131.   200    CONTINUE
132.       C
133.       C   CALL PLOTTING ROUTINES
134.       C
135.          CALL STARTG('GENIL,LINEMX=8*',0.0)
135.1         CALL SUBJTG(-10.,-45.,5.,15.)
135.2         CALL SETSPG(132,1.)
136.          CALL GRAPEG('VERIT*',1,101,ZG,VZLOG,0,'Z*','V(Z) IN DB*',
137.         1'VITRINITE  XDAF = 83.5          V(Z)  F=2.6 GHZ*')
138.          CALL EXITG
139.          STOP
140.          END
141.       SDATA
142.         2.6
143.         24.     66.
144.        -10.     5.
145.          0.28946D 00   -C.59930D-17
146.          0.28944D CO    0.89902D-17
147.        [ IN ALL, 100 VALUES OF REFLECTANCE AMPLITUDE & PHASE.]
148.        [ THIS IS OUTPUT OF REFLEC.SIA PROGRAM. ]
243.          0.60330D 0C   -C.31385D C1
244.          0.69871D 00   -0.31406D 01
245.      0.23119E-02 -0.35547E 01
246.      0.23117E-02 -0.35553E 01
247.        [ IN ALL, 201 VALUES OF U1PLUS, E.G. FROM ATALAR'S PROGRAM.]
444.      0.86933E-03 -0.39522E 01
445.      0.86843E-03 -0.39556E 01
446.          3.5592       3.5597       3.5612       3.5637       3.5672
447.          3.5718       3.5775       3.5842       3.5921       3.6012
448.        [ IN ALL, 81 VALUES OF PUPIL FUNCTION AMPLITUDE,
449.         E.G. LENS TRANSMISSION FUNCTION FROM LEMONS'
450.         PROGRAM, MODIFIED AS PUPIL.80.]
461.          0.7489       0.7084       0.6686       0.6291       0.5897
462.          0.5499
463.         -0.6708      -0.6713      -0.6728      -0.6753      -0.6788
464.         -0.6833      -C.6885      -0.6955      -0.7031      -0.7118
465.        [ IN ALL, 81 PUPIL FUNCTION PHASES TO GO WITH AMPLITUDE.]
478.          0.1830       C.1764       0.1701       0.1640       0.1578
479.          0.1515
500.       SSTOP
```

```
0.1
0.2
0.3                        APPENDIX  C
0.4
0.5                  PROGRAM TO CALCULATE THE PHOTOACOUSTIC
0.6                  RESPONSE IN A 2-REGION SYSTEM.
0.7
0.8
0.9
1.       //OPTAC2 JOB 'F17SE7,181','R BRAY',CLASS=E,REGION=512K
1.5      /*JOBPARM DEST=SELF
2.       // EXEC WATFIV NOLIST
3.       //GO.SYSIN DD *
4.       $WATFIV NOLIST
5.       C     THIS FORTRAN PROGRAM SOLVES FOR THE ACOUSTIC POWER
6.       C  RADIATED INTO TWO SEMI-INFINITE HALF-SPACES, REGIONS
7.       C  1 AND 2, AND GENERATED BY OPTICAL ABSORBTION IN MEDIUM
8.       C  2.  THE
9.       C  INCOMING OPTICAL POWER IS ASSUMED TO BE INCIDENT
10.      C  THROUGH TRANSPARENT MEDIUM 1, AND IS ASSUMED TO HAVE
11.      C  UNIT INTENSITY.
16.      C   THE ACOUSTIC GENERATION IS SOLVED BY THE
17.      C  METHOD OF COUPLED MODES IN A DISTRIBUTED FINITE
18.      C  SOURCE REGION AS PRESENTED IN E.A. AULD'S TEXT V.I, CH.6.
20.      C   THE PRESENT PROGRAM WAS WRITTEN BY RC BRAY IN
21.      C  SEPTEMBER 1980.
36.      C
37.            DIMENSION RHO(2), C(2), C11(2), BETATH(2), ALPHA(2),
38.           1A(2), Z(2),  TAUL(200), STR(200)
39.            REAL K(2), KK(2), B,G,R0,R1,L,LMAX,LINCR,S1(201),
39.1          1 S2(201),F1(201),F2(201),FMIN,FMAX,F(201)
40.            COMPLEX TAU(2),ZTH(2), R,TE11,TE20,TH22,
41.           1JAY,UU,VV,BETA,AP2P,AM1P,AP20,AM10
43.      C
44.      C     FREQ  =  FREQUENCY OF MODULATION OF LIGHT
45.      C     BET   =  OPTICAL ABSORBTION COEFFICIENT OF 2
46.      C
47.            READ, FMIN, FMAX
48.            WRITE(6,133) FMIN, FMAX
49.       133  FORMAT('1 FMIN = ',E18.8,3X,'FMAX = ', E18.8//)
50.            READ,BET
51.            WRITE(6,50) BET
52.       50   FORMAT('0  OPTICAL ABS COEFF BET =  ', E20.8,'  1/M')
53.            BETA = CMPLX(BET,0.)
54.            WRITE(6,30)
55.       30   FORMAT('0          KK                    RHO                    C
56.           1              C11                    BETATH')
57.            DO 45 I=1,2
58.      C
59.      C       KK(I) = THERMAL CONDUCTIVITY OF ITH REGION
60.      C       RHO(I) = DENSITY
61.      C       C(I)  = SPECIFIC HEAT
62.      C       C11(I) = ELASTIC STIFFNESS C11
63.      C       BETATH(I) = THERMAL COEFFICIENT OF LINEAR EXPANSION
64.      C
65.            READ, KK(I), RHO(I), C(I), C11(I), BETATH(I)
66.            WRITE(6,40) KK(I), RHO(I), C(I), C11(I), BETATH(I)
67.       40   FORMAT('0',5E20.8)
68.       45   CONTINUE
70.      C  SET UP LOOP TO CALCULATE RESULTS FOR 201 VALUES OF FREQUENCY
```

- 89 -

```
70.1   C
70.2           FINCR = (ALCG1C(FMAX)-ALCG10(FMIN))/200.
70.3           DO 73 N = 1,201
70.4           FREQ = ALCG10(FMIN) + (N-1)*FINCR
70.5           FREQ = 10.**FREQ
70.7           F(N)=FREQ
73.    C  CALCULATE  ALPHA(I) = THERMAL DIFFUSIVITY OF ITH LAYER
74.    C                A(I)     = THERMAL DIFFUSION COEFFICIENT
75.    C                TAU(I)   = (1+J)*A(I)
76.    C                Z(I)     = ACOUSTIC IMPEDANCE
77.    C                K(I)     = ACOUSTIC PROPAGATION CONSTANT
77.1   C                ZTH(I)   = THERMAL IMPEDANCE
77.2   C
78.            JAY=(0.,1.)
79.            DO 60 I=1,2
80.            ALPHA(I)  = KK(I)/(RHO(I)*C(I))
81.            A(I) = SQRT((2.*3.14159*FREQ)/(2.*ALPHA(I)))
82.            Z(I) = SQRT(RHC(I)*C11(I))
83.            TAU(I) = CMPLX(A(I),A(I))
84.            K(I)=2.*3.14159*FREQ*SQRT(RHC(I)/C11(I))
85.            ZTH(I)=(1.+JAY)*SQRT(3.14159*FREQ*RHO(I)*C(I)
86.          1*KK(I))
91.       60   CONTINUE
92.            TSD = 1./A(2)
92.5   C       WRITE(6,65) TSD
93.    C  65  FORMAT('0  THERMAL SKIN DEPTH  A(2) =   ', E20.8)
98.    C
99.            CALL TRAPS(1,1,10000,1,1)
106.   C
107.   C    CALCULATE TH11, TH20, AND TH22, TEMPERATURE
108.   C AMPLITUDES AT THE Z=0 BOUNDARY.
109.   C
110.           TH11 = BETA/(ZTH(1)*(1.+ZTH(2)/ZTH(1))*(BETA+TAU(2)))
111.   C
112.           TH20 = BETA*(BETA*(ZTH(2)/ZTH(1))+TAU(2))
113.           TH20 = TH20/(ZTH(2))
114.           TH20 = TH20/(1.+ZTH(2)/ZTH(1))
115.           TH20 = TH20/(BETA*BETA - TAU(2)*TAU(2))
116.   C
117.           TH22 = BETA*TAU(2)/ZTH(2)
118.           TH22 = TH22/(BETA*BETA-TAU(2)*TAU(2))
118.5          TH22 = -TH22
119.   C  THAT - SIGN ON TH22 WAS INSERTED DEC. 23, 1981
120.5  C
121.   C    CALCULATE AP20, THE POSITIVE TRAVELLING MODE AT
121.5  C Z=0.
122.   C
122.5          UU = 2.*Z(2)/(Z(1)+Z(2))
123.           UU = UU*(-JAY*K(1)*BETATH(1)*C11(1)*TH11)
123.5          UU = UU/(TAU(1)+JAY*K(1))
124.   C
124.5          VV = TH22/(BETA+JAY*K(2))+TH20/(TAU(2)+JAY*K(2))
125.           VV = VV+JAY*K(2)*C11(2)*BETATH(2)
125.5          VV = ((Z(1)-Z(2))/(Z(1)+Z(2)))*VV
126.   C
126.5          AP20 = UU - VV
127.   C
127.5  C  CALCULATE AM10, THE NEGATIVE TRAVELLING MODE AT
128.   C THE BOUNDARY Z=0.
128.5  C
```

```
129.            UU = TH22/(BETA+JAY*K(2))+TH20/(TAU(2)+JAY*K(2))
130.            UU = UU+JAY*K(2)*C11(2)*BETATH(2)
131.            UU = UU*(-2.*Z(1)/(Z(1)+Z(2)))
132.     C
133.            VV = (Z(1)-Z(2))/(Z(1)+Z(2))
134.            VV = VV+JAY*K(1)*BETATH(1)*C11(1)*TH11
135.            VV = VV/(TAU(1)+JAY*K(1))
136.     C
137.            AM10 = UU + VV
138.     C
140.     C
141.     C    NOW CALCULATE FAR FIELD MODE AMPLITUDES AP2F
142.     C    AND AM1F.
143.     C
144.            AP2F = JAY*K(2)*C11(2)*BETATH(2)*TH22
145.            AP2F = AP2F/(JAY*K(2)-BETA)
146.            AP2F = AP2F + JAY*K(2)*C11(2)*BETATH(2)*TH20
147.          1          /(JAY*K(2)-TAU(2))
148.            AP2F = AP2F + AP20
149.     C
150.     C
151.            AM1F = JAY*K(1)*C11(1)*BETATH(1)*TH11
152.            AM1F = AM1F/(JAY*K(1)-TAU(1))
153.            AM1F = AM1F + AM10
154.     C
155.     C    CALCULATE ACOUSTIC POWER AND STRAIN IN THE
156.     C    FAR FIELDS OF REGIONS 1 AND 2.
157.            P2(N) = CABS(AP2F*CONJG(AP2F)/8./Z(2))
158.            P1(N) = CABS(AM1F*CONJG(AM1F)/8./Z(1))
159.     C
160.     C
161.            S1(N) =SQRT(2.*Z(1)*P1(N))/C11(1)
162.            S2(N) = SQRT(2.*Z(2)*P2(N))/C11(2)
163.     C
163.1      73 CONTINUE
165.     C
166.     C  .PRINT OUT SOME ANSWERS
167.     C
168.            WRITE(6,367)
169.      367 FORMAT('1          F               S1               S2
170.          1P1               P2 '/)
170.5           DO 74 I = 1,201
171.            WRITE(6,368)  F(I),S1(I),S2(I),P1(I),P2(I)
171.5       74 CONTINUE
172.      368 FORMAT(' ',E18.8,3X,E18.8,3X,E18.8,3X,E18.8,3X,E18.8)
176.     C
211.     C    CALL PLOTTING ROUTINES
212.     C
213.            CALL STARTG('GENIL,LINEEX=8**',0.0)
213.5           CALL SETSMG(23,1.0)
214.            CALL SETSMG(24,1.0)
215.            CALL SUPJEG(1.0E6,1.0E-20,1.0E10,1.0E-16)
216.            CALL SETSMG(132,1.)
220.            CALL GRAPHG('VERIT**',1,201,F,P2,0,'FREQ**','  I2**',
221.          1'1E-5 AIR///SILICON   ALPHA = 3.29E6   I2 **')
222.     C     CALL LINESG('VERIT**',201,F,P1),
226.            CALL EXITG
229.     C     WHAT FOLLOWS IS A TABLE OF DATA FOR DIFFERENT MATERIALS
230.     C        K        REC        C            C11         BETATH
231.     C PYREX DATA:   ADJUSTED BETATH 1/8/80
```

```
232.    C .12600D1      .2290CC4     .97500D3       .73000D11      .27000D-6
233.    C MOLYBDENUM DATA: ADJUSTED BETATH 1/8/80
234.    C .17900D3      .1C22CD5     .1380003       .47000D12      .28600D-5
235.    C GOLD DATA: ACJUSTIC EETATH 1/8/80
236.    C .34500D3      .1920CD5     .13000D3       .18900D12      .13000D-4
237.    C WATER DATA
238.    C .65000D0      .10000D4     .41850D4       .23700D10      .69000D-4
239.    C ACETONE DATA:
240.    C .19800D0      .7900CD3     .21760D4       .10600D10      .50000D-3
241.    C METHANOL DATA:
242.    C .15500D0      .79100D3     .25470D4       .83000D9       .40000D-3
243.    C HELIUM (4K) DATA:
244.    C .20000D-1     .146CCD3     .52C0CD4       .74000D7       .13700D0
245.    C ARGON (85K) CATA:
246.    C .12100D0      .14170D4     .98400D4       .10360D10      .15000D-2
247.    C NITROGEN (75K) CATA:
248.    C .13800D0      .8240CD3     .19480D4       .63800D8       .17000D-3
249.    C SILICON DATA:   ACJCSTED BETATH 1/8/80
250.    C .83500D2      .23400D4     .72800D3       .1657D12       .4480D-5
251.    C ALUMINUM DATA:  AIJUSTED BETATH 1/8/80
252.    C .30000D3      .26989D4     .91700D3       .10900D12      .1780D-4
253.    C QUARTZ DATA:
254.    C .13500D1      .220CC4      .93700D3       .86700D11      .5500D-6
255.    C GALLIUM ARSENIDE CATA:
256.    C .46000D2      .5307D4      .35000D3       .11880D12      .5900D-5
257.    C CHROMIUM DATA:
258.    C .87000D2      .7100C4      .4600D3        .35000D12      .65000D-5
259.    C TANTALUM DATA:
260.    C .68000D2      .1660C5      .1420D3        .26700D12      .65000D-5
261.    C SAPPHIRE DATA:  ACJUSTED BETATH 1/8/80
262.    C .33000D2      .39860C4     .43300D3       .49400D12      .30000D-5
263.    C CARBON DATA:   ADJCSTED BETATH 1/8/80
264.    C .80000D2      .20000C4     .7110CD3       .32000D11      .52000D-5
264.1   C AIR (GASEOUS) CATA: NEW!
264.2   C .24100D0      .1225CC1     .74100D3       .14160D6       .34100D-2
264.3   C 1E-5 ATM AIR DATA (CALCULATED PFOM 1 ATM):
264.4   C .24100D-5     .1225CD-4    .74100D3       .14160C1       .34100D-2
265.    C
266.    C   WHAT FOLLOWS IS A TABLE OF ATTENUATION CONSTANTS AND REFL-
267.    C ECTANCES FOR CERTAIN MATERIALS (AIP HER, SEC. 6G)
268.    C     MATERIAL   OPTICAL WAVE-      POWER ATTEN      REFLECTANCE-
269.    C                LENGTH, MICRCNS    CONST, 1/M       (POWER)
270.    C
271.    C AL,EVAP        .492              1.40D8           .922
272.    C AL,EVAP        .95               1.12D8           .912
273.    C AU,EVAP        .50               4.60D7           .504
274.    C AU,EVAP        1.00              7.60D7           .981
275.    C SI,SNGL CRST   .515              2.44D6           .375
276.    C SI,BULK LC FOR 1.25              2.96D6           .330
277.    C SI,EVAP        .500              1.86D7           .399
278.    C SI,EVAP        .800              3.29D6           .367
279.    C MOLY, BULK     .501              7.54D7           .520
280.    C MOLY, BULK     1.000             4.46D7           .574
281.    C
321.        STOP
322.        END
323.    SDATA
324.      .10000E7   .10000E11
325.      3.29E6
326.      .24100D-5   .12250C-4   .74100D3   .14160D1      .34100D-2
```

327.   .83500D2   .234CCD4   .72800D3   .1657D12   .4480D-5
328. $STOP

```
0.1
0.2
0.3                              APPENDIX  D
0.4
0.5                    PROGRAM TO CALCULATE THE PHOTOACOUSTIC
0.6                    RESPONSE IN A 3-REGION SYSTEM.
0.7
0.8
0.9
1.      //DOPT3 JOB 'F17SE7,181','R BRAY',CLASS=E,REGION=512K
2.      /*JOBPARM DEST=SELF
3.      // EXEC WATFIV
4.      //GO.SYSIN DD *
5.      $WATFIV NOLIST
9.      C      THIS FORTRAN PROGRAM SOLVES FOR THE ACOUSTIC STRAIN
10.     C   RADIATED INTO TWO SEMI-INFINITE HALF-SPACES, REGIONS
11.     C   1 AND 3, AND GENERATED BY OPTICAL ABSORBTION IN MEDIUM
12.     C   2 WHICH SEPARATES THEM AND HAS THICKNESS L. THE
13.     C   INCOMING OPTICAL POWER IS ASSUMED TO BE INCIDENT
14.     C   THROUGH TRANSPARENT MEDIUM 1, AND IS ASSUMED TO HAVE
15.     C   UNIT INTENSITY.
16.     C      MEDIUM 3 IS ALSO TRANSPARENT. MEDIUM 1 EXTENDS FROM
17.     C   X=-INFINITY TO X=0. MEDIUM 2 EXTENDS FROM  X=0. TO X=L.
18.     C   MEDIUM 3 EXTENDS FROM X = L TO INFINITY. THE HEAT FLOW
19.     C   IS CALCULATED USING THE METHOD OF COUPLED MODES
20.     C   AS WELL. THE ACOUSTIC GENERATION IS SOLVED BY THE
21.     C   METHOD OF COUPLED MODES IN A DISTRIBUTED FINITE
22.     C   SOURCE REGION AS PRESENTED IN B.A. AULD'S TEXT V.I, CH.6.
23.     C      THIS VERSION CALCULATES FOR A RANGE OF THICKNESSES
24.     C   OF REGION 2 FROM 0 TO 6 THERMAL SKIN DEPTHS.
25.     C   IT THEN PRODUCES A VERSATEK PICT OF STRAIN INTO 3
26.     C   VERSUS A*L, A = THERMAL DIFFUSION COEFFICIENT,
27.     C   L = LENGTH OF REGION 2.
28.     C      THIS VERSION PICTS POWER INTO REGION 3 P3 AND
29.     C   POWER INTO REGION 1 P1. A TABLE OF
30.     C   DATA IN FORMAT READY TO USE (REMOVE COMMENT C IN
31.     C   COLUMN 1) IS STORED IMMEDIATELY BEFORE THE DATA CARD.
32.     C      TO RUN OTHER DATA, CHANGE THE PLOT LABELLING
33.     C   IN THE CALL TO GRAPHG; CHANGE THE X AND Y RANGE IN
34.     C   THE CALL TO SUBJEG; TRY A CHANGE IN THE 'LINEMX=8'
35.     C   OPTION IN THE CALL TO STARTG IF AN ERROR IN THE
36.     C   STARTG CALL RESULTS. (E.G. 'LINEMX=6')
37.     C
38.            REAL S1(2,200), S3(2,200), STR(200), TAUL(200),
39.           1 P1(2,200),P3(2,200),PWR(200)
40.            REAL*8   RHO(3), C(3), C11(3), BETATH(3), ALPHA(3),
41.           1AA(3), ZO(3),
42.           2K(3), KK(3), L,LMAX,LINCR,DEL21,DEL23
43.            COMPLEX*16 TAU(3), AM12,AP31,AP3Z,
44.           1 JAY, C1,C3,C20,C22,
45.           2 BETA, ZTH(3), TH02,A,B,CD,D21,D23,TH11,
46.           3TH30,TH20,TH21,TH22,UU,VV,WW,CDA
48.     C
49.     C      FREQ  =  FREQUENCY OF MODULATION OF LIGHT
50.     C      BET   =  OPTICAL ABSORPTION COEFFICIENT OF 2
51.     C
52.            READ, FREQ
53.            WRITE(6,140)FREQ
54.       140  FORMAT('1   FREQUENCY  =  ',E20.8,'  HZ')
55.            READ,BET
```

```
56.          WRITE(6,50) BET
57.     50   FORMAT('0  OPTICAL ABS COEFF BET = ', E20.8,'  1/M')
58.          BETA = CMPLX(BET,0.)
59.          WRITE(6,30)
60.     30   FORMAT('0            KK                    RHO                    C
61.         1               C11                    BETATH')
62.          DO 45 I=1,2
63.   C
64.   C         KK(I) = THERMAL CONDUCTIVITY OF ITH REGION
65.   C         RHO(I)= DENSITY
66.   C         C(I)  = SPECIFIC HEAT
67.   C         C11(I)= ELASTIC STIFFNESS C11
68.   C         BETATH(I) = THERMAL COEFFICIENT OF LINEAR EXPANSION
68.1  C                    NOTE: ADJUST HANDBOOK VALUE OF BETATH
68.2  C                    BY MULTIPLYING BY BULK MODULUS, DIVIDING BY C11.
69.   C
70.          READ, KK(I), RHO(I), C(I), C11(I), BETATH(I)
71.          WRITE(6,40) KK(I), RHO(I), C(I), C11(I), BETATH(I)
72.     40   FORMAT('0',5E20.8)
73.     45   CONTINUE
74.          DO 180 N = 1,2
75.          READ, KK(3),RHO(3),C(3),C11(3),BETATH(3)
76.          WRITE(6,47) KK(3),RHO(3),C(3),C11(3),BETATH(3)
77.     47   FORMAT('1',5E20.8)
79.   C  CALCULATE  ALPHA(I) = THERMAL DIFFUSIVITY OF ITH LAYER
80.   C             AA(I)     = THERMAL DIFFUSION COEFFICIENT
81.   C             TAU(I)    = (1+J)*AA(I)
82.   C             Z0(I)     = ACOUSTIC IMPEDANCE
83.   C             K(I)      = ACOUSTIC PROPAGATION CONSTANT
84.   C             ZTH(I)    = THERMAL IMPEDANCE
85.   C             D21       = ZTH(2)/ZTH(1)
86.   C             D23       = ZTH(2)/ZTH(3)
87.   C             DEL21     = Z0(2)/Z0(1)
88.   C             DEL23     = Z0(2)/Z0(3)
89.   C
90.          JAY=(0.,1.)
91.          DO 60 I=1,3
92.          ALPHA(I)  = KK(I)/(RHO(I)*C(I))
93.          AA(I) = DSQRT((2.*3.14159*FREQ)/(2.*ALPHA(I)))
94.          Z0(I) = DSQRT(RHO(I)*C11(I))
95.          TAU(I) = DCMPLX(AA(I),AA(I))
96.          K(I)=2.*3.14159*FREQ*DSQRT(RHO(I)/C11(I))
97.          ZTH(I) = (1.+JAY)*DSQRT(3.14159*FREQ*RHO(I)*C(I)*KK(I))
98.          WRITE(6,560) I
99.     560  FORMAT('0 I = ', I1)
100.         WRITE(6,562) ALPHA(I),AA(I),Z0(I),K(I)
101.    562  FORMAT('   ALPHA(I),AA(I),Z0(I),K(I) = ', 5D18.6)
102.         WRITE(6,564) TAU(I),ZTH(I)
103.    564  FORMAT('   TAU(I),ZTH(I) = ', 2D18.6,3X,2D18.6)
104.         WRITE(6,566) ZTH(I)
105.    566  FORMAT('   ZTH(I) = ', 2D18.6)
106.    60    CONTINUE
107.   C
108.         D21 = ZTH(2)/ZTH(1)
109.         D23 = ZTH(2)/ZTH(3)
110.         DEL21 = Z0(2)/Z0(1)
111.         DEL23 = Z0(2)/Z0(3)
112.         WRITE(6,568) D21,D23
113.    568  FORMAT('   D21,D23 = ', 2D18.6,3X,2D18.6)
114.         WRITE(6,570) DEL21,DEL23
```

```
115.      570  FORMAT(' CEL21,CEL23 = ',1D18.6,3X,1D18.6)
116.    C
117.           TSD = 1./AA(2)
118.           WRITE(6,65) TSD
119.      65   FORMAT('0  THERMAL SKIN DEPTH   1/AA(2) =    ', E20.8)
120.    C
122.    C     SET UP LOOP TO INCREMENT LENGTH FROM 0 TO LMAX,
123.    C WHERE LMAX IS SUCH THAT A(2)*LMAX = 6., IN 200 STEPS
124.    C RECALL 1/AA IS THE THERMAL SKIN DEPTH.
125.    C
126.           CALL TRAPS(1,1,10000,1,1)
127.           LMAX =  6.0/AA(2)
128.           LINCR = LMAX/200.
129.           L = 0.
130.           DO 200 M = 1, 200
131.           L = L + LINCR
133.    C
134.    C     CALCULATE TEMPERATURE AMPLITUDES TH11, TH30 IN REGIONS
135.    C 1 AND 3, AND THEN TH20 (EXP(-TAU*Z), TH21(EXP(+TAU*Z), AND
136.    C TH22(EXP(-BETA*Z)). THO2 IS A UBIQUITOUS COLLECTION OF
137.    C CONSTANTS, AS ARE A, B, AND CD (= COMMON DENOMINATOR).
138.    C
139.           THO2 = BETA/(TAU(2)*ZTH(2))
140.           THO2 = THO2/((BETA*BETA)/(TAU(2)*TAU(2))-1.)
141.    C
142.           A = BETA/(BETA+TAU(2))
143.           A = A*(CDEXP(-(BETA+TAU(2))*L)-1.)
144.    C
145.           B = BETA/(BETA-TAU(2))
146.           B = B*(CDEXP(-BETA*L) - CDEXP(-TAU(2)*L))
147.    C
148.           CD = (1.-D21)*(1.-D23)*CDEXP(-TAU(2)*L)
149.           CD = CD - (1.+D21)*(1.+D23)*CDEXP(TAU(2)*L)
150.    C
151.           TH11 = B*(1.-D23) - A*(1.+D23)*CDEXP(TAU(2)*L)
152.           TH11 = -TH11/(ZTH(1)*CD)
153.    C
154.           TH30 = B*(1.+D21)*CDEXP(TAU(2)*L) - A*(1.-D21)
155.           TH30 = TH30/(ZTH(3)*CD)
156.    C
157.    C
158.           TH20 = (1.-D23)*(1.-(D23*BETA)/TAU(2))*CDEXP(-BETA*L)
159.           TH20 = TH20 - (1.+D23)*(1.+(D21*BETA)/TAU(2))*CDEXP(TAU(2)*L)
160.           TH20 = TH20*(THO2/CD)
161.    C
162.           TH21 = (1.-D23)*(1.+(D21*BETA)/TAU(2))*CDEXP(-TAU(2)*L)
163.           TH21=TH21-(1.+D21)*(1.-(D23*BETA)/TAU(2))*CDEXP(-BETA*L)
164.           TH21 = TH21*(THO2/CD)
165.    C
166.           TH22 = -THO2
167.    C
169.    C
170.    C     CALCULATE C1, C20, C22, AND C3, WHICH ARE COMMON
171.    C COLLECTIONS OF CONSTANTS SEEN IN THESE PARTS.
172.    C
173.           C1 = -JAY*K(1)*C11(1)*BETATH(1)*TH11
174.           C1 = C1/(JAY*K(1) + TAU(1))
175.    C
176.           C3 = -JAY*K(3)*C11(3)*BETATH(3)*TH30
177.           C3 = C3/(JAY*K(3) + TAU(3))
```

```
178.     C
179.            UU = CDEXP(-(JAY*K(2)+TAU(2))*L) - 1.
180.            UU = UU*(TH20/(JAY*K(2)+TAU(2)))
181.     C
182.            VV = CDEXP(-(JAY*K(2)-TAU(2))*L) - 1.
183.            VV = VV*(TH21/(JAY*K(2)-TAU(2)))
184.     C
185.            WW = CDEXP(-(JAY*K(2)+BETA)*L) - 1.
186.            WW = WW*(TH22/(JAY*K(2)+BETA))
187.     C
188.            C20=JAY*K(2)*C11(2)*BETATH(2)*(UU+VV+WW)
189.     C
190.     C.
191.            UU = CDEXP((JAY*K(2)-TAU(2))*L) - 1.
192.            UU = UU*(TH20/(JAY*K(2)-TAU(2)))
193.     C
194.            VV = CDEXP((JAY*K(2)+TAU(2))*L) - 1.
195.            VV = VV*(TH21/(JAY*K(2)+TAU(2)))
196.     C
197.            WW = CDEXP((JAY*K(2)-BETA)*L) - 1.
198.            WW = WW*(TH22/(JAY*K(2)-BETA))
199.     C
200.            C22 = -JAY*K(2)*C11(2)*BETATH(2)*CDEXP(-JAY*K(2)*L)
201.            C22 = C22*(UU+VV+WW)
202.     C
203.     C        THERE ARE TWO COMMON DENOMINATORS. THE THERMAL
204.     C  ONE WE CALLED CD. THE ACOUSTIC ONE WE SHALL CALL CDA
205.     C
206.            CDA = (1.+DEL21)*(1.+DEL23)*CDEXP(JAY*K(2)*L)
207.            CDA = (1.-DEL21)*(1.-DEL23)*CDEXP(-JAY*K(2)*L) - CDA
208.     C
209.     C
210.     C
211.     C        CALCULATE AM12, THE FAR-FIELD MODE AMPLITUDE IN
212.     C  MEDIUM 1
213.     C
214.            WW = -(1.-DEL23)*C22 - 2.*DEL23*C3
215.            WW = -(1.+DEL23)*C20*CDEXP(JAY*K(2)*L) + WW
216.            VV = (1.+DEL23)*(JAY*K(1) + DEL21*TAU(1))*CDEXP(JAY*K(2)*L)
217.            UU = (1.-DEL23)*(JAY*K(1) - DEL21*TAU(1))*CDEXP(-JAY*K(2)*L)
218.            UU = UU - VV
219.            UU = -C1*UU
220.            UU = UU/(JAY*K(1)-TAU(1))
221.     C
222.            AM12 = UU + WW
223.            AM12 = AM12*(2./CDA)
224.     C
225.     C
226.     C        NOW SOLVE FOR AP3L, THE VALUE OF THE POSITIVE TRAVELLING
227.     C  MODE IN MEDIUM 3 AT THE BOUNDARY WITH MEDIUM 2
228.     C
229.            WW = .5*(1.+DEL21)*(2.*C22-(1.-DEL23)*C3)*CDEXP(JAY*K(2)*L)
230.            VV = .5*(1.-DEL21)*(1.+DEL23)*C3*CDEXP(-JAY*K(2)*L)
231.            UU = 2.*DEL21*C1 + (1.-DEL21)*C20
232.     C
233.            AP3L = -2.*((UU+VV+WW)/CDA)
234.     C
235.     C        NOW CALCULATE AP3Z, THE FAR FIELD MODE AMPLITUDE IN
236.     C  MEDIUM 3
237.     C
238.            AP3Z = JAY*K(3)*C11(3)*BETATH(3)*AB30
```

- 97 -

```
239.          AP3Z = AP3Z/(JAY*K(3)-TAU(3)) * AP3L
240.     C
263.     C
264.     C
266.     C      CALCULATE STRAIN S1 RADIATED INTO REGION 1, AND
267.     C   S1 RADIATED INTC REGION 3. UNIT INTENSITY
268.     C   IS ASSUMED FOR THE INCIDENT LIGHT.
269.     C
270.      202  S1(N,M) = SNGI(CDABS(AM1Z)/(2*C11(1)))
271.           S3(N,M) = SNGI(CDABS(AE3Z)/(2*C11(3)))
272.           P1(N,M) = SNGI(CDABS(AM1Z*DCONJG(AM1Z)/8./Z0(1)))
273.           P3(N,M) = SNGI(CDABS(AP3Z*DCONJG(AP3Z)/8./Z0(3)))
274.     C
275.     C   LOOP UNTIL 200 INCREMENTS OF LENGTH HAVE BEEN MADE
276.     C
277.           TAUL(M) = SNGI(AA(2)*L)
278.      200  CONTINUE
279.           WRITE(6,150)
280.      150  FORMAT('0    PCWER INTO 1         PCWER  INTO 3')
281.           DO 170 M=1,200
282.           WRITE(6,160) P1(N,M), P3(N,M)
283.      160  FORMAT(' ', 2E20.8)
284.      170  CONTINUE
285.      180  CONTINUE
286.     C
287.     C   CALL PLOTTING ROUTINES
288.     C
289.           CALL STARTG('GENIL,LINEMX=6*',0.0)
290.           CALL SETSEG(24,1.0)
291.           CALL SUBJEG(0.0,1.0E-20,6.00,1.0E-15)
292.           CALL SETSEG(132,1.)
293.           DO 220 J=1,200
294.           PWR(J) = P3(1,J)
295.      220  CONTINUE
296.           CALL GRAPHG('VERIT*',1,200,TAUL,PWR,0,'AL*','I2, W/M*',
297.          1'SAPPHIRE/SILICCN  // WATER  I3   1 GHZ*')
298.           DO 230 J =1,200
299.           PWR(J) = P3(2,J)
300.      230  CONTINUE
301.           CALL LINESG('VERIT*',200,TAUL,PWR)
302.           CALL EXITG
304.     C    WHAT FOLLCWS IS A TABLE OF DATA FOR DIFFERENT MATERIALS
305.     C      K        RHO        C        C11        BETATH
306.     C PYREX DATA:   ADJUSTED BETATH 1/8/80
307.     C .12600D1    .2290CD4   .97500D3   .73000D11   .27000D-6
308.     C MOLYBDENUM DATA: ADJUSTED BETATH 1/8/80
309.     C .17900D3    .10220D5   .13800D3   .47000D12   .28600D-5
310.     C GOLD DATA: ADJUSTED BETATH 1/8/80
311.     C .34500D3    .19200D5   .13000D3   .18900D12   .13000D-4
312.     C WATER DATA
313.     C .65000D0    .10000D4   .41850D4   .23700D10   .69000D-4
314.     C ACETONE DATA:
315.     C .19800D0    .79000D3   .21760D4   .10600D10   .50000D-3
316.     C METHANOL DATA:
317.     C .15500D0    .7910CD3   .25470D4   .83000D9    .40000D-3
318.     C HELIUM (4K) DATA:
319.     C .20000D-1   .1460CD3   .52000D4   .74000D7    .13700D0
320.     C ARGON (85K) DATA:
321.     C .12100D0    .1417CD4   .98400D4   .10360D10   .15000D-2
322.     C NITROGEN (75K) DATA:
```

- 98 -

```
323.     C .13800D0      .8240CD3      .19480D4      .63E00D8      .17000D-3
324.     C SILICON DATA:  ADJUSTED BETATH 1/8/80
325.     C .83500D2       .23400D4      .72800C3      .1657D12      .4480D-5
326.     C ALUMINUM DATA:  ACJUSTED BETATH 1/8/80
327.     C .30000D3       .26989D4      .91700C3      .10900D12     .1780D-4
328.     C QUARTZ DATA:
329.     C .13500D1       .2200D4       .93700D3      .86700D11     .5500D-6
330.     C GALLIUM ARSENICE CATA:
331.     C .46000D2       .5307C4       .35000D3      .11880D12     .5900D-5
332.     C CHROMIUM DATA:
333.     C .87000D2       .7100C4       .460CD3       .35000D12     .65000D-5
334.     C TANTALUM DATA:
335.     C .68000D2       .1660E5       .1420D3       .26700D12     .65000D-5
336.     C SAPPHIRE DATA:  ACJUSTED BETATH 1/8/80
337.     C .33000D2       .39860C4      .43300D3      .49400D12     .30000D-5
338.     C CARBON DATA:  ADJCSTED BETATH 1/8/80
339.     C .80000D2       .2000CC4      .71100D3      .32000D11     .52000D-5
340.     C AIR (GASEOUS) DATA: NEW!
341.     C .24100D0       .12250C1      .74100D3      .14160D6      .34100D-2
342.     C 1E-5 ATM AIR CATA (CALCULATED FROM 1 ATM):
343.     C .24100D-5      .12250D-4     .74100D3      .14160D1      .34100D-2
344.     C
345.     C   WHAT FOLLOWS IS A TABLE OF ATTENUATICN CONSTANTS AND REFL-
346.     C ECTANCES FOF CERTAIN MATERIALS (AIP HBK, SEC. 6G)
347.     C    MATERIAL     CPTICAL WAVE-      POWER ATTEN      REFLECTANCE
348.     C                 LENGTH, MICRONS    CCNST, 1/M       (PCWER)
349.     C
350.     C AL,EVAP         .492               1.40D8           .922
351.     C AL,EVAP         .95                1.12D8           .912
352.     C AU,EVAP         .50                4.60D7           .504
353.     C AU,EVAP         1.00               7.60D7           .981
354.     C SI,SNGL CRST    .515               2.44D6           .375
355.     C SI,BULK LO PUR  1.25               2.96D6           .330
356.     C SI,EVAP         .500               1.86D7           .399
357.     C SI,EVAP         .800               3.29D6           .367
358.     C MOLY, BULK      .5C1               7.54D7           .520
359.     C MOLY, BULK      1.000              4.46D7           .574
360.     C
400.         STOP
401.         END
402.     $DATA
403.       .10000D10
404.       3.29E6
405.       .33000D2      .3986CD4      .43300D3      .49400D12     .30000D-5
406.       .83500D2      .23400D4      .72800D3      .1657D12      .4480D-5
407.       .65000D0      .10000D4      .41850D4      .23700D10     .69000D-4
408.       .65000D0      .10000C4      .41850D4      .23700D10     .69000D-4
409.     $STOP
```

REPORT DOCUMENTATION PAGE	READ INSTRUCTIONS BEFORE COMPLETING FORM

1. REPORT NUMBER AFOSR-TR- 81-0435	2. GOVT ACCESSION NO. AD-AC98804	3. RECIPIENT'S CATALOG NUMBER

4. TITLE (and Subtitle) ACOUSTIC MICROSCOPY FOR NONDESTRUCTIVE EVALUATION OF MATERIALS.	5. TYPE OF REPORT & PERIOD COVERED Semiannual Technical rept. 1 Aug 1980 — 31 Jan 1981
	6. PERFORMING ORG. REPORT NUMBER G.L. Report No. 3232

7. AUTHOR(s) C.F. Quate	8. CONTRACT OR GRANT NUMBER(s) F49620-78-C-0098 ARPA Order-3569

9. PERFORMING ORGANIZATION NAME AND ADDRESS Edward L. Ginzton Laboratory Stanford University Stanford, California 94305	10. PROGRAM ELEMENT. PROJECT, TASK AREA & WORK UNIT NUMBERS 2306/B2 61102F

11. CONTROLLING OFFICE NAME AND ADDRESS AFOSR/NE Bolling AFB, DC 20332	12. REPORT DATE March 1981
	13. NUMBER OF PAGES 100

14. MONITORING AGENCY NAME & ADDRESS(if different from Controlling Office)	15. SECURITY CLASS. (of this report) UNCLASSIFIED
	15a. DECLASSIFICATION/DOWNGRADING SCHEDULE

16. DISTRIBUTION STATEMENT (of this Report)

"Approved for public release; distribution unlimited"

17. DISTRIBUTION STATEMENT (of the abstract entered in Block 20, if different from Report)

18. SUPPLEMENTARY NOTES

19. KEY WORDS (Continue on reverse side if necessary and identify by block number)

Acoustic microscopy	Acoustic Scattering	Photoacoustics
Transducer	Backscattering	
Alloy	Reflectance	
Adhesion	Layered Media	

20. ABSTRACT (Continue on reverse side if necessary and identify by block number)

Our work consisted of further improvements in the acoustic microscope. We have extended the operation to higher frequencies (3.6 GHz with a wavelength of 0.4 micrometers). We have built new hardware and developed new software to enable us to record the image in digital form on floppy discs. We have devised a system for recording two simultaneous images, each with a different frequency. The difference frequency can be varied as we wish. We have done further work on materials — both Inconel and manganese ferrite.

DD FORM 1473 EDITION OF 1 NOV 65 IS OBSOLETE
1 JAN 73
S/N 0102-LF-014-6601

11